International Earth Rotation and Reference Systems Service (IERS)
Service International de la Rotation Terrestre et des Systèmes de Référence

IERS Technical Note No. 34

The International Celestial Reference System and Frame

ICRS Center Report for 2001–2004

Jean Souchay and Martine Feissel-Vernier (eds.)

IERS ICRS Centre

Observatoire de Paris/CNRS UMR8630
SYstèmes de Référence Temps-Espace (SYRTE)

61 Av. de l'Observatoire
75014 Paris
France

Verlag des Bundesamts für Kartographie und Geodäsie
Frankfurt am Main 2006

The International Celestial Reference System and Frame
ICRS Center Report for 2001–2004

Jean Souchay and Martine Feissel-Vernier (eds.)

(IERS Technical Note ; No. 34)

Technical support: Wolfgang Schwegmann

International Earth Rotation and Reference Systems Service
Central Bureau
Bundesamt für Kartographie und Geodäsie
Richard-Strauss-Allee 11
60598 Frankfurt am Main
Germany
phone: ++49-69-6333-273/261/250
fax: ++49-69-6333-425
e-mail: central_bureau@iers.org
URL: www.iers.org

ISSN: 1019-4568 (print version)
ISBN: 3-89888-802-9 (print version)

An online version of this document is available at:
http://www.iers.org/MainDisp.csl?pid=46-1100077

Druckerei: Appel &Klinger Druck und Medien GmbH, Kronach

Table of Contents

Foreword

The IERS established in 2001 an ,,ICRS Center", responsible for the maintenance of the International Celestial Reference System and Frame (ICRS, ICRF). This Center is operated jointly by the Paris Observatory (OP) and the U.S. Naval Observatory (USNO), with an agreed share of tasks. It accomplishes these tasks in coordination with the International VLBI Service for Geodesy and Astrometry (IVS) and the IAU Working Group on Reference Frames. It has two co-directors (one from each institution), and a representative to the IERS Directing Board, which rotates between institutions on a four-year term. The representation for the first term (2001-2004) was by the Paris Observatory. In addition to service activities reported yearly through the IERS Annual Reports, research was conducted concerning the various tasks of the Product Center. This Technical Note presents a number of studies in the fields of the maintenance of the International Celestial Reference System and Frame, future realizations of the ICRS, the monitoring of extragalactic radio sources, the link to celestial reference frames at other wavelengths, and information dissemination.

Jean Souchay, Co-director, ICRS Center
Martine Feissel-Vernier Paris Observatory/SYRTE

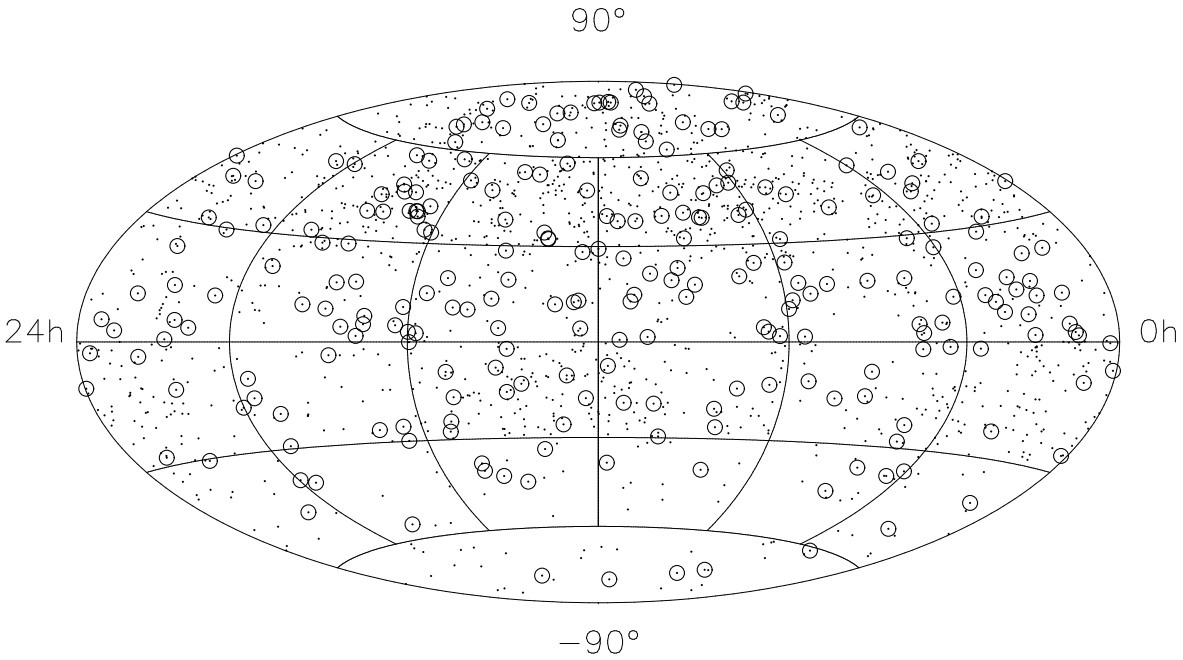

Fig. 1. Sky distribution of the 1500 extragalactic radio sources whose VLBI positions are available for the International Celestial Reference Frame ICRF. The circled dots are the 250 sources that are considered stable on the basis of the ICRS Center studies.

Maintenance of the ICRF using the most stable sources

A.-M. Gontier[1], E.F. Arias[2,1], and C. Barache[1]

[1] *Observatoire de Paris - SYstèmes de Référence Temps-Espace (SYRTE) - UMR 8630/CNRS*
[2] *BIPM - Section du Temps*

Abstract. In preparation for the next realization of the VLBI-based International Celestial Reference Frame (ICRF), we have studied representations of the ICRS by different sets of selected sources. The axes of the ICRS are realized by the coordinates of sources qualified as *defining* object in the ICRF. A different selection of sources has been proposed by Feissel-Vernier based on an analysis of time series of radio source coordinates. We studied the impact of the two sets of sources by using the results of recent analyses representing the state of the art for the next ICRF realization. We shown that the non-rotation condition of the axes with respect to ICRF would not be realized with a better accuracy than 20 μas. We notice an indetermination of 10 to 40 μas in right ascension axes and the presence of an equator tilt with respect to the ICRF of about 22 μas. We conclude that the use of proposed set of stable sources would allow an improvement in the maintenance of the ICRF axes and in the source position precision, to reach 30 μas for the 253 stable sources.

1 Introduction

As was originally proposed by Guinot (1979), the IAU, in its 1991 Recommendations on Reference Systems (Bergeron, 1992), decided to select distant extragalactic objects as the basis of its new celestial reference system and to adopt directions that would remain fixed with respect to a selected set of these objects. Continuity between the old and new system was mandatory so that these directions would be consistent with their previous realizations, i.e., the pole and origin of right ascensions in the new reference system should be close to the FK5 pole and right ascension origin, within the uncertainties of the FK5. A fundamental advantage of selecting extragalactic objects is that they are so distant that their proper motions are currently undetectable, even by the most precise techniques. The choice of extragalactic objects to realize the fiducial directions was made possible by the availability of a mature and highly precise observing technique, Very Long Baseline radio Interferometry (VLBI).

At its 23rd General Assembly in August 1997, the IAU decided (Appenzeller, 1998),

- That, as from 1 January 1998, the IAU celestial reference system shall be the International Celestial Reference System (ICRS) as specified in the 1991 IAU Resolution on Reference Systems and as defined by the International Earth Rotation Service (IERS);
- That the corresponding fundamental reference frame shall be the International Celestial Reference Frame (ICRF) constructed by the IAU Working Group on Reference Frames (WGRF);
- That the Hipparcos Catalogue shall be the primary realization of the ICRS at optical wavelengths;
- That IERS should take appropriate measures, in conjunction with the IAU Working Group on Reference Frames, to maintain the ICRF and its ties to the reference frames at other wavelengths.

The ICRS (Arias et al., 1995) complies with the conditions specified by the 1991 IAU Recommendations. The origin of the ICRS axes is

located at the barycentre of the solar system and the directions of its axes are fixed relative to distant extragalactic sources. For the sake of continuity with the FK5 pole, the ICRS pole is in the J2000.0 direction defined by the conventional IAU models for precession (Lieske et al., 1977) and nutation (Seidelmann, 1982). The origin of right ascensions is also defined consistently with that of the FK5 by fixing the right ascension of 3C 273B to the Hazard et al. (1971) FK4 value transformed to the J2000(FK5) System (Kaplan et al., 1982).

The ICRF consists of a catalogue of equatorial coordinates of 608 extragalactic radio sources derived from about 1.6 million observations accumulated by a worldwide network over 1979-1995. It was derived by a sub-group of the WGRF that agreed on an optimal data analysis strategy (Ma et al., 1998). It includes three lists of objects, with

- the most compact and best observed 212 *defining* sources, with a median uncertainty of 0.4 mas on individual positions,
- compact sources (294) named *candidate* whose positions are likely to be improved when more observations are accumulated in the future,
- sources less appropriate for astrometric purposes (102) named *other*, but which are provided for possible ties of reference frames at other wavelengths or for other objectives.

The accuracy of the ICRF realization of the ICRS axes is estimated to be 20 μas (Ma & Feissel, 1997).

The Hipparcos stellar reference frame was astrometrically aligned to ICRF to within $\pm$0.6 mas for the orientation at 1991.25 and to within $\pm$0.25mas/a for the spin (Kovalevsky et al., 1997). Consequently the Hipparcos Catalogue provides the master realization of the ICRS in the optical domain with the above uncertainties. As the complete FK5 catalogue was observed by Hipparcos, the directions of the pole and origin of right ascensions of the FK5 relative to Hipparcos were determined, with an accuracy of 2.3 mas at the mean epoch J1991.25. The directions of the FK5 axes in the ICRS were estimated (Fig. 1), taking into account the propagation of the uncertainty of the Hipparcos tie to the ICRS (Mignard & Froeschlé, 1997).

Using a state of the art precession-nutation model (Mathews et al., 2002), the analysis of long VLBI series of the observed motion of the celestial pole in the ICRS allows us to derive the coordinates of the mean pole at J2000.0 in the ICRS (IERS, 2001). Combining VLBI and LLR Earth orientation and terrestrial reference frames and using the JPL planetary ephemeris DE200, Folkner et al. (1994) derived the offset of the mean equinox at J2000.0 relative to the ICRS origin of right ascensions. Resulting values are summarized in Fig. 1.

Practical consequences of the adoption of the ICRS/ICRF are given in Feissel & Mignard, 1998.

The main objectives of the maintenance and extension of the ICRF were:

- to provide positions of extragalactic sources observed since July 1995,
- to refine the positions of candidate sources from additional observations,
- to monitor sources to ascertain whether they continue to be suitable for their use in the ICRF,
- to improve the data analysis.

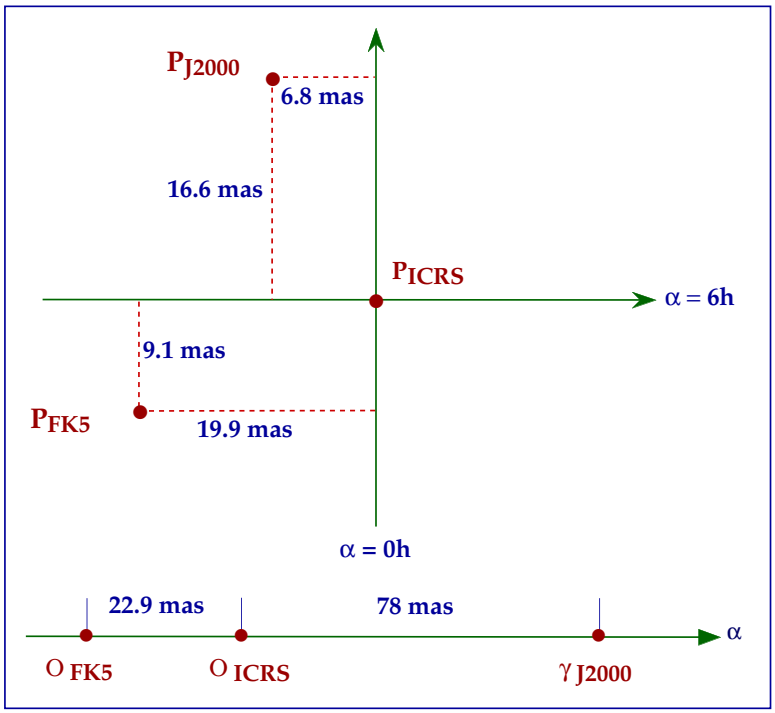

Fig. 1. Location of the poles and the origin of right ascensions of the FK5 and that of the celestial pole and equinox at J2000.0 with respect to the ICRS.

Since 1998, two extensions of the ICRF have been elaborated, ICRF-Ext.1 (IERS, 1999) and ICRF-Ext.2 (Fey et al., 2004), they were both oriented towards the densification of the frame.
The consistency of each maintenance/extension catalogue with the ICRF and the ICRS is of fundamental importance. Improvements in the VLBI analysis can be made but without introducing systematic effects or changing the positions generally beyond the ICRF error threshold. Consequently the main features of the ICRF analysis (Ma et al., 1998) were retained for the extension solutions and only limited changes were made to ensure better modelling.

The data added to the ICRF in ICRF-Ext.1 spanned from December 1994 through April 1999 and were obtained from both geodetic and astrometric observing programs. In the 600,000 observations from 461 sessions added, 59 *new* sources were observed. The ICRF-Ext.1 catalogue contains the positions and uncertainties of 667 extragalactic radio sources (IERS, 1999). As in the original ICRF, the formal errors were inflated applying an additive variance of 0.25 mas and a scaling factor of 1.5 to provide more realistic errors. The positions and errors of the *defining* sources are those of the ICRF one. For *candidate* and *other* sources the refined positions and errors reflect the changes in the data set and the analysis (Gontier et al., 2002). The time series of source positions have been updated. Based on the work of Fey & Charlot (2000), 392 source structure indices were made available, they qualifies the level of position disturbance expected from the source structure (Fey & Charlot, 1997).

The ICRF-Ext.2 solution differed from that of the ICRF and ICRF-Ext.1 solutions primarily in the use of the NMF mapping function (Niell,

1996) for troposphere modeling. The data added in ICRF-Ext.2 spanned from 1999 May through 2002 May and were obtained from both geodetic and astrometric observing programs. Approximately 1.2 million new observations from 400 sessions were added. There were 50 additional new sources. The positions and errors for the *defining* sources were unchanged from the ICRF. Revised positions and errors for the *candidate* and *other* sources were estimated and reflect the changes in the data set and the analysis (Fey at al., 2004). ICRF-Ext.2 marks a milestone in that it utilizes the available VLBA (Very Long Baseline Array) data. A total of over 652,000 delay observations (almost 20% of all observations) from 30 VLBA geodesy/astrometry sessions were included in the solution.

Meanwhile, the general improvements in VLBI technology, the development of the observing network and the extension of the set of observed objects that took place in operational VLBI, brought the astrometric results to its current precision towards the end of the first decade of operation. Starting about 1990, individual time series of source coordinates stabilize (Gontier et al., 2001). In a study of individual source motions, Feissel-Vernier (2003) devised a stability selection scheme based on a statistical assessment of source stability. A set of 199 well observed and stable sources was identified and 163 well observed but highly unstable or drifting sources were pinpointed. Another set of 358 sources were observed too sparsely in this time frame for a statistical evaluation of their stability. The use of the stable sources in the definition of the axes of a celestial reference frame was shown to lower the medium-term instability of the celestial reference frame from 28 to 6 μas when compared to the ICRF (Gontier & Feissel, 2003). Background information on this selection process is given by Feissel-Vernier (2005).

The Feissel-Vernier (2003) scheme was applied to time series of source coordinates that were derived taking subsets of the ICRF *defining* sources as the background reference, but it was shown that a sizable part of these are unstable. One could not rule out the possibility that the intrinsic instability of the set of reference sources create spurious instabilities in the sources under study. Using as a reference a VLBI solution in which the set of stable sources are used to define the orientation of the frame (no-net-rotation condition) and all the sources are global parameters except the unstable ones treated as arc parameters, time series of the unstables or sparsely observed sources were derived. The standard Feissel-Vernier (2003) scheme was applied to this time series and, as expected, a number of sources (54) were detected as stable (Feissel-Vernier, 2005).

The total number of stable sources selected by the Feissel-Vernier process is 253 (199 original + 54 additional) and will be referred as F-V stable sources in the present study.

Analysis by Arias & Bouquillon (2004), on a set of two VLBI independent solutions obtained in 2002, demonstrated that the orientation of the axes of the ICRS is better realized by using the 199 F-V stable sources. This indicates that in the selection of the more stable sources for the realization of the celestial reference system, statistical tests on the time-varying behaviour of source coordinates should be included. The present study extends the Arias & Bouquillon analysis to a larger number of individual celestial frames with different characteristics, and to the total set of 253 F-V stable sources, to assess the previous results and to contribute to a future redetermination of the ICRF.

In section 2 of this report we describe the five VLBI celestial reference frames elaborated in 2003-2004 with the purpose of contributing to the

ICRF maintenance. In section 3 we compare the individual frames with the ICRF-Ext.2 by using two different sets of common sources, the ICRF defining sources and the F-V stable sources.
In section 4 we discuss the impact of the F-V stable sources selection on the definition of axes and on the source coordinates precision. Finally we summarize in section 5 the arguments in favour of a new ICRF realization.

2 Data analyzed

Five VLBI solutions are used for this study and are briefly described in this section. All have referred their respective celestial frames to ICRS by applying a no-net-rotation constraint based on a subset of the ICRF defining sources.

RSC(AUS) 04 R 01 was derived by Geoscience Australia from VLBI observations acquired in the period April 1980- May 2004. OCCAM 6.1 software has been used for the solution. The orientation of the celestial frame has been defined through a no-net-rotation constraint applied to the positions of 207 ICRF defining sources. IERS 1996 and MHB2000 (Mathews et al., 2002) have been adopted as the a priori precession and nutation model respectively.

RSC(BKG) 04 R 01 was derived by the Federal Agency for Cartography and Geodesy and the geodetic Institute of the University of Bonn, in Germany. The software used for the solution is CALC 9.13, SOLVE release 2004.03.18. The celestial reference frame has been oriented by a no-net-rotation constraint applied to the positions of the 212 defining ICRF sources. The time span of the observations used in the solution is January 1984- March 2004. The a priori precession and nutation models are both IERS 1996.

RSC(CGS) 04 R 01 was derived by the Space Geodesy Centre in Matera (Italy) from observations in the period April 1980- October 2003. The software used is CALC 9.12 SOLVE release 2002.10.04 and SOLVE revision 2002.10.11. The celestial frame has been oriented by a no-net-rotation imposed to the positions of 141 ICRF defining sources. The a priori precession and nutation models are both IERS 1996.

RSC(GAOUA) 03 R 01 was derived by the Main Astronomical Observatory of the National Academy of Sciences of Ukraine, from observations acquired in the period August 1979- September 2003. The software used is SteelBreeze-2.0.2. The orientation of the celestial frame has been made by a no-net-rotation constraint applied to the positions of 23 ICRF defining sources. The IAU-2000A precession-nutation models have been chosen as a priori models.

RSC(GSFC) 03 R 03 was derived by the Goddard Space Flight Centre from observations made during the period 1980.0-2002.7. A not-net-rotation constraint has been applied on the defining sources to orient the celestial frame. All observed sources except the unstables are global parameters in this solution. Unstable sources pinpointed by Feissel-Vernier scheme (2003) are treated as arc parameters and therefore have not been included in the catalogue.

For each individual frame, table 1 gives the total number of sources, the number of ICRF defining sources, the number of F-V stable sources present in the catalogue, the number of sources used for the no-net-rotation condition and the declination range.

Table 1. Individual celestial reference frames analyzed.

Frame	Total	IERS def.	F-V stable	NNR const.	Dec. range (^{o})
RSC(AUS) 04 R 01	571	202	188	207 def.	-81 ; +84
RSC(BKG) 04 R 01	668	207	253	207 def.	-81 ; +84
RSC(CGS) 04 R 01	554	183	252	141 def.	-80 ; +84
RSC(GAOUA) 03 R 01	1571	211	253	23 def.	-81 ; +86
RSC(GSFC) 03 R 03	562	152	208	152 def.	-85 ; +84

3 Catalogue comparison

In order to study the influence of the set of selected sources on the orientation of the celestial frame, we compared the five VLBI catalogues listed in table 1 with the ICRF.

The relative orientation of two celestial reference frames is modeled by three rotation angles A_1, A_2, A_3 around the axes of the equatorial coordinate system and systematic effects by three deformation parameters (D_α, D_δ and dz). These parameters are estimated using equations (1) and (2), where α, δ are the source coordinates and $\Delta\alpha$, $\Delta\delta$ are the differences of coordinates in the two frames. The D_α and D_δ parameters represents a slope in right ascension as a function of the declination and a slope in declination as a function of the declination respectively. The dz parameter is a fictitious equator tilt in declination that reflects systematic differences in declination that may be caused by inaccuracy of the tropospheric propagation correction for sources observed at low elevations.

$$\Delta\alpha = A_1 \tan\delta \cos\alpha + A_2 \tan\delta \sin\alpha - A_3 + D_\alpha(\delta - \delta_0) \quad (1)$$

$$\Delta\delta = -A_1 \sin\alpha + A_2 \cos\alpha + D_\delta(\delta - \delta_0) + dz \quad (2)$$

The transformation parameters are evaluated by a weighted least squares fit; the equations are weighted by using the inverse of the variance of the coordinate differences $(\Delta\alpha, \Delta\delta)$. For the assignment of weights, formal coordinate uncertainties smaller than 10 μas in the individual frames are set to this value in order to have more realistic weights. Radio sources with residuals higher than 2.5 the rms residual of the fit are considered as outliers, and consequently deweighted. One could note that we usually have either none, one or four outlier sources in the following comparisons.

The catalogues have been compared to the ICRF-Ext.2 by using common sources of two different sets:

- the ICRF defining sources
- the F-V stable sources

VLBI observations from 1979-1995 were used in the construction of the ICRF and in the classification of its radio sources (Ma et al., 1998). The ICRF has three types of sources, in decreasing order of astrometric quality: *defining, candidate* and *other*. The classification of sources in the ICRF has been done over the 608 sources for the first realization of the frame; 212 fulfilled the criteria for the *defining* sources, 294 were classified as *candidate* sources and 102, showing excessive position variation, had been included in the category *other*. The two extensions of ICRF densify the frame by adding coordinates of *new* sources; the coordinates and uncertainties of the *defining* sources remain the same as in ICRF; for

candidate and *other* sources the positions and uncertainties reflect the changes in the data set and the analysis.

The alignment of the axis of the various realizations of the system is assessed by the *defining* sources.

The F-V analysis is based on time series of source coordinates produced by an independent analysis centre (USNO). It consists of a two step process on about 700 radio sources observed in the period 1989.5-2002.4. A first selection, made on the basis of continuity criteria for one-year weighted average coordinates, retained 362 sources. The second step of the procedure consists of selecting a set of stable sources by applying various criteria like the computation of standard deviation, the Allan standard deviation and the normalized linear drift and looking at their intersection. A subset of 253 sources has been retained as *stable* after these tests. The originality with respect to previous classification is that in F-V selection, studies are conducted on the stability of radio source positions by statistical analyses of the time series of the yearly averaged coordinates.

Whilst in the ICRF work sources have been classified by applying criteria based on the quality of the data, the observational history of the radio sources, the consistency of coordinates derived from different data subsets and the radio source structure, F-V classification is mainly supported by the observational history of sources and the analysis of time series of radio source coordinates.

One could note that from the set of 253 F-V stable sources 101 are previously classifed as *defining*; 87 as *candidate* and 61 as *other* sources. This means that 74% of the F-V selected sources are either *defining* in the ICRF or *candidate* which are potentially *defining* sources in the future. A consequence of using ICRF-Ext.2 as reference catalogue is that some of the F-V stable sources could have revised coordinates with respect to ICRF.

3.1 Catalogue comparison using ICRF defining sources

The five individual frames of table 1 were compared with ICRF-Ext.2 using the usual catalogue comparison model of the ICRS-product centre of IERS. The number of defining sources used in the comparisons is shown in the "IERS defining" column of table 1. The global relative orientation and the deformation parameters between ICRF and the individual frames given in table 2 and 3 were estimated by a weighted least squares fit.

Following the usual practice in VLBI work, constraints described in the data analyzed section, have been applied to align the axes of the individual solutions to those of ICRS; the angles of table 2 show that they are aligned better than 50 μas. The deformation parameters D_α, D_δ of table 3 indicate that no systematic effects are present under the form of slopes varying with the declination. No significant bias of the principal plane of the frames are observed except for RSC(CGS) 04 R 01 where a dz of 35 μas is seen.

3.2 Catalogue comparison using F-V stable sources

The number of common stable sources used in the comparisons is shown in the column "F-V stable" of table 1. Results of comparison of individual frames with ICRF-Ext.2 are shown in tables 4 and 5.

Table 2. Comparison of individual VLBI frames with ICRF-Ext.2 by using common ICRF defining sources. A_1, A_2, A_3 are the rotation angles which transform coordinates from the individual frames into ICRF; unit is μas.

Frame	A_1	A_2	A_3
RSC(AUS) 04 R 01	-24 ± 19	$+50 \pm 19$	-04 ± 25
RSC(BKG) 04 R 01	-04 ± 18	-19 ± 18	-32 ± 23
RSC(CGS) 04 R 01	$+16 \pm 22$	$+39 \pm 22$	$+07 \pm 31$
RSC(GAOUA) 03 R 01	$+14 \pm 19$	$+39 \pm 19$	-22 ± 24
RSC(GSFC) 03 R 03	$+19 \pm 19$	$+24 \pm 20$	-22 ± 28

Table 3. Comparison of individual VLBI frames with ICRF-Ext.2 by using common ICRF defining sources. D_α, D_δ are the slopes in right ascension and declination respectively, dz is the bias in declination; units are μas/deg for the slopes and μas for the bias.

Frame	D_α	D_δ	dz
RSC(AUS) 04 R 01	-1.8 ± 0.8	$+0.1 \pm 0.4$	$+15 \pm 21$
RSC(BKG) 04 R 01	-0.9 ± 0.7	-0.8 ± 0.4	$+20 \pm 19$
RSC(CGS) 04 R 01	-0.7 ± 1.0	-0.8 ± 0.6	$+35 \pm 27$
RSC(GAOUA) 03 R 01	-0.8 ± 0.8	-0.4 ± 0.4	-08 ± 19
RSC(GSFC) 03 R 03	-1.6 ± 0.8	$+0.4 \pm 0.4$	$+04 \pm 21$

Table 4. Comparison of individual VLBI frames with ICRF-Ext.2 by using common F-V stable sources. A_1, A_2, A_3 are the rotation angles which transform coordinates from the individual frames into ICRF; unit is μas.

Frame	A_1	A_2	A_3
RSC(AUS) 04 R 01	-05 ± 13	$+39 \pm 12$	$+06 \pm 13$
RSC(BKG) 04 R 01	-02 ± 10	-11 ± 09	$+09 \pm 10$
RSC(CGS) 04 R 01	$+26 \pm 12$	$+38 \pm 11$	$+46 \pm 13$
RSC(GAOUA) 03 R 01	$+18 \pm 10$	$+47 \pm 09$	$+12 \pm 10$
RSC(GSFC) 03 R 03	$+18 \pm 09$	$+11 \pm 09$	$+18 \pm 10$

Table 5. Comparison of individual VLBI frames with ICRF-Ext.2 by using common F-V stable sources. D_α, D_δ are the slopes in right ascension and declination respectively, dz is the bias in declination; units are μas/deg for the slopes and μas for the bias.

Frame	D_α	D_δ	dz
RSC(AUS) 04 R 01	-1.4 ± 0.5	$+0.1 \pm 0.3$	$+14 \pm 13$
RSC(BKG) 04 R 01	-0.2 ± 0.3	-0.9 ± 0.2	$+36 \pm 10$
RSC(CGS) 04 R 01	-0.3 ± 0.4	$+0.0 \pm 0.3$	$+12 \pm 13$
RSC(GAOUA) 03 R 01	-0.3 ± 0.4	-0.0 ± 0.3	-19 ± 11
RSC(GSFC) 03 R 03	-0.7 ± 0.3	$+0.1 \pm 0.2$	$+22 \pm 10$

4 Discussion

Results in tables 2 and 4 show that the set of F-V stable sources defines the axes of the ICRS better than the defining sources. Except for RSC(CGS) 04 R 01 and RSC(GAOUA) 03 R 01 which have the smallest number of defining sources used initially for the alignment, the directions of the axes are closer to those of ICRS when they are represented by the F-V stable sources. In all cases, the uncertainties of the evaluated angles are smaller when the F-V stable sources are used in the comparison. For A_1 and A_2 angles, the differences between the values estimated using F-V stable or defining sources of an individual frame are not significant. From the differences observed on A_3 angle we could note a global rotation weakly significant of 10 to 40 μas. Except for A_3 the scattering of the rotation parameters obtained in the different comparisons indicate that the axes are stable within 20 μas which is the accuracy claimed for the ICRF.

The results in tables 3 and 5 show that in general the deformations represented by slopes in the coordinates are not significant for both comparisons. The values of the slopes Dα and Dδ indicate for both sets of sources that the radio source coordinates in the five catalogues do not present any systematic effect varying with the declination. As for the rotation angles the uncertainties of the evaluated parameters are smaller when the F-V stable sources are used in the comparison.

One could note that the equator of the individual frame are biased with respect to the ICRF for both sets of sources. The RSC (GAOUA) 03 R 01 dz bias is of opposite sign with respect to all other values which might be explained by the small number of defining sources used for the alignment. The mean quadratic dz term is 20 ± 22 μas when using defining sources and 22 ± 11 μas for the F-V stable sources. In the pre-ICRF celestial frames, significant values of dz were found when comparing solutions obtained by different analysts. However, McMillan and Ma (1997) showed that adding the so-called gradient parameter in the modeling of the tropospheric delay minimizes this defect. The gradient parametrization is now commonly used in VLBI analysis. Although the dz parameter is expected to be negligible, it is still significant when the F-V stable sources are used for the comparison. This could be due to the better sky coverage of the F-V stable sources with respect to the defining ones (Fig. 2) in the declination range $[+30^o\ ; -30^o]$ where the effect of the tropospheric mismodelling is larger. This effect should be discussed in the framework of the next ICRF realization.

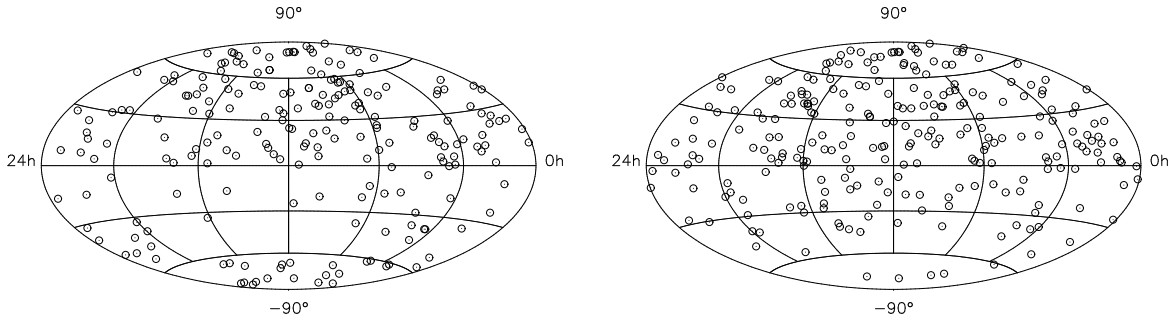

Fig. 2. Sky distribution of the ICRF defining sources (left) and the F-V stable sources (right).

Table 6. Rms residual after fitting the global rotations and the deformation parameters between individual frames and ICRF- Ext.2 by using the common ICRF defining sources (Def.), and by using the common F-V stable sources (Stab.); unit is μas.

Frame	rms α $cos\delta$		rms δ	
	Def.	Stab.	Def.	Stab.
RSC(AUS) 04 R 01	202	136	268	157
RSC(BKG) 04 R 01	189	110	246	145
RSC(CGS) 04 R 01	212	142	303	181
RSC(GAOUA) 03 R 01	182	108	267	153
RSC(GSFC) 03 R 03	182	97	240	126

The post-fit rms residuals in α $cos\delta$ and in δ for both comparisons are given in table 6, where "Def." indicates that the comparison has been made on the basis of common defining sources, and "Stab." on common F-V stable ones. This residuals illustrate the fit to the model.

By inspecting the table, we can conclude that the rms residuals in α $cos\delta$ and in δ are better for the F-V stable set of sources by at least a factor 1.5, which means that the comparison model represents better the inconsistencies in the orientation of the catalogues with respect to ICRS when the frames are compared on the basis of F-V stable sources.

Figure 3 plots for the frame RSC(GSFC) 03 R 03 the normalized residuals (ratio of the postfit residuals to the uncertainty of the coordinate difference between frames) in two dimensional local plane for the fit based on the common defining sources (left) and for the fit based on the common F-V stable sources (right). A circle of radius one has been plotted. A large number of ICRF defining sources show residuals dispersed out of the circle of unit radius, with values that be up to 2, whereas most of F-V stable sources are limited to the unit radius circle. The same behaviour is observed for the other frames analyzed.

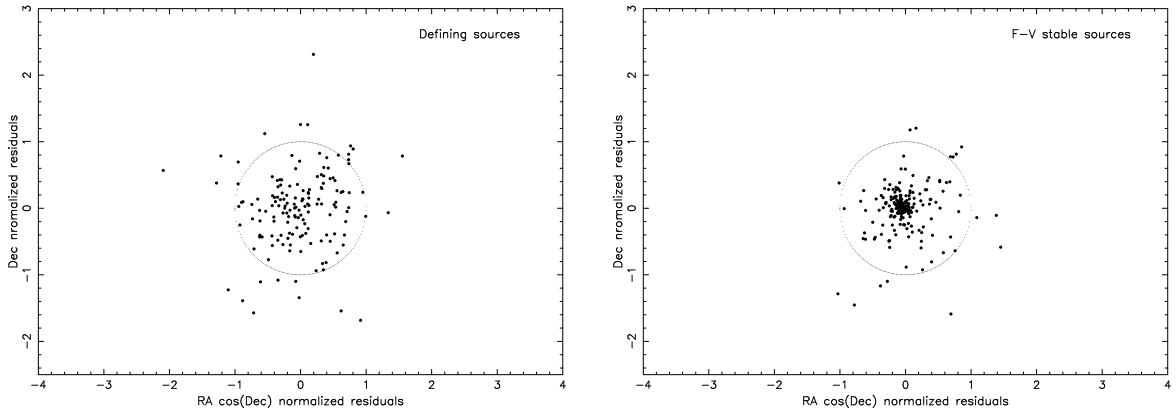

Fig. 3. Normalized residuals in two dimensional local plane for the fit based on defining sources (left) and the F-V stable sources (right).

To evaluate the impact of F-V selection of sources on the precision of the source positions, we compare pairs of independant celestial frames. In each comparison, the two frames are rotated to common axes in a least square adjustment of the equations (1) and (2) applied to the 199

F-V stable sources common to the frames. In the set of F-V stable sources, only the 199 initial set was used because the three-cornered-hat method requires that the tested population be homogeneous. The variances of the post fit residuals $\Delta\alpha cos\delta$ and $\Delta\delta$ are computed. In this process, the estimated parameters A_1, A_2, A_3 and dz absorb systematic differences that can be expected from the construction schemes of the compared reference frames. The variance of the residuals is a measure of the residual differences. The three-cornered-hat method is then applied to these variances. This method allows to estimate the variance of the noises of three or more sets of measurements of the same quantities, here the source right ascensions and declinations, under the assumption that the errors are independent in the three data sets. Considering the variances of the differences between two data sets i and j, one can write

$$var(\alpha_i \cos\delta - \alpha_j \cos\delta) = var(\alpha_i \cos\delta) + var(\alpha_j \cos\delta) \quad (3)$$

$$var(\delta_i - \delta_j) = var(\delta_i) + var(\delta_j) \quad (4)$$

If three reference frames are considered, one gets three sets of the above equations, that can be solved to obtain the individual residual variances $var(\alpha_k \cos\alpha)$ and $var(\delta_k)$ for $k = 1, 3$. If more than three data sets with independent errors are available, the individual residual variances can be estimated by means of a least squares algorithm.

Table 7 gives the individual standard deviations thus derived for the reference frames of table 1. The RSC(AUS) 04 R 01 catalogue was excluded from the comparison because only 155 out of the 199 F-V stable sources are present in the frame. The robustness of the estimations was tested by associating the data in various ways. The results remain stable within 5 μas. We conclude from the values of table 7 that the precision of sources coordinates for the set of stable sources is better than 30 μas.

Table 7. Standard deviations of source positions for the set of 199 F-V stable sources; unit is μas.

Frame	Standard deviations	
	$\Delta\alpha \cos\delta$	$\Delta\delta$
RSC(BKG) 04 R 01	21	26
RSC(CGS) 04 R 01	27	29
RSC(GAOUA) 03 R 01	22	29
RSC(GSFC) 03 R 03	23	18

5 Conclusion

The ICRF was defined on the basis of the pre-1995 astrogeodetic VLBI observations. Since, the core of the *defining* sources was kept fixed in the composition and coordinates, and the two subsequent updates were limited to extending the list of sources with coordinates referred to the original ICRF. Analyses recently published show that a set of 253 stable sources can be selected by applying statistical test on the time-varying behaviour of source coordinates (Feissel-Vernier et al., 2005).

We have compared five individual reference frames obtained from independent VLBI analysis using the *defining* sources on one side, and the *F-V stable* sources on the other side. The analysis performed confirm the Arias & Bouquillon (2004) result that the orientation of the ICRS

axes is better determined when the set of F-V stable sources is used for the comparison. We have noted that also the gradient parametrization is used in VLBI analysis, we still have an equator tilt in declination which is significant at the level of accuracy better than 20 μas.
The intrinsic stability of the sources would allow to reach 5 μas in the maintenance of the ICRF axes, provided that the coherence defaults are solved, else the accuracy will be kept between 10 to 20 μas.
The use of selected stable sources for the definition of the axes and the realization of the pimary frame (source coordinates treated as global parameter in the data analysis) would allow an improvement by a factor of eight in the source position precision, to reach 30 μas with respect to the 250 μas claimed for the ICRF.

Therefore we support the elaboration of the next ICRF on the basis of a set of stable sources by applying criteria based on data quality, observationnal history, source structure as well as statistical tests on the time-varying behaviour of source coordinates.

References

Appenzeller I. (ed.), 1998, Proceedings of the 23rd General Assembly, Transactions of the IAU 23B.

Arias E. F., Charlot P., Feissel M., Lestrade J.-F., 1995, A&A 303, 604.

Arias E. F., Bouquillon S., 2004, A&A 422, 1105.

Bergeron J. (ed.), 1992, Proceedings of the 21st General Assembly, Transactions of the IAU 21B, 41.

Feissel M., Mignard F., 1998, A&A 331, L33.

Feissel-Vernier M., 2003, A&A 403, 105.

Feissel-Vernier M., 2005, this IERS Technical Note, J. Souchay and M. Feissel-Vernier eds.

Feissel-Vernier M., Ma C., Gontier A.-M., Barache C., 2005, "Analysis strategie issues for the maintenance of the ICRF axes", submitted to A&A.

Fey A. L., Charlot P., 1997, ApJs 111, 95.

Fey A. L., Charlot P., 2000, ApJs 128, 17.

Fey A. L., Ma C., Arias E. F., Charlot P., Feissel-Vernier M., Gontier A.-M., Jacobs C. S., Li J., McMillan D. S., 2004, AJ 127, 3587.

Folkner W. M., Charlot P., Finger M. H., et al., 1994, A&A 287, 279.

Guinot B., 1979, Basic problems in the kinematics of the rotation of the Earth, Proc. IAU Symp. 82, Time and the Earth's Rotation, D. D. McCarthy, J. D. H. Pilkington eds., D. Reidel - Dordrecht, 7.

Gontier A.-M., Le Bail K., Feissel M., 2001, A&A 375, 661.

Gontier A.-M., Ma C., Arias E. F., Eubanks T. M., Fey A. L., Jacobs C. S., Sovers O. J., Archinal B. A., Charlot P., 2002, Adv. Space Res. Vol. 30, N^o2, 185.

Gontier A.-M., Feissel-Vernier M., 2003, IAU XXV, Proc. JD16, (Gaume, McCarthy, Souchay eds.).

Hazard C., Sutton J., Argue A. N., Kenworthy C. N., Morrison L.V., Murray C.A., 1971, Nature Phys. Sci. 233, 89.

IERS, 1999, 1998 IERS Annual Report, Observatoire de Paris, 87.

IERS, 2001, 2000 IERS Annual Report, Verlag des Bundesamts für Kartographie und Geodäsie Frankfurt am Main, IV.2-31.

Kaplan G. H., Josties F. J., Angerhofer P. E., Johnston K. J., Spencer J. H., 1982, AJ 87, 570

Kovalevsky J., Lindegren L., Perryman M. A. C., Hemenway P. D., Johnston K. J., Kislyuk V. S., Lestrade J.-F., Morrison L. V., Platais I., Röser S. et al., 1997, A&A 323, 620.

Lieske J. H., Lederle T., Fricke W., Morando B., 1977, A&A 58, 1.

Ma C., Feissel M. (eds.), 1997, Definition and Realization of the International Celestial Reference System by VLBI Astrometry of Extragalactic Objects, IERS Technical Note No 23, Observatoire de Paris.

Ma C., Arias E. F., Eubanks T. M., Fey A. L., Gontier A.-M., Jacobs C. S., Sovers O. J., Archinal B. A., Charlot P., 1998, AJ 116, 516.

Mathews P. M., Herring T. A., Buffett B. A., 2002, JGRB 107, 1029.

McMillan D. S., Ma C., 1997, GRL 24, 453.

Mignard F., Froeschlé M., 1997, Linking the FK5 to the ICRF, JD12, 23rd IAU General Assembly (August 1997). Highlights in Astronomy.

Niell A. A., 1996, J. Geophys. Res. 101, 3227.

Seidelmann P. K., 1982, 1980 IAU Nutation, Celest. Mech. 27, 79.

Future Realizations of the ICRF: Radio and Optical

A. Fey and R. Gaume

US Naval Observatory (USNO), Washington DC, USA

Abstract. At the XXIII General Assembly of the International Astronomical Union (IAU), held August 1997 in Kyoto, Japan, the International Celestial Reference Frame (ICRF) (Ma et al., 1998) was adopted as the fundamental astronomical celestial reference frame. As a consequence, the definitions of the axes of the celestial reference system are no longer related to the equator or the ecliptic but have been superseded by the defining coordinates of the ICRF. The ICRF is currently defined by the radio positions of 212 extragalactic objects obtained using the technique of Very Long Baseline Interferometry (VLBI) at frequencies of 2.3 and 8.4 GHz over the past 20+ years. A number of astrometric space programs have been proposed over the last few years. Since the astrometric accuracy of these missions is expected to exceed that of the current radio-based ICRF, the success of these space missions may motivate a future redefinition of the ICRF at optical wavelengths. We review the potential for future realizations of the current radio wavelength ICRF, and review the status of various space astrometric missions having the capability to produce high accuracy optical wavelength reference frames.

1 The Future of the ICRF: Radio

1.1 The ICRF-Ext.1

The primary objectives of ICRF-Ext.1 (Gambis, 1998, Fey et al., 2004), the first extension of the ICRF, were to provide positions for extragalactic radio sources observed since the definition of the ICRF (July 1995) and to refine the positions of candidate and other sources using additional observations. A secondary objective was to monitor sources to ascertain whether they continue to be suitable for use in the ICRF. The data added to the ICRF in this extension spanned December 1994 through April 1999 and was obtained from both geodetic and astrometric observing programs. Approximately 0.6 million new observations from 461 sessions were added. There were 59 new sources. The positions and errors for the defining sources were unchanged from the ICRF. Improved positions and errors for the candidate and other sources were estimated and reflect the changes in the data set and the analysis. The 59 new sources were added with ICRF coordinates. As in the original ICRF, the formal errors were inflated applying an additive variance and a scaling factor to provide more realistic errors.

1.2 The ICRF-Ext.2

The primary objective of ICRF-Ext.2 (Fey et al., 2004), the second extension of the ICRF, was to provide positions for extragalactic radio sources observed since the definition of the ICRF (July 1995) and its first extension (April 1999) and to refine the positions of candidate and other sources using additional observations. The data added to the ICRF in this extension spanned May 1999 through May 2002 and was obtained from both geodetic and astrometric observing programs. Approximately 1.2 million new observations from approximately 400 sessions were added. There were 50 new sources. The positions and errors for the defining sources were unchanged from the ICRF. Improved positions and errors for the candidate and other sources were estimated and reflect the changes in the data set and the analysis. The 50 new sources were added with ICRF coordinates. As in the original ICRF, the formal

errors were inflated applying an additive variance and a scaling factor to provide more realistic errors.

1.3 The VLBA Calibrator Surveys

The VLBA Calibrator Survey (VCS1) (Beasley et al., 2002) is the largest high-resolution radio survey ever undertaken and triples the number of sources available to the radio astronomy community for VLBI applications. The VCS1 resulted in a catalog containing milliarcsecond-accurate positions of 1332 extragalactic radio sources distributed over the northern sky. The positions were derived from astrometric analysis of dual-frequency 2.3 and 8.4 GHz VLBA snapshot observations. The VCS1 observations were carried out in 10 24 hr sessions (epochs) spanning the period 1994 August to 1997 August. In total, 1811 radio sources were observed in the VCS1 campaign. The final VCS1 catalog contains positions of 1289 sources from dual-frequency solutions, and 43 source positions derived from an 8.4 GHz only solution. To align the VCS1 positions with the reference frame defined by ICRF-Ext.1, the positions of 315 ICRF-Ext.1 reference sources observed were fixed at their catalog values during the astrometric processing. The formal errors were inflated applying an additive variance and a scaling factor to provide more realistic errors.

The VCS2 (Fomalont et al., 2003) resulted in a catalog containing milliarcsecond-accurate positions of an additional 276 extragalactic radio sources. This survey fills in regions of the sky that were not completely covered by the previous surveys including sources near the Galactic plane, $-45^\circ < \delta < -30^\circ$, and VLA calibrators.

The VCS3 (Petrov et al., 2005) resulted in a catalog containing milliarcsecond-accurate positions of an additional 360 extragalactic radio sources. This survey fills in regions of the sky that were not completely covered by the previous surveys including sources with $\delta > -45^\circ$ where the calibrator density is less than one source within a 4° radius.

1.4 Extending the ICRF to Higher Radio Frequencies

Because the positions in the ICRF now form the underlying basis for all astrometry, subsequent IAU resolutions have encouraged the astrometric community to extend the ICRF to other wavelengths. In 2001, a program was initiated to observe the ICRF at higher radio frequencies using the Very Long Baseline Array (VLBA) telescope of the National Radio Astronomy Observatory (NRAO). A multi-institutional team consisting of scientists from the National Aeronautics and Space Administration (NASA), the U.S. Naval Observatory (USNO), NRAO and Bordeaux Observatory was assembled and VLBA observations at 24 and 43 GHz were started in May 2002 (Jacobs et al., 2002). The long term goals of the program are to 1) develop higher frequency reference frames for improved deep space navigation, 2) extend the VLBA calibrator catalog at 24 and 43 GHz, 3) provide the benefit of the ICRF catalog to new applications at these higher frequencies, and 4) study source structure variation at 24 and 43 GHz in order to improve the astrometric accuracy. Preliminary results of the astrometry have been presented by Jacobs et al. (2002b). Preliminary results of the imaging have been presented by Fey et al. (2002) and Fey et al. (2004b).

1.5 Densification of the ICRF in the Southern Hemisphere

The goals for ICRF observing include: 1) obtaining additional data on astrometric sources for more precise positions, 2) obtaining source position stability information from time series at useful time resolution, 3) densification of defining sources, especially in the southern hemisphere and 4) source structure monitoring. To accomplish these goals, various observing programs are underway. The International VLBI Service (IVS) schedules regular Celestial Reference Frame (CRF) experiments for the specific purpose of maintenance of the ICRF. In recent years, these CRF experiments have concentrated primarily on observing sources in the southern hemisphere. The U.S. Naval Observatory currently has a joint program with the Australia Telescope National Facility (ATNF) for astrometry and imaging of southern hemisphere ICRF sources (Fey et al., 2000). The goals of this USNO/ATNF joint 5-year program are to image all southern hemisphere ICRF sources at least twice for structure monitoring and to search for new astrometric sources for densification. This program has yielded, to date, milli-arcsecond accurate positions for a total of 47 southern hemisphere sources (Fey et al., 2004c, Fey et al., 2004d). The positions for all 47 sources are south of $\delta = -30°$. Images at 8.4 GHz for a total of 69 southern hemisphere extragalactic sources in the ICRF have been presented by Ojha (2004). These imaging observations represent the first large, comprehensive VLBI survey in the southern hemisphere, significantly extending the existing limited VLBI surveys and, along with some well-known objects, contain many sources that have never been imaged at milliarcsecond resolution.

1.6 Densification of the ICRF in the Northern Hemisphere

The ICRF suffers from a deficit of sources with an average of only one object per 8x8 degrees on the sky (Charlot et al., 2000). Additionally, the distribution of the 667 ICRF-Ext.1 sources is found to be largely non-uniform. For example, the distance to the nearest ICRF source for any randomly-chosen sky location is up to 13 degrees in the northern hemisphere and 15 degrees in the southern hemisphere. In many cases, this precludes the use of the ICRF as a catalog of calibrators serving as fiducial points to determine the relative positions of nearby weaker objects (radio stars, pulsars, weak quasars) with the phase-referencing technique, because the separation between the calibrator and the target source should be a few degrees at most in such observations. The non-uniform source distribution also makes it difficult to assess and control any local deformations in the ICRF. Such deformations might be caused by tropospheric propagation effects and the apparent motions of the sources due to variable intrinsic structure.

To address these concerns, an observing program was proposed (Charlot et al, 2000) and is currently underway to densify the ICRF using an approach that will also improve the overall sky distribution of the sources. A secondary objective of the program is to identify new sources of high astrometric value which could potentially be used as defining sources in a future realization of the ICRF. This program concentrates on observations of northern hemisphere sources using the existing standard VLBI networks such as the European VLBI Network (EVN) and the VLBA.

1.7 Connecting the ICRF to Future Optical Realizations Through Stars

Although the present day ICRF is based on the VLBI determined radio positions of extragalactic sources, astrometric positions of galactic and extragalactic sources from future space-based missions at optical wavelengths will likely surpass the accuracy of the current ICRF, and may define the next generation ICRF. However, there will continue to be a need for an accurate link between a radio reference frame and future optical realizations of the ICRF. Of the proposed future astrometric missions, only GAIA will accurately measure astrometric positions of a large number of extragalactic sources. Proposed missions such as SIM will be limited to a small number of only the brightest extragalactic sources. As a result, it is still desirable to obtain the astrometric positions of a number of galactic sources visible in both the radio and the optical to provide a connection between the two frames. Personnel at the U.S. Naval Observatory continue to build upon a program of radio star astrometry begun in the late 1970's using the NRAO Very Large Array (VLA) (Johnston et al., 1985, Johnston et al., 2003). Recent observations using the VLA in its A-configuration in conjunction with the Pie Town VLBA antenna (Boboltz et al., 2003) were used to determine the astrometric positions of 19 radio stars in the ICRF. Average values for the errors in our derived positions for all sources were 13 and 16 mas in $\alpha \cos \delta$ and δ, respectively. U.S. Naval Observatory personnel will continue work on this radio star observing program. Additional VLA observations and observations recorded with the Multi-Element Radio Linked Interferometer Network (MERLIN) are currently being reduced.

2 The Future of the ICRF: Optical

The accuracy level of the current radio wavelength based ICRF significantly surpasses the accuracy of any existing optical astrometric catalog derived from ground based observations. However, the promised astrometric accuracy and target density of future space-based optical astrometric missions will likely motivate a future redefinition of the ICRF at optical wavelengths. Hipparcos was the world's first, and up to this point only, dedicated space astrometry mission. Owing in part to the great success of the Hipparcos mission, a number of follow-up space astrometry missions have been discussed, planned, proposed, funded, scheduled for launch, rescoped, descoped, and in some cases, canceled. These missions include DIVA, AMEX (SMEX), AMEX (MIDEX), FAME, JASMINE, SIM-PlanetQuest, Gaia, and OBSS. It is often difficult to keep track of the current status of the various space astrometry missions due in part to the quickly changing nature of the organizational priorities and funding resources of the major national and international space astronomy agencies. Currently, the list of funded space astrometry missions progressing toward launch has been reduced to two: SIM-PlanetQuest and Gaia. The salient features of these two missions are outlined below:

2.1 SIM PlanetQuest

- **Synopsis:** SIM PlanetQuest is a space-based optical interferometer operating in an earth-trailing orbit.
- **Acronym:** **S**pace **I**nterferometer **M**ission
- **Funding Agency:** NASA
- **Launch:** 2010 (planned). Five year baseline mission, potential ten year extended mission.
- **ConOps:** SIM PlanetQuest is a pointed mission with predefined targets
- **Number of Objects:** about 10,000 stars (1,300 grid stars)
- **Magnitude Range:** brighter than (a limiting magnitude of) about 20^{th}.
- **Astrometric Accuracy:** 4 microarcseconds wide angle, 1 microarcsecond narrow angle
- **Reference Frame:** Should SIM achieve 4 microarcseconds wide angle astrometric accuracy, the resultant grid will form the basis of the most accurate reference frame ever produced, easily exceeding the accuracy of the current radio-based ICRF. SIM will also be capable of observing a fair number of extragalactic sources. Detailed plans are currently being developed with regard to SIM observations of the extragalactic frame sources.
- **Additional Information:** SIM Planetquest is currently in mission development Phase B (Preliminary Design phase).[1]

Fig. 1. Artist's conception of the SIM-PlanetQuest spacecraft

[1] See: http://planetquest.jpl.nasa.gov/SIM

2.2 Gaia

- **Synopsis:** Gaia is a funded space astrometry mission intended to launch in 2010-2012. Operating at L2, Gaia consists of three instruments which provide astrometric, photometric, and spectroscopic data.
- **Funding Agency:** ESA
- **Launch:** before 2012 (planned). Five year operation phase.
- **ConOps:** Continuous scanning. Two optically combined fields of view.
- **Number of Objects:** 10^9
- **Magnitude Range:** 7-20^{th} magnitude
- **Astrometric Accuracy:** 15-20 microarcseconds @ 15^{th} m_v
- **Reference Frame:** The stated accuracy goal of Gaia (Perryman, 2004) is somewhat less than that of SIM-PlanetQuest. What Gaia loses in accuracy, however, is easily overcompensated in the number of mission objects, of order 10^5 more than SIM-PlanetQuest. Gaia will also detect and measure the positions of about 400,000 QSOs, enabling an extremely rigid attachment of the impressively dense Gaia stellar frame to the extragalactic frame.
- **Additional Information:** In addition to astrometry, Gaia will provide 12 band millimagnitide photometry, radial velocity data for brighter stars to an accuracy of a few km/s and spectrophotometry in the visible and near-IR to m_v 17.5.[2]

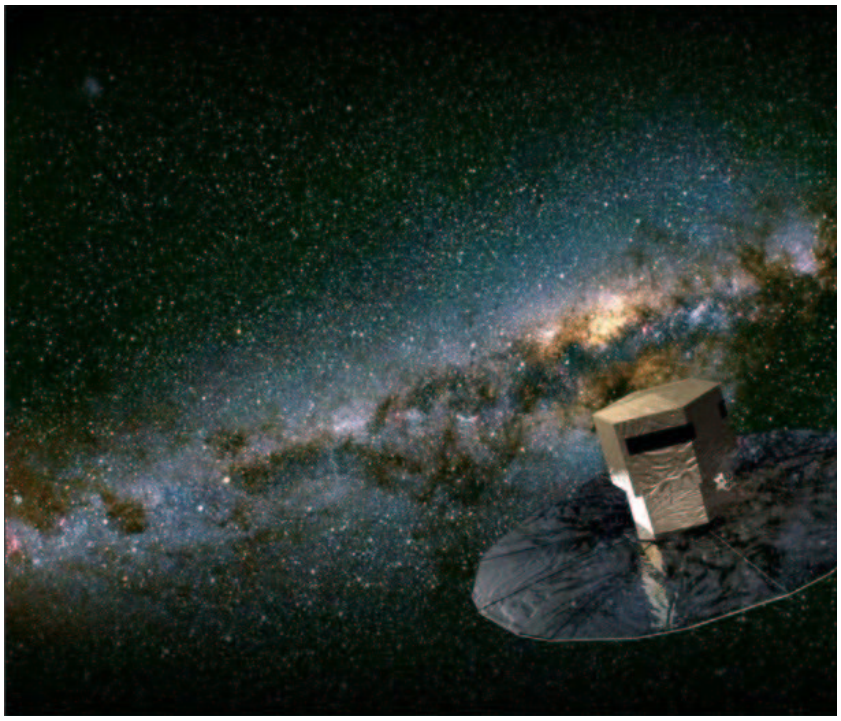

Fig. 2. Artist's conception of the Gaia spacecraft, on orbit

[2]See: http://www.rssd.esa.int/gaia/

References

Beasley, A. J., Gordon, D., Peck, A. B., Petrov, L., MacMillan, D. S., Fomalont, E. & Ma, C. 2002, ApJS, 141, 13

Boboltz, D. A., et al. 2003, AJ, 126, 484

Charlot et al. 2000, in International VLBI Service for Geodesy and Astrometry 2000 General Meeting Proceedings, edited by Nancy R. Vandenberg and Karen D. Baver, NASA/CP-2000-209893

Fey et al. 2000, in International VLBI Service for Geodesy and Astrometry 2000 General Meeting Proceedings, edited by Nancy R. Vandenberg and Karen D. Baver, NASA/CP-2000-209893

Fey, A. L., et al. 2002, AAS, 201, 7611

Fey, A. L., Ma, C., Arias, E. F., Charlot, P., Feissel-Vernier, M., Gontier, A.-M., Jacobs, C. S., Li, J., & MacMillan, D. S. 2004, AJ, 127, 3587

Fey, A. L., et al. 2004b, AAS, 205, 9112

Fey, A. L., et al. 2004c, AJ, 127, 1791

Fey, A. L., et al. 2004d, AJ, 128, 2593

Fomalont, E. B., Petrov, L., MacMillan, D. S., Gordon, D., & Ma, C. 2003, AJ, 126, 2562

Gambis, D., editor, 1998 IERS Annual Report, Observatoire de Paris, p. 87-114.

Jacobs et al. 2002, in International VLBI Service for Geodesy and Astrometry 2002 General Meeting Proceedings, edited by Nancy R. Vandenberg and Karen D. Baver, NASA/CP-2002-210002

Jacobs, C. S., et al. 2002b, AAS, 201, 7610

Johnston et al. 1985, AJ, 90, 1343

Johnston, K., Vegt, C. d., & Gaume, R. 2003, AJ, 125, 3252

Ma, C., et al. 1998, AJ, 116, 516

Ojha, R., et al. 2004, AJ, 127, 3609

Petrov, L., Kovalev, Y. Y., Fomalont, E., & Gordon, D. 2005, AJ, 129, 1163

Perryman, M. 2004, Gaia in 2003, WG-STATUS-013, 23 February 2004

Pulsars: timing reduction at Nançay's radio-telescope and construction of an astrometric catalog

J. Souchay[1] and I. Cognard[2]

[1] *Observatoire de Paris/CNRS UMR8630, 61 Av. de l'Observatoire, 75014, Paris, France*
[2] *CNRS/Laboratoire de Physique et Chimie de l'Environnement, 34 Avenue de la Rercherche Scientifique, 45071 Orléans, France*

Abstract. After summarizing the general physical properties of pulsars ans the basis of pulsar timing reduction we emphasize the possibility to construct an astrometric catalogue of pulsars starting from the pulsar observations at Nançay's radiotelescope, not sensitive to the ephemerides used for the reduction.

1 Introduction

Pulsars, discovered by radioastronomers in 1967, not only offer the opportunity to study fundamental physics in conditions not reachable on Earth, but also can play an essential role in modern astrometry. Indeed, pulsar timing analysis is directly dependent on the way by which the position of the Earth on its orbit is modelized. The arrival times of the pulses are shifted by the Doppler effect due to the relative speed of the Earth on its orbit, whose direction and amplitude vary along the year with respect to the line of sight. Therefore, pulsar timing provides precious information about the location of the ecliptic, i.e. a dynamical frame related to the revolution of the Earth, with respect to a frame related to the pulsars, as galactic objects.

Thus after recalling fundamental principles both related to pulsars physical properties and to pulsar timing reduction, we explain how radio pulses observations of pulsars carried out at Nançay's radiotelescope can participate actively to the construction of both a very accurate catalogue of the coordinates of pulsars, which should give birth to a Pulsar Reference Frame, and to a very accurate positioning of the ecliptic with respect to inertial directions. A set of about 20 pulsars are regularly observed at Nançay, among which PSR1937+21 and PSR1821-21 have been subject to a very intensive campaign for more than 15 years. We show the advantages of all these observations to accomplish the objectives above.

2 Physical characteristics of pulsars

Pulsars are radio-sources which emit radio pulses periodically. During each period, the information received from the pulsar covers a very limited time span. The period P of the pulsar can be defined as the time interval between two consecutive pulses. Presently more than 1500 pulsars have been discovered. Their period covers a range between $1\ ms\ <\ P\ <\ 8\ s$, with a bi-modal distribution (one peak at 4 ms and another one at 0.6 s) and with a slowing down typically at the level of $\dot{P} = 10^{-15} s\ /\ s$. The magnetic fields of the pulsars are the strongest ones observed among galactic sources. All the pulsars are emitting in radio frequencies, but some of them, as the Crab pulsar, are emitting in other frequencies, as in the optical, X, and γ bands.

2.1 Pulsar emission: the physical explanation.

The periodicity of the signal as well as the hypothesis of a rotational object strongly suggests that the emissive part of the beam is very small. The beam accompanying the pulsar in its rotation is crossing the line of sight of the observer located on Earth at each period of the pulsar, as it is a case for the light coming from a lighthgouse. The mechanism of emission of the pulsars is not still well understood, but the theoritical explanation involves a strong magnetic field around a neutron star. A scenario often considered is the following one: the magnetic field creates itself a strong electric field which brings the light particules towards the upper magnetosphere. The electrons are dragged away from the surface along the lines of force, thus creating a vacuum several hundreds of meters high above the surface. The difference of electric potential in this vacuum enables to accelerate the electrons along the lines of magnetic forces, with overwhelming energies leading to emissions of γ rays reaching a few Mev. These γ rays at their turn interact with the magnetic field to create electron-positron pairs. These pairs are themselves re-accelerated to produce new γ rays. This scenario re-produced in an unlimited way is at the origin of the coherent radio emission usually observed.

2.2 Evolution of a pulsar

The emission of the electro-magnetic radiations is responsible of a decreasing of the speed of rotation of the underlying neurtron star, i.e. an increasing of its period of rotation P. The decreasing law has been set already 30 years ago by Manchester and Taylor (1977):

$$\dot{P} = \frac{8\pi R^6 B_0^2 \sin^2 \alpha}{3Ic^3 P} \tag{1}$$

where :

- B_0 is the value of the magnetic field at the surface of the star
- R is the radius of the neutron star
- α is the angle between the axis of rotation and the magnetic axis
- I is the angular momentum of the star
- c is the speed of light
- P is the period of the pulsar

2.3 Magnetic field

Therefore it is possible to evaluate roughly the intensity of the magnetic field B_0 of a pulsar by measuring its period P and the derivative of its period $\dot{P}$ (Manchester et al., 1988; Rawley, 1986). B_0 is generally ranging between 10^4 T and 10^8 T. Such an amplitude is possible if the magnetic flux $\Phi = BR^2$ is conserved during the contraction of the initial star towards a neutron star. For instance, if the Sun radius should contract from $R_\odot = 7 \times 10^5 km$ to $R_\odot = 10 km$, then the intensity of the magnetic field, initially of $B = 10^{-4}$ T should reach 10^6 T. According to the equation (1), the product $P\dot{P}$ gives an estimate of the value of the magnetic field, which currently degenerates in a time scale of 10^6 to 10^7 years.

As the strength of the pulsar magnetic field is decreasing, the period becomes longer and its derivative smaller. As the magnetic field is at

the basis of the emission, it could happen that the field is not strong enough to create γ rays energetic enough to sustain the emission, and thus leads to the extinction of the pulsar.

2.4 Phase and period of a pulsar

The short periods observed for pulsars are explained by the conservation of the angular momentum. For instance, if the Sun, whose the period of rotation (at the equator) is roughly 26 days and the radius approximatively $7 \times 10^5 km$, would contract as a neutron star, then its period of rotation should be 4 ms.

The pulse of a pulsar has a mean feature characteristic for each pulsar which does not depend on time. Profiles can exhibit several peaks. The principal one is called "pulse", whereas the other ones are quoted as "interpulses". Each individual pulse is made itself of a stream of subpulses, themselves consisting in micro pulses, whose intensity and phase can vary. The study of these variations is precious for the understanding of the scenarios of emission mechanisms.

The emission of a pulsar is observed as a periodic sequence of pulses, associated with the periodicity of its rotation. Therefore it is natural to introduce the terminology of *phase* to describe the time along a sequence of pulses.

2.5 Variations of the period

The rotation of a pulsar is slowing down because of the conversion of its rotational energy into electro-magnetic emissions. This loss of energy lengthens the period in a stable way, so that the period can be modelled in the following way:

$$P(T) = P_0 + \dot{P}_0(T - T_0) \tag{2}$$

Where P_0 and $\dot{P}_0$ are the period and its derivative with respect to the time, at a given epoch T_0. Nevertheless, the period can undergo sudden and hasardous changes with large amplitudes. These changes, called *glitches*, recently observed for a millisecond pulsar by the second author (Cognard and Backer, 2004) are explained by a re-equilibrium of the internal forces of the pulsar consecutive to a "starquake", i.e. a quake of the external crust. One of the explanations for these starquakes are the changes provoked by the slowing down of the pulsar: the centrifugal forces leading to the flattening of the neutron star are decreasing and the lack of elasticity of the crust leads to a crunch whose the manifestation is a starquake.

3 A specific class of objects: the millisecond pulsars

The theory according which pulsars are neutron stars enables to consider pulsars with period of the order of 1 *millisecond*. In fact a lot of such objects have been discovered, following the detection of the first candidate, PSR1937+14, in 1982 (Backer et al.,1982). Their period is always larger than 1 *millisecond*, but the existence of sub-millisecond pulsars is presently investigated. Whereas the very small period of rotation of ms pulsars suggests that these objects are very young, the magnetic field calculated starting from the equation (1) as well as the lack of nebula

generally surrounding the pulsar suggest that they are in fact very old objects.

The basic scenario to explain the presence of a millisecond pulsar is the following one: one of the member of a binary star is evolving on the main sequence more rapidly as its companion star. After it explodes as a supernova, it becomes a neutron star and forms a pulsar. Then its magnetic field is gradually decreasing whereas its period increases, thus leading to a complete extinction. At this stage a binary system is made of as star located on the main sequence together with an old and non emitting pulsar. When the star companion leaves the main sequence to reach the phase of expansion, its external material is undergoing an accretion from the dense pulsar. Therefore angular momentum is transferred, which re-accelerates the pulsar. This explains why this last object can be subject to a large angular speed of rotation mixed with a low magnetic field, properties which are generally found for the rapid pulsars observed.

The quantity of material being subject to accretion is limited, because of the pressure exerted by the pulsar radiation (Eddington, 1926) and its magnetic field. The maximum of accretion rate has been set to roughly $10^{-8}\ M\odot/y$. The minimum period under which the rotation of the pulsar is too fast to accrete some material has been given by Van der Heuvel (1984).

$$P = (2.4ms)B^{6/7}R^{15/7}M^{-\frac{5}{7}}\dot{m}^{-frac37} \tag{3}$$

where :

- B is the magnetic field of the pulsar in unit of $10^9 G$
- R is the radius in unit of 10^4 m
- M is the mass in unit of solar mass
- $\dot{m}$ is the accretion rate in units of $M_\odot/y$

Although the scenario above is generally accepted, some millisecond pulsars, as PSR1937+214 do not show the presence of any companion star. For these kinds of objects, alternative theoretical investigations are proposed, which are not in the scope of the present paper.

4 Pulsar timing and the de-dispersion technique at Nancay's radio-telescope

The major part of the informations concerning the physical properties of pulsars are obtained at radio wavelengths, between 10 MHz and 10 GHz. The radio signals emitted are affected by the ionizated interstellar medium according to the frequency of emission. The lower the frequency, the longer the time delay due to the presence of interstellar medium. The consequence is that the pulses are wide instead of showing a thin profile. Therefore, a specific technique consists in a de-dispersion of the signal in order to study the pulses properly. Recently, the N.R.T. (Nançay Radio Telescope) is equipped with a battery of 80 bi-processors and an instrumentation intended to catch the signal and to send it to a calculator for de-dispersion and synchronous integration with the period of rotation of the pulsar. The sensistivity of observations has been noticably improved by this new technical configuration.

5 Pulsar timing, astrometry and dynamics of the solar system

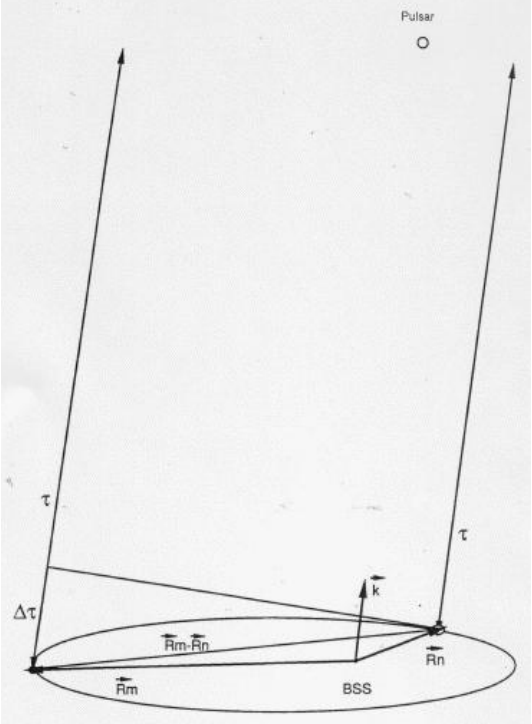

Fig. 1. Geometric configuration for pulsar timing

Analysis of pulsar timing data consists in comparing the observed arrival times of pulses with those obtained from the theory. These calculations involve a physical model describing the trajectory of an electro-magnetic signal from the pulsar (the emitter) to the observer (the receiver). For that purpose it is necessary to include the modeling of various astronomical motions (see Figure 1), as:

• The motion of the pulsar with respect to the Barycentric Reference System (BRS) centered on the barycenter of the solar system (this motion is generally considered as linear and uniform). Indeed, any pulsar is undergoing a motion around the center of the galaxy and consequently a relative motion with respect to the Earth, characterized by a radial velocity (along the line of sight) as well as a proper motion (perpendicular to the line of sight).

• The motion of the Earth barycenter with respect to the BRS, due to its annual revolution around the Sun and to the influence of the planets. Pulsar timing is affected by the position of the Earth with respect to the barycenter of the solar system. Therefore it is influenced by the small perturbations caused by the planets. For instance, the giant planets (Jupiter, Saturn, Uranus and Neptune) cause a displacement of the Sun and of the Earth with respect to the barycenter, this gravitational action having itself an influence on the motion of the Earth.

• The motion of the observer (i.e. the radiotelescope antenna) with respect to the Earth's barycenter, mainly due to the diurnal rotation of the Earth. Moreover the oscillations of the axis if figure of the Earth due to the combined effect of precession and nutation must also be taken into account.

5.1 Basic equation for pulsar timing

Let us call T_n the date of emission of a pulse and t_n the instant when the pulse reaches the observatory. We can write:

$$t_n = T_n + \tau \tag{4}$$

where τ is the interval of time necessary for the pulse to come from the pulsar to the observatory. For the analysis, t_n is measured and compared to the calculation of $T_n + \tau$. In fact $T_n + \tau$ cannot be directly calculated, because the date of emission of the pulse is unknown. Nevertheless, pulses are emitted periodically and as a consequence, if we denote T_m the date of emission of a pulse after T_n, we can write:

$$T_m = T_n + NP \tag{5}$$

P being the period of one pulse and N an integer. If t_m is the date of reception at the observatory of the pulse emitted at T_m, then:

$$t_m - t_n = (T_m + \tau + \delta\tau) - (T_n + \tau) = (T_m - T_n) + \frac{(\vec{R}_m - \vec{R}_n).\vec{k}}{c} \tag{6}$$

where c is the speed of light, $\vec{R}_m$ and $\vec{R}_n$ are the positions of the observatory respectively at t_m and t_n with respect to the barycenter of the solar system, and $\vec{k}$ is a unit vector directed towards the direction of the pulsar (cf. Figure 1).

6 A complete modeling of the arrival time

In order to calculate with a very high precision the propagation time of the pulses between the pulsar and the observer, it is necessary to elaborate a sophisticated modeling including the time delays due to the propagation of an electro magnetic signal through a ionized interstellar medium, as well as relativistic effects on the geometric space time due to the solar gravitational field. This model must be set at a precision of a few *nanoseconds* level in order to match the present accuracy of pulsar timing measurements.

6.1 Relativistic effects: geometric delay and time measurements

When adopting the Minkowski's metric, the trajectories of the photons coming from a pulsar are following the null geodesics corresponding to this metric and their coordinates must satisfy the following equation:

$$\mathrm{d}\tau^2 = (1 - 2\phi)c^2\mathrm{d}t^2 - (1 + 2\gamma\phi)(\mathrm{d}x^2 + \mathrm{d}y^2 + \mathrm{d}z^2) = 0 \tag{7}$$

This can be reduced at the first order to:

$$c\mathrm{d}t = (1 + (1 + \gamma)\phi)[\mathrm{d}x^2 + \mathrm{d}y^2 + \mathrm{d}z^2]^{1/2} \tag{8}$$

This equation gives the interval of time between the emission of the photon at T and its reception at the antenna at t, after covering a distance $(\mathrm{d}x^2 + \mathrm{d}y^2 + \mathrm{d}z^2)^{1/2}$. After replacing the gravitational potential ϕ by its expression, we find:

$$c(t - T) = \mid \vec{R}' - R \mid -(1 + \gamma) \sum_p \frac{GM_p}{c^2} ln\left[\frac{\vec{k}.\vec{r}^p + r^p}{\vec{k}.\vec{R}^p + R^p}\right] \tag{9}$$

where $\vec{R}'$ and R are the positions of the pulsar and of the station with respect to the origin (barycenter of the solar system), $\vec{r}^p$ and $\vec{R}^p$ respectively the positions of the pulsar and of the antenna with respect to the planet p, and $\vec{k}$ the unit vector towards the pulsar.

6.2 Proper time and coordinate-time

A transformation is necessary which enables to make the correspondence between the physical time τ in which the observations are measured, and the coordinate time t from which the equations are given. Relativity introduces a difference between these two time-scales. In order to make the correspondence, we can write the invariance of the element of distance $\mathrm{d}s^2$ in any change of coordinates:

$$\mathrm{d}s^2 = c^2\mathrm{d}\tau^2 = g_{ij}\mathrm{d}x^i\mathrm{d}x^j \tag{10}$$

τ is the proper time of the station, and the x^i are the space-time coodinates. Therefore we obtain the differential equation which gives t as a function of τ:

$$\frac{\mathrm{d}\tau}{\mathrm{d}t} = 1 - \left[U(\vec{r}_h) + \frac{1}{2}(\frac{v}{c})^2\right] \tag{11}$$

where $\vec{r}_h$ is the position of the clock insuring the pulsar timing, v its speed with respect to the barycenter of the solar system, and U is the gravitationnal potential.

6.3 Interstellar dispersion

The model used to express arrival time of the pulses must include the time delay $\mathrm{d}t$ due to the interstellar dispersion given by:

$$\mathrm{d}t = \frac{kDM}{\nu_b^2} \tag{12}$$

where ν is the frequency of the signal and:

$$k = \frac{e^2}{8\pi^2 c\varepsilon_0 m_e} = 4.14879 \times 10^3 cm^3 pc^{-1} MHz \tag{13}$$

with: $e = 1.60219\times10^{-19}C$ (electronic charge), $\varepsilon_0 = 8.85419\times10^{-12}AsV$ and: $m_e = 9.10956 \times 10^{-31}kg$ (electron mass). DM is the dispersion measure in pc/cm^3, corresponding to the integral of the electron density along the line of sight to the pulsar studied. ν_b is the frequency at the barycenter of the solar system, and consequently corresponds to the frequency ν_s of the signal at the station, corrected with the Doppler effect:

$$\nu_b = \frac{\nu_s}{1 + \frac{\vec{k}.\vec{v}}{c}} \tag{14}$$

6.4 Correction due to the curvature of the wavefront

The wavefront which reaches the solar system is not flat but curved. Some time delay $\delta\tau$ is due to this curvature (see Figure 2). The curvature is of course depending on the distance of the pulsar. As an example, for the pulsar PSR1937+214, which is located at a distance $\approx$ 2 kpc, the time delay of the signal is of the order of $1\mu s$, which is quite significant in view of the precision of the observations, which is at the level of the nanosecond.

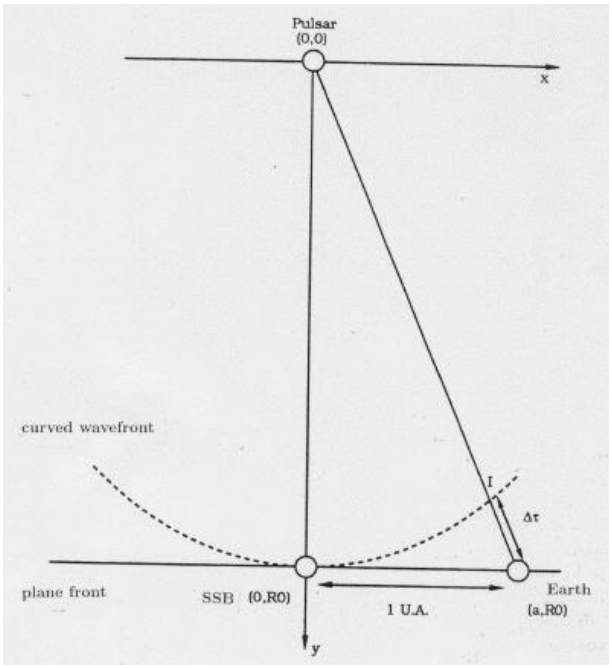

Fig. 2. Curvature of the wave front

6.5 Modeling of the arrival time of the pulse

Finally, after taking into account all the effects above, the initial equation (6) giving the difference of arrival of the pulses is becoming much more complicated, and has the following form:

$$t_n - t_0 = (T_n - T_0) + \frac{V_R}{c}(T_n - T_0) - \left(\frac{\vec{k}_n.\vec{R}_n}{c} - \frac{\vec{k}_0.\vec{R}_0}{c}\right)$$
$$+\left[\frac{r_n^2 - r_0^2 - (\vec{k}_n.\vec{r}_n)^2 + (\vec{k}_0.\vec{r}_0)^2}{2cR_0}\right] - \frac{(\vec{V}_T.\vec{r}_n)}{cR_0}(T_n - T_0) + \frac{V_T^2}{2cR_0}(T_n - T_0)^2$$
$$-\frac{(1+\gamma)}{c^3}\sum_p GM_p ln\left[\frac{\vec{k}\vec{r}_n^p + r_n^p}{\vec{k}.\vec{r}_0^p + r_0^p}\right] + 4.15 \times 10^3 DM(\nu_{b,n}^{-2} - \nu_{b,0}^{-2}) \quad (15)$$

In this equation all the parameters have already been defined previously except V_R and V_T which stand respectively for the radial and the tangential velocities of the pulsar with respect to the barycenter of the solar system. Notice that the first term $(T_n - T_0)$ at the right hand side of the equation is known: indeed the pulsar is emitting a number of pulses which is an integer between the initial date T_0 and the date T_n, as it was shown from (5).

7 Towards a Pulsar reference Frame constructed at Nancay's radiotelescope

Since 1988, the NRT (Nancay Radio Telescope, see Figure 3) has been largely involved in the detection of millisecond pulsars as well as in a huge and regular specific monitoring concerning some of them. High precision mesurements have accumulated since more than 10 years for various studies among which one of the most important were those concerning

the interstellar medium. More particularly the very long and consistent data concerning the two millisecond pulsars PSR1821-24 and 1937+21 to which we added the long Arecibo PSR1855+09 data and the two shorter PSR13-02 and PSR1643-12 data lead us to begin an analysis devoted to the very accurate determination of the reciprocical position of the pulsars, as well as the position of the ecliptic, i.e. the trajectory of the Earth, with respect to them.

7.1 Influence of the ephemerides of the Earth orbital motion

As it is clearly shown by equation (15) the pulse coming from a given pulsar is directly dependent on the model chosen for the position of the Earth, through the intermediary of the vectors $\vec{r}_0$ and $\vec{r}_n$ which represent the radius vectors of the Earth with respect to the BRS (Barycenter Reference System) centered at the barycenter of the solar system. Moreover it is also dependent on the way by which the position of the pulsar is determined through the intermediary of $\vec{k}_0$ and $\vec{k}_n$ which are the unit radius vectors from the barycenter of the solar system to the pulsar at dates T_0 and T_n respectively. Therefore the combination of the adoption of any given ephemerides of the orbital motion of the Earth with respect to the barycenter together with datation of pulses arrival times lead to a specific determination of the celestial coordinates of the pulsar.

Thus we can naturally point out the following questions: what is the uncertainty of the positioning of a given pulsar in the celestial sphere due to the uncertainty of the orbital ephemerides of the Earth used for the calculations ? Even if the coordinates are subject to changes according to the ephemerides, what about the angular distance between two pulsars ? At which extent does it depend of the ephemerides used ?

8 Tests with a small set of pulsars.

In order to give a preliminary answer to the questions above, we have used 3 different ephemerides from the JPL (Jet Propulsion Laboratory), i.e. DE200, DE405 and DE407 (Standish, 1982; Standish, 1990) in order to reduce the pulsar timing observations.

In Table 1 we list our determinations of the coordinates for each pulsar selected above according to the ephemerides used, whereas in table 2 we give our determinations for the angular distances between the pulsars chosen. We can remark that these angular distances are poorly affected by the ephemerides used: the difference according to the ephemerides used does not exceed 3 milliarcseconds (Table 2). On the opposite the differences in the determination of the equatorial coordinates (α, δ) of the pulsars (Table 1) can reach roughly 15 millisarseconds.

These results are a clear support for the possible construction of a celestial reference frame with optimal accuracy based on the intrinsic relative position of pulsars rather than using an intermediate modelling of the position of the ecliptic which should worsen the quality of the astrometric measurements. Such an application has been done with success for the construction of the ICRF (International Celestial reference Frame) starting from the relative positions of quasars (IERS, 2001).

Table 1. List of the pulsars used for the astrometric analysis, together with their equatorial coordinates for J2000.0 obtained from 3 different ephemerides for the orbital motion of the Earth.

Name of pulsar	α DE200	δ DE200	$\Delta\alpha$ DE405 - DE200	$\Delta\alpha$ DE407 - DE200	$\Delta\delta$ DE405 - DE200	$\Delta\delta$ DE407 - DE200
	h mn s	° ' "	10^{-3} "	10^{-3} "	10^{-3} "	10^{-3} "
PSR1821-24	18 24 32.007721 ± 0.020	- 24 52 10.803114 ± 5.44	7.470 ± 0.42	7.095 ± 0.42	-2.772 ± 7.61	- 4.702 ± 7.61
PSR1937+21	19 39 38.560135 ± 0.002	+ 21 34 59.139705 ± 0.04	16.650 ± 0.04	14.205 ± 0.04	-6.069 ± 0.06	- 6.577 ± 0.06
PSR1855+09	18 57 36.393499 ± 0.014	+ 09 43 17.323676 ± 0.40	12.660 ± 0.29	10.860 ± 0.29	-4.144 ± 0.56	- 5.096 ± 0.56
PSR0613-02	06 13 43.972992 ± 0.024	- 02 00 47.110967 ± 0.72	14.025 ± 0.49	12.480 ± 0.49	-1.386 ± 1.00	- 2.781 ± 1.00
PSR1643-12	16 43 38.157313 ± 0.024	- 12 24 58.711054 ± 1.98	10.980 ± 0.50	9.855 ± 0.50	-3.611 ± 2.78	- 1.531 ± 2.78

Table 2. Determination of the angular distances between the pulsars listed in Table 1, with respect to the ephemerides used for the orbital motion of the Earth.

Pulsar	Pulsar	arc inter-pulsar (degree)	Δ arc DE405-DE200 (mas)	Δ arc DE407-DE200 (mas)
1	2	49.90547948	0.2005	0.7722
1	3	35.51839847	-0.2010	0.4275
1	4	152.98996546	-0.7606	-1.4015
1	5	26.87642586	0.0214	0.3235
2	3	15.57641855	1.1884	1.1476
2	4	151.36653030	1.0796	1.0650
2	5	54.96006368	-1.2473	-1.2708
3	4	166.64788112	2.6505	2.5836
3	5	39.963920275	-2.7859	-2.7557
4	5	153.380677482	0.0979	0.1354

References

Backer, D. C., Kulkarni, S. R., Heiles C., Davis, M. M., Goss W. M., 1982,*Nature* 300, 615

Cognard, I., Backer, D. C., 2004, *ApJ* 612, L215

Eddington, A. S., 1926, *The Internal Constitution of stars*, Cambridge Univ. Press

Fairhead, L., 1989, *PhD Thesis*, Observatoire de Paris

IERS Annual Report, 2001 (BKG Editions, Frankfurt, 2002)

Manchester, R. N., Taylor, J. H., 1977, *Pulsars*, W. H. Freeman and Company

Rawley, L. A., *PhD Thesis*, Princeton

Rawley, L. A., Taylor, J. H., Davis M. M., Allan D. W. 1988, *Ap.J.* 326, 947

Standish, E. M., 1982 *Astronomy and Astrophysics* 114, 297

Standish, E. M., 1990 *Astronomy and Astrophysics* 233, 252

Source Structure

D. A. Boboltz

U.S. Naval Observatory (USNO), Washington D.C., USA

Abstract. The International Celestial Reference Frame (ICRF) as realized by Very Long Baseline Interferometry (VLBI) (Ma, 1998), depends on the assumed point-like nature of the extragalactic radio sources whose positions define the frame. It has long been known (Charlot, 1990; Fey et al., 1996) that these sources exhibit spatially extended structure on the milliarcsecond scales achievable with VLBI. This intrinsic structure can be variable in both time and frequency, and it will set limits on the ultimate accuracy of the source positions determined from the astrometric/geodetic VLBI. We describe efforts underway to determine the structure of individual ICRF sources, quantify the effect of measured source structure with regard to the resultant accuracy of source positions, and mitigate the negative effects of source structure on the accuracy of the ICRF source positions. We also describe an active effort to extend the ICRF to higher radio frequencies, where the effect of source structure is less pronounced.

1 Introduction

Currently, the accuracy of VLBI astrometry/geodesy is limited by instrumental phase stability and the effects of the Earth's troposphere on the observations. Contributions of the VLBI delay observables due to intrinsic source structure can be as high as tens to even hundreds of picoseconds. The current level of accuracy for ICRF source positions is approximately 250 microarcseconds ($\sim$ 20 ps delay on a typical baseline) (Ma, 1998). With improvements in tropospheric modeling and VLBI instrumentation, source structure may become a primary contributor to the overall "error budget" in future ICRF realizations based on VLBI observations.

There are two ways in which source structure can be dealt with in astrometric/geodetic VLBI. One can either attempt to filter-out sources with the worst structure, at a cost of perhaps losing a significant fraction of the sources in the reference frame, or one can use models of the effects based on the source maps to attempt to correct the VLBI data. The former approach is addressed in a recent article (Feissel-Vernier, 2003) by Feissel-Vernier in which a suitable set of astrometrically stable sources was identified based on the analysis of source position time-series. Source filtering is also the basis for the development of the source "structure index" by Fey and Charlot (1997, 2000). The second approach, in which corrections for structure effects are determined and applied to the VLBI data, has been tested on a massive scale by Sovers et al. (2002). In the following sections, developments in source imaging, modeling source structure effects and application to VLBI observables, and the possible reduction of source structure effects by moving the ICRF to higher radio frequencies are all discussed.

2 Imaging Extragalactic Source Structure

Prior to any modeling of source structure or application of structure corrections to VLBI data, a complete database of VLBI images is required from which to compute the corrections. Ideally, one would like to make images from the astrometric/geodetic VLBI observations themselves, however, these data are not optimized for source imaging. Often there is a limited amount of data from a less than desirable network of

stations making the production of reliable images of the ICRF sources difficult. Fortunately, there are a number of ongoing programs designed specifically for the purpose of imaging extragalactic sources.

The largest effort to image ICRF sources is a series of experiments using the Very Long Baseline Array (VLBA) in conjunction with up to 10 additional geodetic antennas. These observations, with the designation RDV, are part of a collaborative effort between the U.S. Naval Observatory (USNO), the NASA Goddard Space Flight Center (GSFC) and the National Radio Astronomy Observatory (NRAO). During each 24-hour RDV session, approximately 80 ICRF sources are observed using dual S/X-band (2.3/8.4 GHz) frequencies. S- and X-band images are produced from these observations and made available on-line from the Radio Reference Frame Images Database (RRFID) at ([1]). The RRFID currently contains 3125 images of 452 ICRF sources. Images of selected sources have also been made available through a series of articles (Fey et al., 1996; Fey and Charlot, 1997, 2000). In addition to being a valuable resource for source imaging, the RDV experiments now provide roughly 20% of the entire database of geodetic/astrometric VLBI observations.

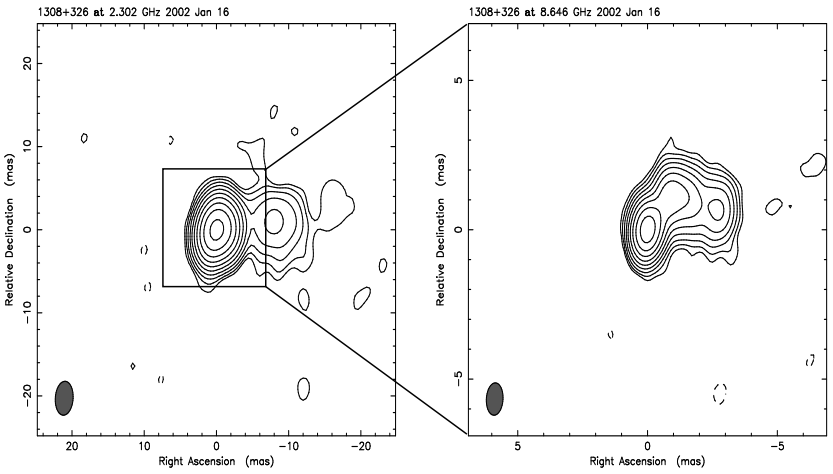

Fig. 1. VLBI radio frequency images at 2.3 GHz (left panel) and 8.4 GHz (right panel) of the ICRF source 1308+326 at epoch 2002 January 16 (RDV-31) taken from the USNO Radio Reference Frame Image Database (RRFID).

The VLBA Calibrator Survey (VCS1) (Beasley et al., 2002) is the largest high-resolution radio survey ever undertaken and triples the number of sources available to the radio astronomy community for VLBI applications. The VCS1 resulted in a catalog containing milliarcsecond-accurate positions of 1332 extragalactic radio sources distributed over the northern sky and in a majority of cases, images of the sources are also available. The images and u-v radius plots for the VCS1 can be accessed on-line via a graphical search engine at ([2]). Additional observations for the Second VLBA Calibrator Survey (VCS2) (Fomalont et al., 2003) were undertaken to fill holes in the sky which were not completely covered by VCS1 and to image ICRF sources with somewhat limited structural information. VCS2 data covers an additional 276 sources including sources near the Galactic plane at declinations $-45° < \delta < -30°$.

[1] http://www.usno.navy.mil/RRFID/
[2] http://magnolia.nrao.edu/vlba_calib/

In an effort to investigate the structure of ICRF sources in the southern hemisphere, the USNO has undertaken a joint program of observations with the Australia Telescope National Facility (ATNF) using the southern hemisphere geodetic stations and ATNF's Long Baseline Array (LBA) (Fey et al., 2000). The goals of this USNO/ATNF program are to image the source structure of all southern hemisphere ICRF sources at least twice and to search for new astrometric sources in order to densify the ICRF in the southern hemisphere. Initial astrometric and imaging results from this joint effort have recently been published in a series of journal articles (Ojha et al., 2004; Fey et al., 2004a, 2004b).

3 Modeling Source Structure

Having a database of reliable VLBI images in hand, one can begin the task of source structure modeling. In VLBI observations for astrometry/geodesy, the primary observable is the delay, τ, which is equal to the derivative of the total phase, ϕ_t, with respect to the observing frequency, ω. For a theoretical point source, the total phase is simply equal to the geometric phase, ϕ_g, which is a function of the interferometer baseline vector, $\mathbf{b}$, and the reference direction vector to the source, $\mathbf{s}_0$. For a source with an extended brightness distribution an additional structure phase, ϕ_s, is introduced, and the delay observable can be written (Charlot, 2002) as

$$\tau = \frac{\partial \phi_g}{\partial \omega} + \frac{\partial \phi_s}{\partial \omega} = -\frac{1}{c}\mathbf{b} \cdot \mathbf{s_0} + \tau_s. \quad (5)$$

The first term is the derivative of the geometric phase with respect to frequency or the geometric delay. The second term, τ_s, is the delay induced by the extended source brightness distribution, a quantity which we would like to remove from the data. In addition to the effect on the delay, source structure has an effect on the total phase as a function of time or the phase-delay rate (Charlot, 2002). The effects of source structure on this phase-delay rate should also be accounted for in a complete analysis of VLBI observations for astrometry and geodesy, but will not be discussed further here. For a comprehensive discussion of the theoretical modeling of the effects of source structure on astrometric/geodetic VLBI observations see (Charlot, 1990).

In theory, structure corrections due to the added delay can be determined from the VLBI maps and applied to the delay observables. In practice, τ_s is computed from a linear fit to the source structure phases determined for each frequency channel in the bandwidth synthesis observations (Charlot, 2002). Because astrometric VLBI data typically consist of dual-frequency S/X-band observations, the structure corrections must be determined for each band individually and applied with weights consistent with the weighting of the S/X-band observables which go into the calculation of the dual-frequency delay. These weighting factors are 1.08 at X band and 0.08 at S band (Fey and Charlot, 1997), thus the S-band data and the structure corrections are down-weighted by a factor of $\sim$1/13 relative to the X-band values.

There are two practical difficulties in the determination and application of the delay structure corrections. The first is the choice of the fiducial reference point $\mathbf{s}_0$ for the source brightness distribution in the maps. The computation of the source structure corrections relies on the choice of this point which also defines the absolute position of the source in the

reference frame. For a typical core-jet VLBI source, one would ideally prefer a dominant compact core with little or no morphological changes in the brightness distribution over time. Since VLBI sources are often not ideal, both the choice of the image reference point and source registration from one epoch to the next are made more difficult. Different methods for determining this reference point over multiple epochs were tested in Charlot (2002) for the ICRF source 2200+420. The results show that the application of source structure corrections based on an incorrect choice of reference point can actually increase the scatter in the source position over time relative to the scatter in the position with no corrections for structure. The best results were obtained in Charlot (2002) by manually choosing the reference position on a per epoch basis, a task which can be tedious for a large number of sources with a long time series of observations.

A second difficulty in the determination of the dual-frequency source structure corrections is the registration of the S- and X-band maps relative to one another. The S- and X- band data recorded simultaneously often produce significantly different structures which are complicated by the factor of ∼4 difference in resolution between the two frequencies. The errors introduced by improper registration are somewhat mitigated by the fact that the computed S-band corrections are down-weighted by the factor of ∼1/13 in the combined dual-frequency source structure corrections.

Despite these difficulties in properly registering the VLBI maps, source structure modeling has been tested for a large multi-epoch S/X-band data set in Sovers et al. (2002). Ten epochs of VLBI data spanning ∼1.5 years comprised of over 200,000 S/X-band observations (delay + delay-rate) of 160 extragalactic radio sources were used in the study. A database of 800 pairs (S- and X-band) of maps from the Radio Reference Frame Image Database (Fey et al., 2002) were used to derived structure corrections from the image CLEAN components. The study found that modeling the delay induced by source structure improved the overall VLBI model by ∼8 ps in quadrature, a significant portion of the ∼30 ps overall weighted root-mean-square delay residuals. For individual sources, improvement in the scatter of the delay residuals over time ranged from 6.5 to 16.8 ps for sources with structure indices ranging from 1 to 4 (see below) (Sovers et al., 2002).

4 Source Structure Selection and Filtering

The modeling and application of source structure corrections is both labor and computationally intensive in practice. However, even if one cannot directly apply structure corrections to VLBI data, source structure can still be a useful indicator of source quality for application to the ICRF. There are two methods by which the sources with the most compatible structure for astrometry/geodesy may be selected. First, one can categorize source structure based on the images of the sources and the structure corrections computed from these images. Second, one can examine the statistical impact of source structure on the astrometric stability of the source position time series. Both of these techniques have been used to filter undesirable sources from astrometric/geodetic observations as discussed below.

Fey and Charlot (1997, 2000) developed the first indicator of astrometric source quality based on structure corrections derived from source images.

They termed this indicator the source "structure index". The structure index is the median value $\tau_{\rm median}$ of the structure delay corrections computed from the VLBI source maps. These structure delay corrections are determined for pixels in a 512×512, u-v grid for all baselines less than the diameter of the Earth (Fey and Charlot, 1997). Fey and Charlot categorize ICRF sources according to structure index as follows:

$$\text{Structure Index} = \begin{cases} 1, & if\ 0\ ps \leq \tau_{\rm median} < 3ps; \\ 2, & if\ 3\ ps \leq \tau_{\rm median} < 10ps; \\ 3, & if\ 10\ ps \leq \tau_{\rm median} < 30ps; \\ 4, & if\ 30\ ps \leq \tau_{\rm median} < \infty. \end{cases} \quad (6)$$

Thus the best astrometric sources receive a structure index of 1 while the worst sources have a value of 4. Figure 2 shows the distribution of S- and X-band structure indices for the 388 ICRF sources observed in Fey and Charlot (2000). At X-band, roughly 60% of the ICRF sources fall into the compact category (structure index of 1 or 2) while 40% of the sources are either marginal (sturcture index of 3) or unacceptable (structure index of 4) for VLBI astrometry. At S-band, approximately 90% of the sources have structure indices of 1 or 2 indicating both compact structure and the fact that the S-band source structure corrections are down-weighted by a factor of $\sim$1/13.

Based on the source structure index, correlations between the observed radio structure and the astrometric position accuracy and stability of the sources have been found (Fey and Charlot, 2000). These correlations indicate that the more extended sources have larger position uncertainties and are less positionally stable than the more compact sources. The structure index therefore provides a reliable tool by which sources for use in astrometric/geodetic VLBI may be selected or eliminated. This

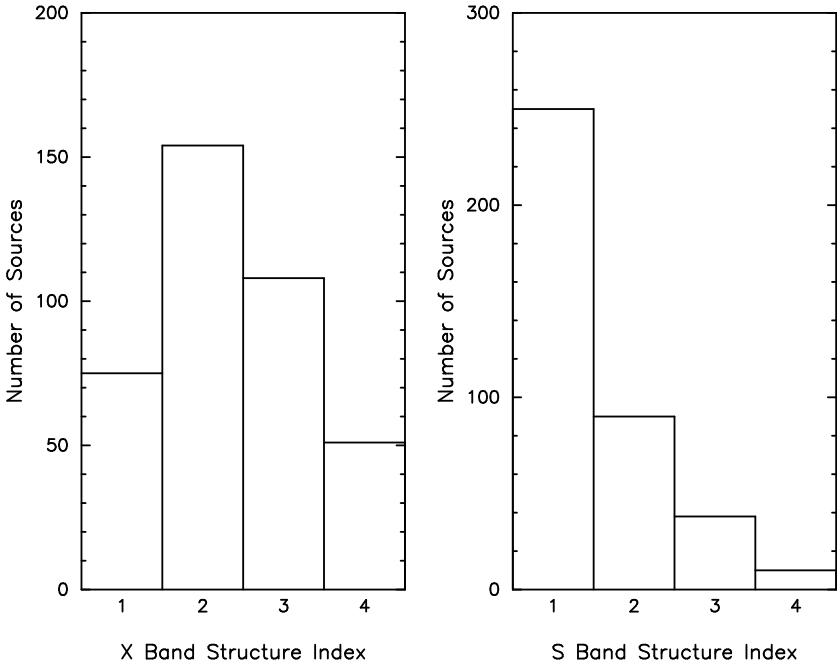

Fig. 2. Distribution of source structure indices for sources at 2.3 GHz (right panel) and 8.4 GHz (left panel) for the 388 sources in Fey and Charlot (2000).

structure index filter requires much less effort (indices can be computed from a single epoch and updated periodically) than would be required to apply actual structure corrections to the VLBI observables in time. The structure index values for many northern hemisphere ICRF sources can be obtained from ([3]).

The second approach to source filtering is discussed in a recent article by Feissel-Vernier (2003), in which various statistical tests applied to the VLBI source position time series were utilized. Specifically, the standard deviation, the Allan standard deviation, the least-squares derived linear drift, and the normalized linear drift were determined for the time series of source positions in right ascension and declination. These quantities were then used alone and in various combinations to select/exclude sources for use in determining reference frames. Testing was performed by computing a set of yearly reference frames based on the sources selected by the various schemes, determining the standard deviation characterizing the scatter of the rotation angles about the axes of the frames, and comparing these standard deviations to that computed for the 212 ICRF defining sources. In all cases, the selection schemes resulted in improved stability of the yearly reference frames over the current ICRF (Feissel-Vernier, 2003). Feissel-Vernier recommends the set of selected sources be considered for use in future realizations of the ICRF and for the scheduling of future VLBI observations.

5 Extension of the ICRF to Higher Frequencies

Prompted by the desire to move the NASA Deep Space Network (DSN) toward Ka-band (32 GHz) frequencies, a pilot program to investigate the possibility of extending the ICRF to higher frequencies, namely K-band (24 GHz) and Q-band (43 GHz). VLBA observations at K- and Q-band were initiated by a collaboration of institutions including NASA/JPL, GSFC, USNO, NRAO, and Bordeaux Observatory in May 2002. There are a number of motivations for this joint program of astrometric observations see Jacobs et al. (2002) for a full description. One of the goals of the program is to study source structure at higher frequencies. The expectation is that at higher frequencies the sources should appear more compact since the extended emission in AGN is usually steep spectrum, and the centroid of the observed emission should be closer to the AGN central engine. The more point-like source structure should enable more precise astrometry than traditional S/X-band VLBI.

Images and u-v radius plots from the program are now available on the RRFID web site. Thus far, 783 images of 231 extragalactic sources have been produced. Figure 3 shows two example maps for the ICRF source 1308+326 at 24 and 43 GHz. Initial imaging results (Fey et al., 2003) show that sources are more spatially compact at K-band than at the current standard X-band. The distribution of structure indices calculated from the first epoch of 24/43 GHz images (Figure 4) shows a shift toward lower values as the frequency of observation increases. Over 95% of the sources observed have structure indices of 1 or 2 at K- and Q-band. For 28 overlapping sources observed at X-band at a similar epoch, only 86% of the sources have structure indices of 1 or 2. For all ICRF sources measured at X-band, this number drops to 60% as discussed above. These preliminary source structure results are consistent with the standard theory of compact extragalactic radio sources and suggest

[3] http://www.observ.u-bordeaux.fr/public/radio/PCharlot/structure.html

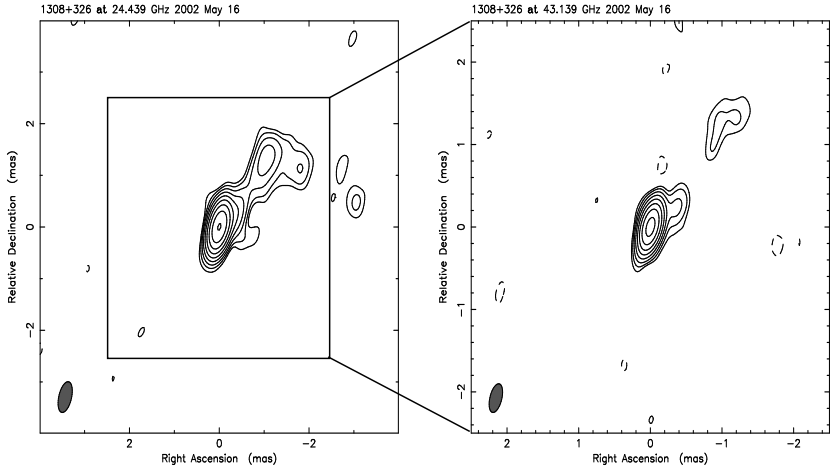

Fig. 3. VLBI radio frequency images at 24 GHz (left panel) and 43 GHz (right panel) of the ICRF source 1308+326 at epoch 2002 May 16 (BR079A) taken from the USNO Radio Reference Frame Image Database(RRFID).

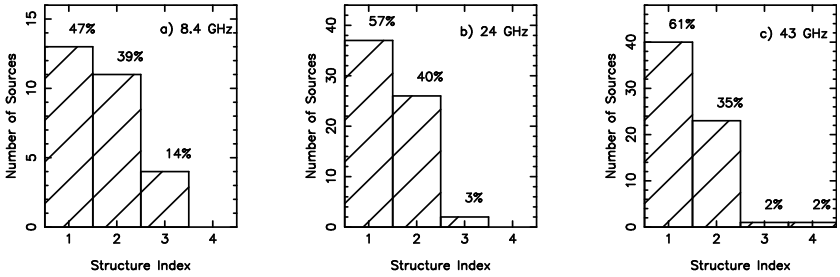

Fig. 4. Distribution of source structure indices for sources at a) 8.4 GHz, b) 24 GHz, and c) 43 GHz. A total of 65 sources were observed at 24 and 43 GHz on 2002 May 15. Also shown are the values for the 28 overlap sources observed at 8.4 GHz on 2002 Jan 16.

that reference frames defined at these higher radio frequencies will be less susceptible to the effects of intrinsic source structure than the current ICRF.

References

Beasley, A. J., Gordon, D., Peck, A. B., Petrov, L., MacMillan, D. S., Fomalont, E. B., & Ma, C. 2002, ApJS, 141, 13

Charlot, P. 1990, ApJ, 99, 1309

Charlot, P. 2002, International VLBI Service for Geodesy and Astrometry, 2002 General Meeting Proceedings, eds. N. R. Vandenberg and K. D. Baver, NASA/CP-2002-210002, 233

Feissel-Vernier, M. 2003, A&A, 403, 105

Fey, A. L., Clegg, A. W., & Fomalont, E. B. 1996, ApJS, 105, 299

Fey, A. L. & Charlot, P. 1997, ApJS, 111, 95

Fey, A. L. & Charlot, P. 2000, ApJS, 128, 17

Fey, A. L., et al. 2000, International VLBI Service for Geodesy and Astrometry, 2000 General Meeting Proceedings, eds. N. R. Vandenberg and K. D. Baver, NASA/CP-2000-209893

Fey, A. L., Boboltz, D. A., Gaume, R. A., & Kingham, K. A., 2002, International VLBI Service for Geodesy and Astrometry, 2002 Annual Report, eds. N. R. Vandenberg and K. D. Baver, NASA/TP-2003-211619, 287

Fey, A. L., et al. 2003, Future Directions in High Resolution Astronomy: A Celebration of the 10th Anniversary of the VLBA, ASP Conference Series, eds. J. D. Romney and M. J. Reid, in press

Fey, A. L., et al. 2004a, AJ, 127, 1791

Fey, A. L., Ojha, R., Reynolds, J. E., Ellingsen, S. P., McCulloch, P. M., Jauncey, D. L., & Johnston, K. J. 2004b, AJ, 128, 2593

Fomalont, E. B., Petrov, L., MacMillan, D. S., Gordon, D., & Ma, C. 2003, AJ, 126, 2562

Jacobs, C. S., et al. 2002, International VLBI Service for Geodesy and Astrometry, 2002 General Meeting Proceedings, eds. N. R. Vandenberg and K. D. Baver, NASA/CP-2002-210002, 350

Ma, C. et al. 1998, AJ, 116, 516

Ojha, R., et al. 2004, AJ, 127, 3609

Sovers, O. J., Charlot, P., Fey, A. L., & Gordon, D. 2002, International VLBI Service for Geodesy and Astrometry, 2002 General Meeting Proceedings, eds. N. R. Vandenberg and K. D. Baver, NASA/CP-2002-210002,243

Assessing astrometric quality: stability of the VLBI-derived extragalactic celestial frame

M. Feissel-Vernier

Observatoire de Paris/CNRS UMR8630, 61 Av. de l'Observatoire, 75014, Paris, France
and Institut Géographique National/LAREG

Abstract. This chapter presents background information of a paper (Feissel-Vernier, 2003) that investigated several stable source selection processes and proposed a list of 199 stable sources that could be used for a future improvement of the ICRF. Their performance in maintening the direction of the ICRF axes ($\pm$ 6 μas) is better by a factor of four or five than that of the current 212 ICRF defining sources.

1 Introduction

The wealth of observational data on extragalactic radio sources accumulated by astro-geodetic VLBI in the last two and a half decades makes possible detailed analyses of the time evolution of the radio sources positions. Time series statistics can be used to describe the spectral characteristics of these time evolutions, and to discriminate both stable and unstable sources. Under a deterministic point of view, systematic investigation of apparent linear drifts is also possible. The impact of source motion or instability on the global stability of the celestial reference frame that they materialize can be evaluated.

This study is based on the series of individual source coordinates derived by A. Fey (2002) over 1979-2002.

Section 2 describes the time and space structure of observational data and gives examples of observed time variation of the source coordinates. Section 3 describes the selection scheme applied to detect on the one hand sources that are stable and on the other hand those that are drifting or unstable. The relationship of the resulting set of stable sources with the current ICRF source categories (defining, candidate, other) and the ICRF structure index is examined in section 4. The respective performances of set of sources in maintening the celestial reference frame axes are evaluated in section 5.

2 The observations

The observations consist of time series derived from a set of three analyses of the existing VLBI observing sessions up to May 2002. Each analysis results in time series of coordinates per session for one third of the sources ("arc" sources), the coordinates of the other sources being treated as "global", i.e. they are assumed to stay fixed in time and are estimated globally. Each analysis includes a no-net-rotation (NNR) condition with respect to the ICRF based on the ICRF defining sources.

To avoid inconsistencies that are due to the NNR condition realization in the three analyses, and that can reach the level of 50 microarcseconds (μas), we consider here for each source the time series of its coordinate differences with their global weighted mean.

The frequency bands used in astrometric and geodetic VLBI are the S and X bands, with respective frequencies 2.3 and 8.4 Ghz and wavelengths 13 and 3.6 cm. Figure 1 shows the sky distribution of the most

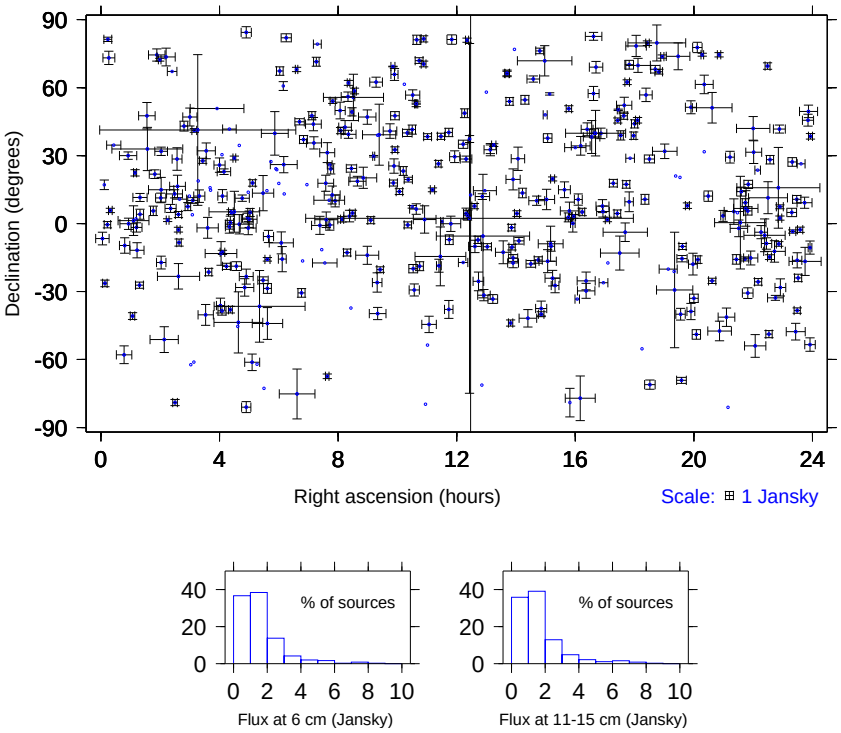

Fig. 1. The most observed ICRF radio sources. Total flux at wavelengths 6 cm (vertical bars), and 11 cm or 15 cm (horizontal bars) is shown when available. Fluxes histograms are shown for sources fainter than 10 Jansky.

observed ICRF sources. The mean flux at 11 or 15 cm, and 6 cm is shown when available at the IERS Celestial Reference System Product Center (IERS 2002).

Figure 2 shows the sky distribution of the most observed sources for one-year time spans centered at the beginning of each year. After a steady extension in the first decade of operation, the sky coverage stabilized during the second one.

Over 700 sources were observed since 1979. The sources observation rates are extremely uneven, as illustrated by the histogram of figure 3. A few sources are observed in nearly all sessions, e.g. 0552+398 has over 205000 observations in over 3000 sessions, while a large number of other sources were observed in less than 20 sessions.

The observed objects are selected by the IVS among quasars and galaxy nuclei that are compact when observed in the X-band and S-band with baseline lengths extending to several thousands kilometers. However, when observed at the current level of precision (a fraction of milliarcsecond, mas), no object is really pointlike. If the source structure is extended or not circular, its apparent direction may change as a function of the length and orientation of the baselines. Most of the known activity of quasars takes the form of jets, i.e., aligned emissive structures that cause an apparent motion of the observed phase center. While the background source structure is assumed to stay fixed, oscillations may exist in the observed direction, as well as apparent drifts that are unlikely to continue indefinitely, but with time characteristics that are not well known. In principle it is possible to accurately correct this effect if repeated maps are available. However, the source structure correction

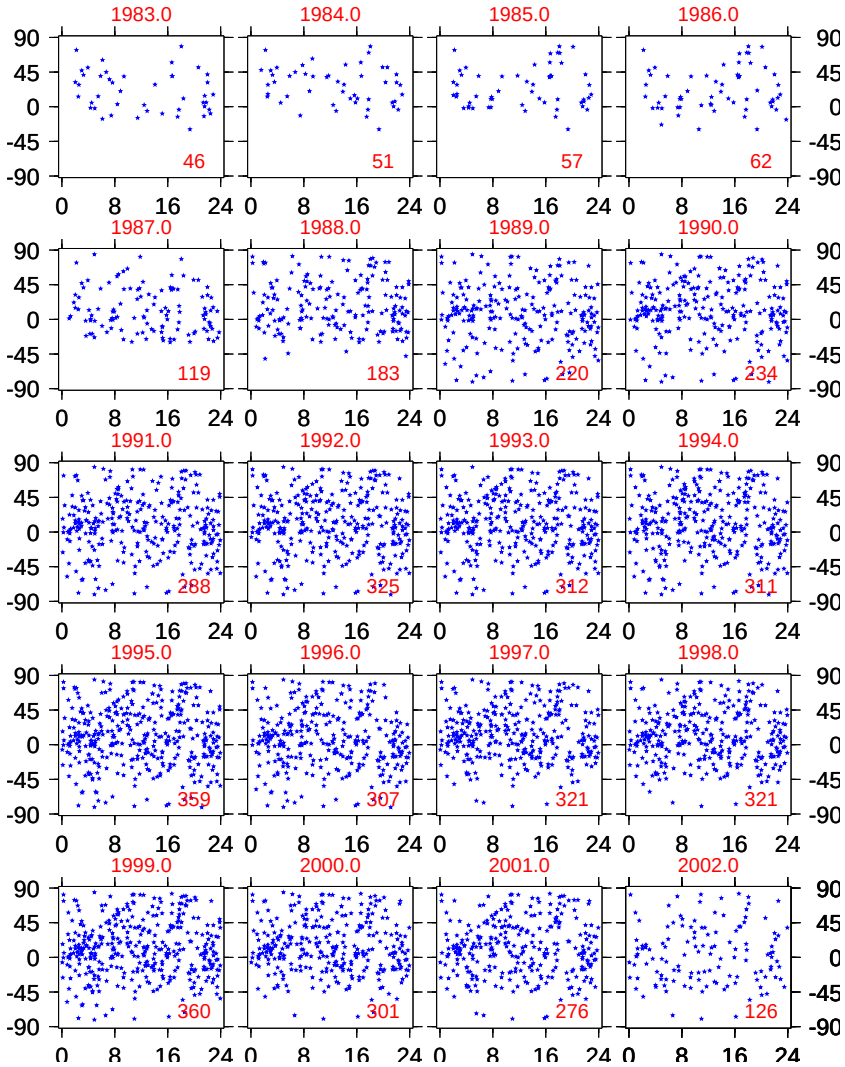

Fig. 2. Year by year sky distribution of the most observed radio sources. The yearly numbers of sources are given in the individual frames.

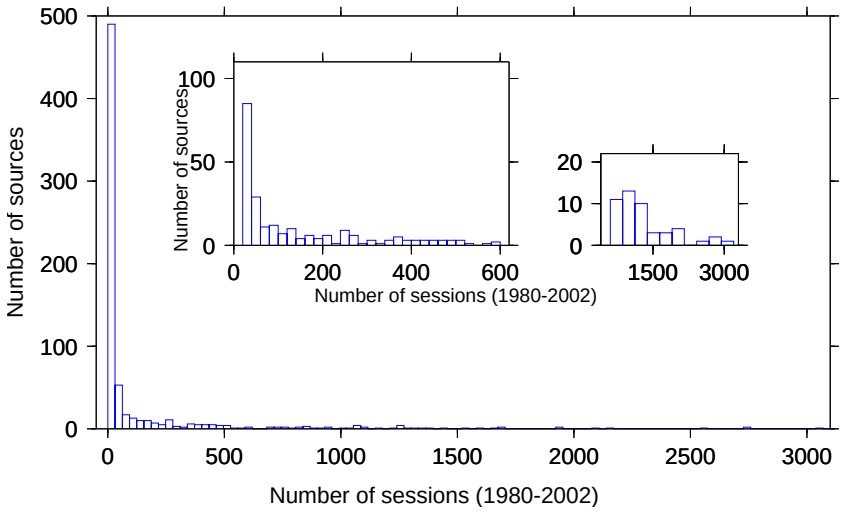

Fig. 3. Observation rates. Number of sessions in which a given source is observed. The leftmost abscissae limit in the right insert is equal

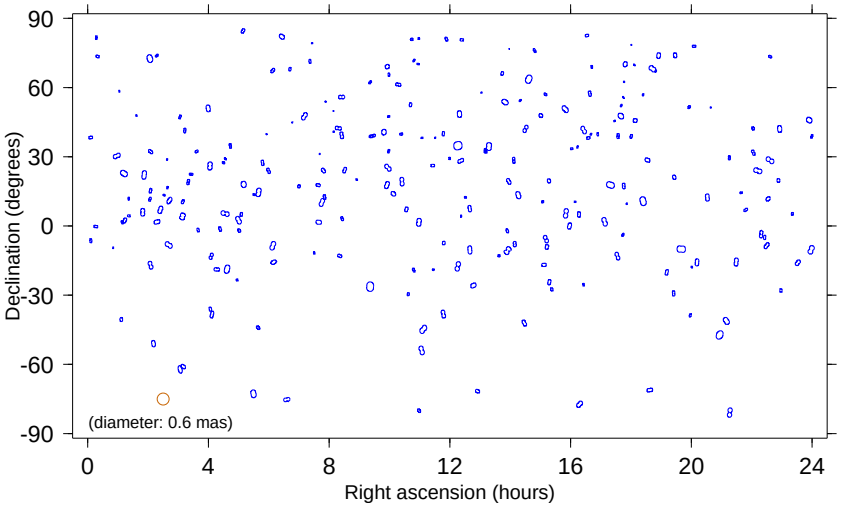

Fig. 4. 245 well observed sources (1989.5-2002.4) with standard deviations of yearly positions smaller than 0.35 mas. Envelops of the standard deviation of the yearly average coordinates in local equatorial frames $(\alpha \cos\delta,\ \delta)$.

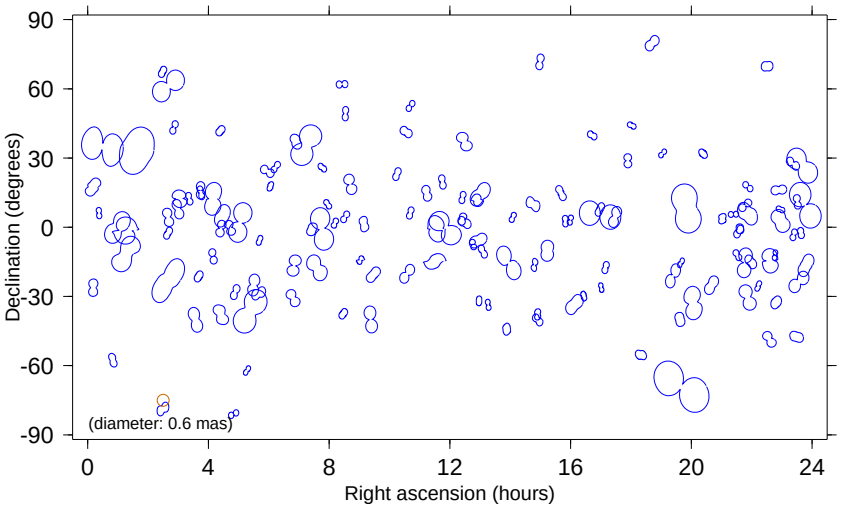

Fig. 5. 143 well observed sources (1989.5-2002.4) with standard deviations of yearly positions larger than 0.35 mas. Envelops of the standard deviation of the yearly average coordinates in local equatorial frames $(\alpha \cos\delta,\ \delta)$.

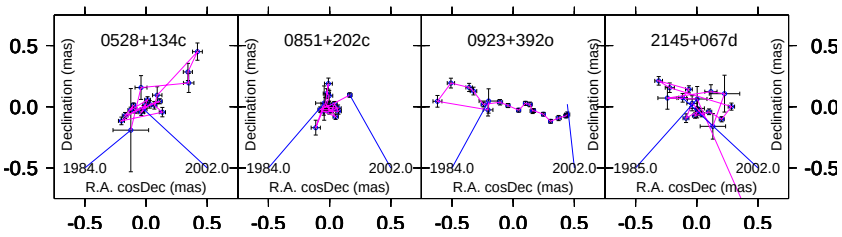

Fig. 6. Observed motion of four radio sources intensively observed over 1984-2002 (yearly averages).

is not implemented in the existing astrogeodetic analysis software. As a result, most objects exhibit time variations of their position in some preferred direction. This is illustrated on Figures 4 and 5, which show the envelopes of the standard deviation of yearly weighted average source positions in local equatorial frames.

Figure 6 shows examples of two-dimensional apparent motions of yearly weighted average source positions in local equatorial frames for four sources: 0528+134 (85517 observations in 2598 sessions), 0851+202, also known as 0J287, (102810 observations in 2788 sessions), 0923+392, also known as 4C39.25, (154589 observations in 2808 sessions), and 2145+067 (61614 observations in 1743 sessions). 0923+392 shows a steady quasi linear motion after 1986, an exceptional situation among the ICRF sources. The other three show a variety of quiet and unquiet behaviours.

Figures 12, 13, 14 and 15 in Annex 1 show the time evolution of the positions of these same four sources in the direction of their maximum variance for 0.1-year weighted average coordinates over 1984-2002. The following comments can be made.

- 0528+134 has a linear drift of 14.8 ± 2.8 μas, with superimposed low frequency oscillations with amplitude of several tens of μas and a high frequency standard deviation equal to 149 μas. The Allan variance analysis (see explanations in section 3) indicates a flicker noise spectrum at the level of 100 μas for sampling intervals up to a few years.
- 0851+202 (0J287) has a slow linear drift (4.8 ± 1.8 μas), with little low frequency oscillations, and a high frequency standard deviation equal to 133 μas. The Allan variance analysis indicates a flicker noise spectrum, also at the level of 100 μas for sampling intervals up to a few years.
- 0923+392 (4C39.25) has a well defined linear drift (57.1 ± 1.4 μas), with relatively strong low frequency oscillations, and a moderate high frequency standard deviation (114 μas). After a flicker noise signal at the level of 100 μas, the Allan variance analysis indicates a random walk for sampling intervals longer than 0.2 years, reaching a level of 300 μas for 5-year sampling times.
- 2145+067 has a slow linear drift (9.0 ± 4.2 μas) and a flicker noise spectrum at a level slightly above 100 μas for sampling intervals up to a few years. Note the large rupture around 1998, raising the high frequency standard deviation to the level of 207 μas.

Apparent source linear velocities give some information on the stability of the sources, at least for the rapidly drifting sources. As an example, a source with a linear drift of 50 μas/year, that would induce a 1 mas source shift after 20 years cannot be considered a "good" source for celestial frame maintenance. Figure 7 shows least-square estimates of source linear drifts over 1989.5-2002.4 as a function of declinations. The inserted histogram shows that a large proportion of sources have apparent drifts smaller than 40 μas/year.

3 The selection scheme

The observational situation is that sources show some level of apparent motions, which may come into contradiction with the basic assumption that, *globally*, the set of selected object has a no net rotation relative

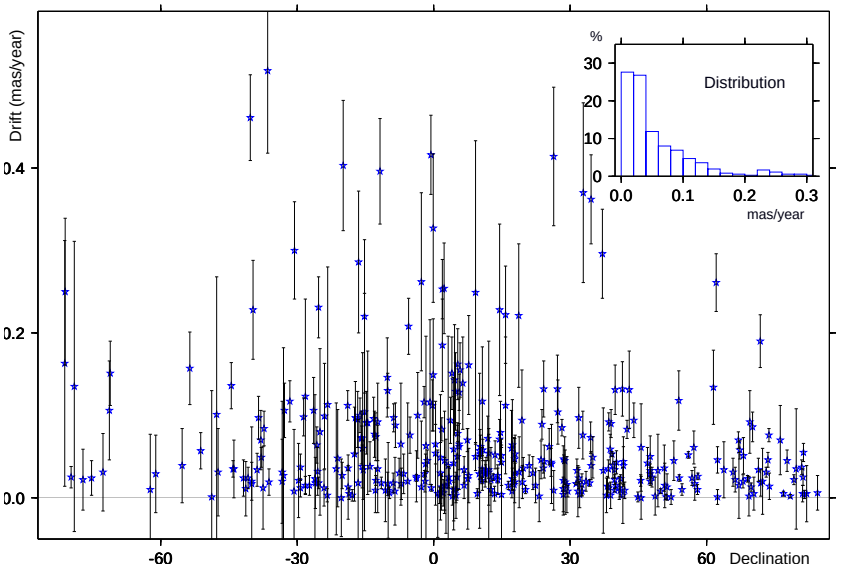

Fig. 7. Sources linear drifts in the direction of maximum variance (1989.5-2002.4), as a function of declination. The insert shows the histogram of the observed drifts.

to the quasi inertial space. However, little is presently known about the actual behaviour of these hundreds of sources, so that a way to solve this difficulty may be to select sources that best match the no-motion model, in order to minimize the uncontrolled global rotation. The authors of the ICRF (Ma et al., 1998) set up three classes of sources, using qualitative and quantitative criteria, such as apparent drift, formal uncertainty of the global coordinates over 1980-1995, source stucture index. They used only the sources they considered as the most reliable (the *defining* sources) for the definition of the ICRF orientation. A second set of apparently reliable sources that had not been enough observed in 1995 were considered as *candidates*. Finally, the remaining sources, considered as unstable, were labelled *other* sources.

The proposed selection scheme is based on a statistical assessment of source stability.

An earlier study (Gontier et al., 2001) had shown that the improvements in VLBI technology, the development of the observing network and the extension of the set of observed objects that took place in operational VLBI, brought the astrometric results to its current precision towards the end of the first decade. Starting about 1990, individual time series of source coordinates stabilize. Therefore, the selection schemes under study are applied to data after 1989.5, i.e. 3.1 million observations of 707 sources, representing 87% of the total observations. Note that values and plots of yearly averages for sources observed since 1984 are available (IERS, 2003).

A set of stable sources is selected in a two-step process, as follows.

1. A first selection is made on the basis of continuity criteria for one-year weighted average coordinates.
   (a) Length of observation period longer than five years.
   (b) Not less than two observations of the source in a given session.
   (c) One-year average coordinates based on at least three observations.

(d) Not more than three successive years with no observations, conditions (b) and (c) being met.
(e) At least half of the one-year averages available over the source observation time span.

This first screening keeps 362 sources for the years centered at 1990.0 through 2002.0. These include 141 defining sources, 130 candidates, 87 other and 4 new sources, i.e. 67% of the defining sources, 44% of the candidates and 85% of the others.

2. The time series of yearly values of $\alpha \cos\delta$ and δ are then analysed in order to derive
   (a) the linear drift (least squares estimation) and the normalized drift. The normalized linear drift is the absolute value of the least-square derived linear drift divided by its formal uncertainty;
   (b) the Allan standard deviation for a one-year sampling time. The Allan variance of a time series x_i with N items and sampling time τ is defined as:

$$\sigma_A^2(\tau) = \frac{1}{2N} \sum_i (x_{i+1} - x_i)^2$$

The Allan variance analysis (Allan, 1966), see a review of these methods in (Rutman, 1978)) allows one to characterize the power spectrum of the variability in time series, for sampling times ranging from the initial interval of the series to 1/4 to 1/3 of the data span, in our case one year through four years. This method allows one to identify white noise (spectral density S independent of frequency f), flicker noise (S proportional to f^{-1}), and random walk (S proportional to f^{-2}). Note that one can simulate flicker noise in a time series by introducing steps of random amplitudes at random dates. In the case of a white noise spectrum (an implicit hypothesis in the current ICRF computation strategy), accumulating observations with time eventually leads to the stabilisation of the mean position. In the case of flicker noise, extending the time span of observation does not improve the quality of the mean coordinates.

The distributions of the above statistics applied to the 362 preselected sources are shown on figure 8.

Based on these statistics, rules are set up to derive source stability indices. For each local coordinate ($\alpha \cos\delta$ and δ), three partial indices are defined, as shown in Table 1. The thresholds are set after the distributions of figure 8. The partial stability indices range from 1 (most stable) through 3 (least stable). A rejection value (10) is associated to very large drifts or standard deviations. Given the length of the available time series (up to 13 years), one could consider the Allan standard deviation for sampling times longer than one year (e.g. two or four years). The one-year interval is preferred because its estimation is expected to be more robust than for longer time spans.

The partial stability criteria derived by applying the thresholds of Table 1 are then combined in five different ways, each one representing a different balance in the roles of the standard deviations and the drifts. Fifty sources were found to have apparent drifts larger than 50 μas/year. They are excluded a priori in the five options.

We reproduce in Annex 2 the table giving detailed statistics on the 362 sources well observed over 1989.5-2002.4, taken from Feissel-Vernier (2003), which is published only in electronic form in A&A.

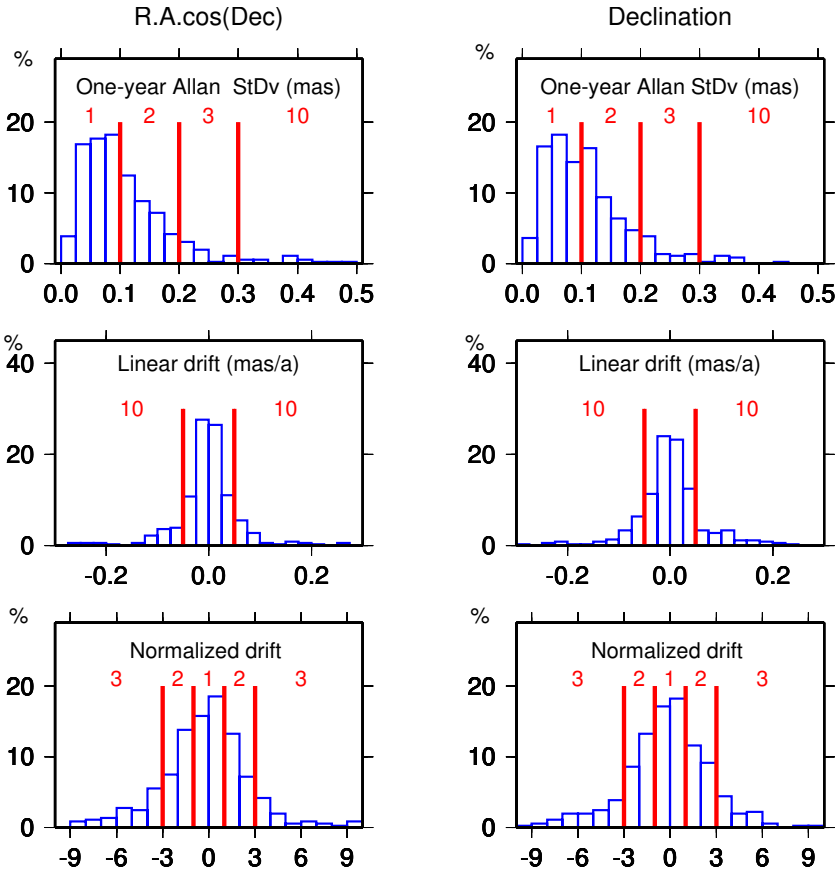

Fig. 8. Distributions of the partial stability criteria for the well observed sources over 1989.5-2002.4. The thresholds and corresponding partial indices listed in Table 1 are shown.

Table 1. Partial stability criteria. The values range from 1 (best) through 3 (worse), with a rejection value of 10.

Statistics	Threshold	Partial index
Allan Standard deviation (AlSd)		
	AlSd $\leq$ 100 μas	1
	100 μas $\leq$ AlSd $\leq$ 200 μas	2
	200 μas $\leq$ AlSd $\leq$ 300 μas	3
	AlSd $\geq$ 300 μas	10
|Drift| (Vel)		
	Vel $\leq$ 10 μas/year	1
	Vel $\geq$ 50 μas/year	10
|Normalized drift| (Nvl)		
	Nvl $\leq$ 1	1
	1 $\leq$ Nvl $\leq$ 3	2
	Nvl $\geq$ 3	3

4 Relationships of the stable sources with the ICRF source qualification

The **partial stability indices** for each of the 362 sources investigated (drift, Allan variance and normalized drift) can be compared with two existing ICRF qualifiers:

- the source status: defining, candidate or other, and
- the source structure index in the X band when available. Structure index values 1 and 2 indicate very good and good astrometric suitability, values 3 and 4 poor and very poor suitability.

The comparison with the source status is plotted in figure 9 for the 312 well observed sources with apparent drifts smaller than 50 μas/year over 1989.5-2002.4. The graphs give the positions of the defining, candidate and other sources as a function of both the one-year Allan standard deviation and the normalized drift. Although a number of defining sources fall in the lower-left zone which correspond to small partial stability indices, some of them are clearly detected as unstable. The candidate sources are globally in the same situation. Conversely, a number of 'other' sources, i.e. considered as having questionable stability in the ICRF work, are detected as stable. Compared to the ICRF selection, the proposed scheme rescues a number of sources that are in fact efficient for maintaining the ICRF axes directions.

The comparison with the source structure indices, plotted on figure 10, also shows moderate cross correlation of the two types of criteria.

Table 2 gives the relationship of the **global stability index** with the ICRF qualifiers. Sources with global stability indices 1 and 2 are considered as stable. Although a number of defining sources get small, i.e. good, partial stability indices, some of them are clearly detected as unstable. The candidate sources are globally in the same situation. Conversely, a number of 'other' sources, i.e. considered as having questionable stability in the ICRF work, are detected as stable. Compared to the ICRF selection, the proposed scheme rescues a number of sources that are in fact efficient for maintaining the ICRF axes directions. For what concerns the source stability indices, 80% of the stable sources have a good structure index (1 or 2), while the ratio is also large for the unstable sources (64%). Altogether, 61% of the well observed sources with a good structure index are detected as stable, and 39% are detected as unstable. This finding is of interest in the context of studying the dynamics of the quasars activity. Similarly, there is no clear relationship of the source total fluxes in the X and S bands with their direction time variability. A possible relationship with the flux variability remains to be investigated.

Figure 11 shows the sky distribution of the proposed stable and unstable sources, together with that of the current ICRF defining sources.

5 Testing source selections

Out of the 362 preselected sources the proposed stability scheme produces 199 stable sources, a number to be compared to the 212 defining sources in the ICRF. To test their efficiency with respect to the maintenance of the axes of the celestial reference frame that they materialize, we consider the 13 yearly differential reference frames (1990.0 - 2002.0) that are formed by the coordinates of the stable sources observed in

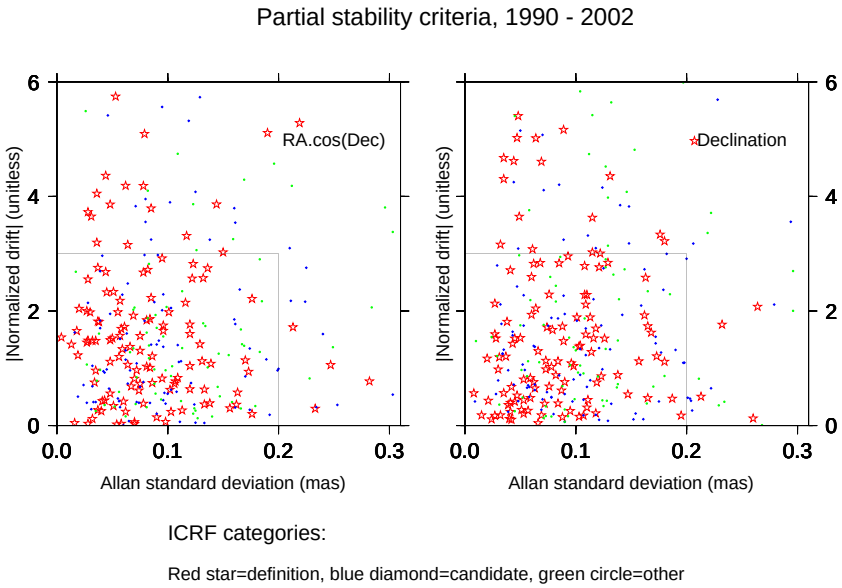

Fig. 9. Partial stability criteria and ICRF source classes

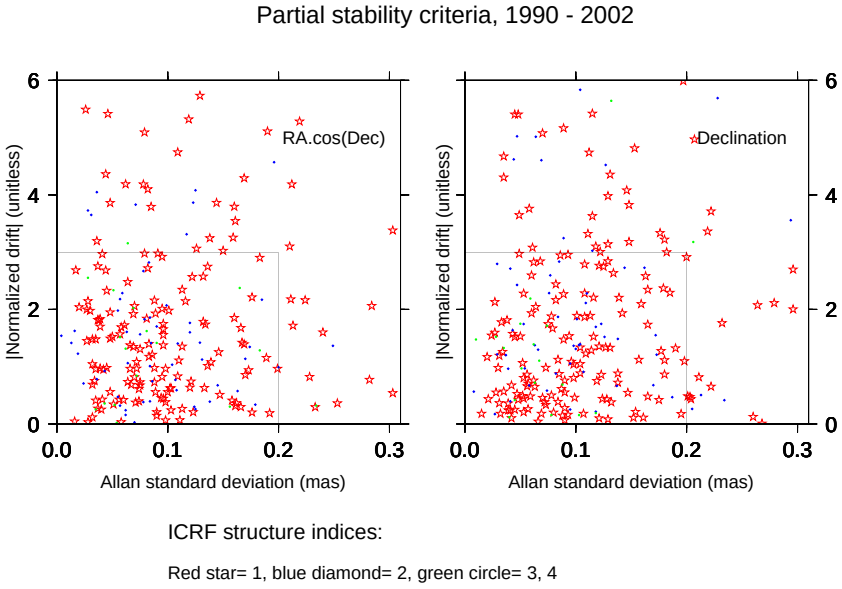

Fig. 10. Partial stability criteria and ICRF source source structure index

Table 2. Stability index and ICRF source qualifiers

Stab.	Source status			Structure index		
index	Def.	Can.	Oth.	1	2	3-4
1	33	26	15	46	11	7
2	48	42	34	76	26	6
3	2	1	4	6	2	0
4	58	61	34	70	26	13

Table 3. Stability test

Source selection scheme	Nb of sources kept	Std dev. μas	Allan Std dev. 1 year μas	4 years μas
Stable	199	10.8	9.4	5.9
ICRF Defining	212	25.6	26.0	27.6

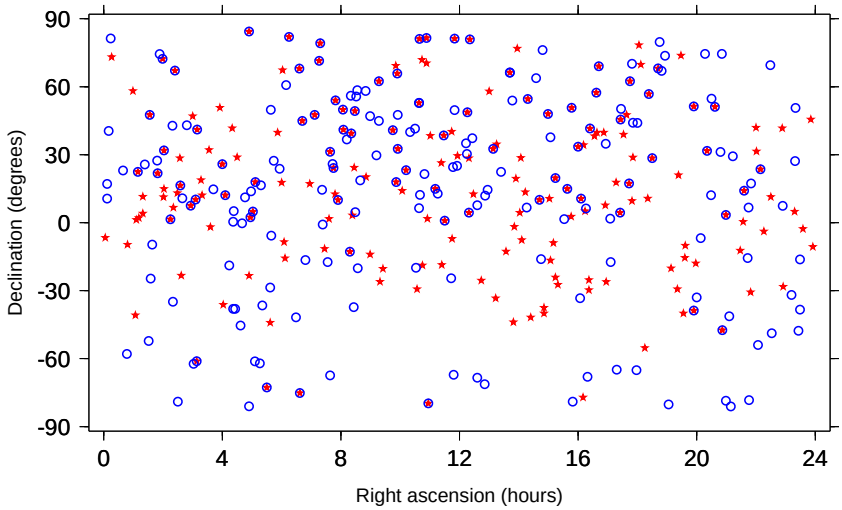

Fig. 11. Detected stable sources (stars) over 1989.5-2002.4 and ICRF defining sources (circles).

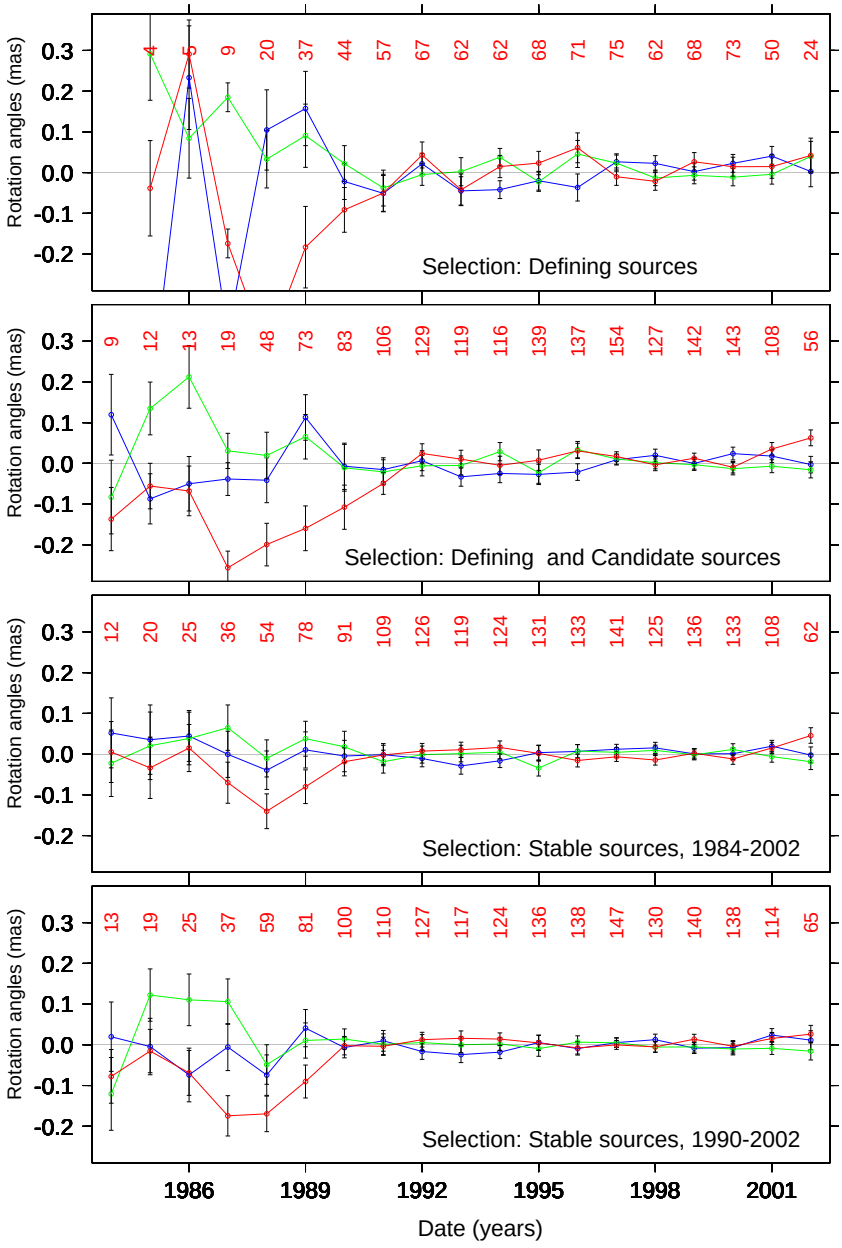

Fig. 12. Rotation angles of yearly differential reference frames - A1: blue (dark) - A2: green (light) - A3: red (medium) - Unit: 0.001" (mas). The numbers of selected sources for each year are given.

each year. The yearly differential rotation angles $A_1(y)$, $A_2(y)$, $A_3(y)$ around the axes of the equatorial coordinate system for year y are then computed for the 13 years.

Table 3 lists efficiency estimates for the stability scheme and for the ICRF defining sources. These estimates are the usual standard deviation that characterizes the scattering of the sets of rotation angles, and their Allan standard deviations for one-year and four-year sampling times, that characterize their stability in time. Note that if the time series of the rotation angles have white noise, the four-year Allan standard deviation will be equal to half (square root of one fourth in sampling time) the one-year one. In the case of flicker noise, both values will be equal.

The estimated efficiency of the ICRF defining sources is worse than that of the proposed selection by nearly a factor of three for the one-year estimates and a factor of five in the longer term.

6 Discussion

When compared to the current ICRF defining sources, the selection scheme developed in this study achieves improved time stability of yearly reference frames, which implies improved internal consistency. This has consequences not only in astrometric applications, but it may also have bearings in the geophysical interpretation of the Earth's orientation in inertial space. As an example, Dehant et al. (2002) have shown that source instabilities perturb precession and long term nutation determinations at the level of tens of μas, a level comparable to that of the discrepancy of VLBI results with the precession constant or the 18.6-year nutation component in the IAU2000 Nutation model.

Finally, we recommend that the set of selected stable sources be considered on the one hand in any future improvement of the International Celestial Reference Frame, and on the other hand in the scheduling of repeated VLBI sessions for Earth rotation, geodesy and astrometry.

Acknowledgements. The data analysis in this study is entirely based on the time series of coordinates of 707 radio source derived by Alan Fey (USNO) using 3.6 millions of observations accumulated in various US and international programs since 1979.

References

Allan, D. W. 1966, Proc. IEEE 54, 221

Dehant, V., Feissel-Vernier, M., de Viron, O., Ma, C., Yseboot, M., Bizouard, C., 2002, JGRB, 108, 2275, DOI 2002JB001763.

Feissel-Vernier, M., 2002, anonymous ftp: ftp://lareg.ensg.ign.fr/pub/martine/crono_vue

Feissel-Vernier, M., 2003, A&A, 403, 105

Fey, A. L., 2002, Private communication

Fey, A. L., Charlot, P., 2000, ApJS 128, 17

Gontier, A.-M., Le Bail, K., Feissel, M., 2001, A&A 375, 661

IERS 1999, ftp://hpiers.obspm.fr/icrs-pc/icrf/iau/icrf-Ext.1

IERS 2002, ftp://hpiers.obspm.fr/icrs-pc/icrf/iau/icrf.car

IERS 2003, http://hpiers.obspm.fr/icrs-pc/icrf/time-series.html

Ma, C., Arias, E. F., Eubanks, T. M., Fey, A. L., Gontier, A.-M., Jacobs, C. S., Sovers, O. J., Archinal, B. A., Charlot, P., 1998, AJ 116, 516

Rutman, J., 1978, Proc. IEEE 66, 1048

7 Annex 1

Time series of source displacement, 1984-2002

- Figure 13: 0528+134
- Figure 14: 0851+202
- Figure 15: 0923+392
- Figure 16: 2145+067

8 Annex 2

We reproduce hereafter the table giving detailed statistics on the 362 sources well observed over 1989.5-2002.4, taken from Feissel-Vernier (2003, referred to as MFV hereafter), which is published only in electronic form in A&A.

The redshift and the total flux at 6 cm, 11/15 cm are given when available. 'AlSd' is the Allan standard deviation for a one-year sampling time.

1. The ICRF source status: d = defining, c = candidate, o = other, n = not available in ICRF Ext-1.
2. The source structure index, when available in ICRF-Ext.1. This index (Fey and Charlot, 2000) qualifies the level of position disturbance expected as a result of the the source structure (1 for the least disturbed, 4 for the most disturbed)
3. The stability index derived in MFV; values 1 and 2 correspond to stable sources, 3 to unstable, and 4 to highly unstable or drifting. The stability indices are rounded off.
4. The same stability criterion as above, but keeping only yearly averages based on at least twelve observations (instead of three).

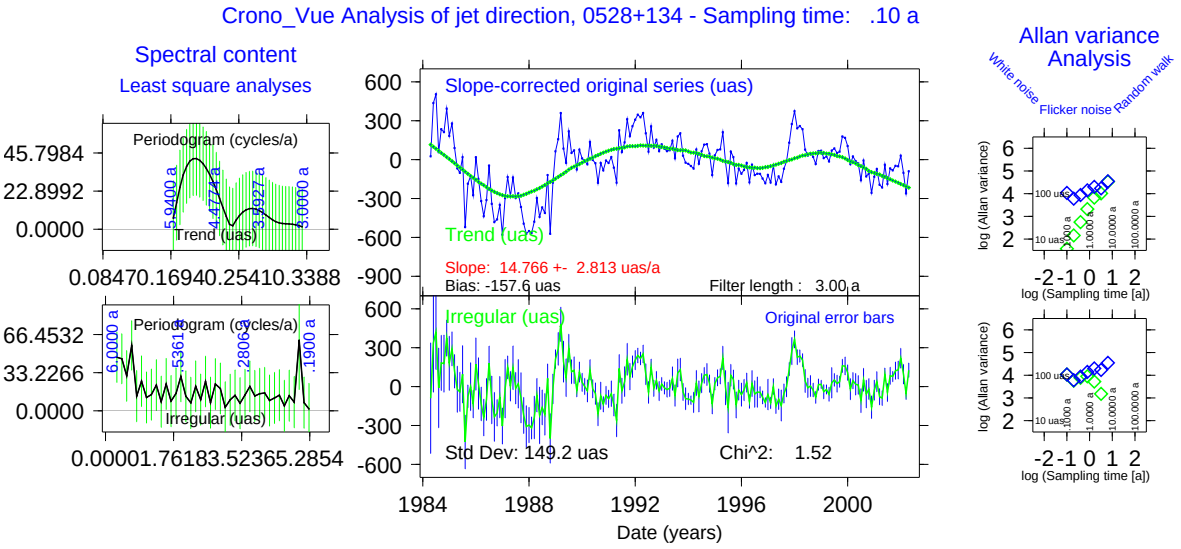

Fig. 13. Time series at 0.1-year intervals showing the apparent motion of source 0528+134 in the direction of maximum variance.

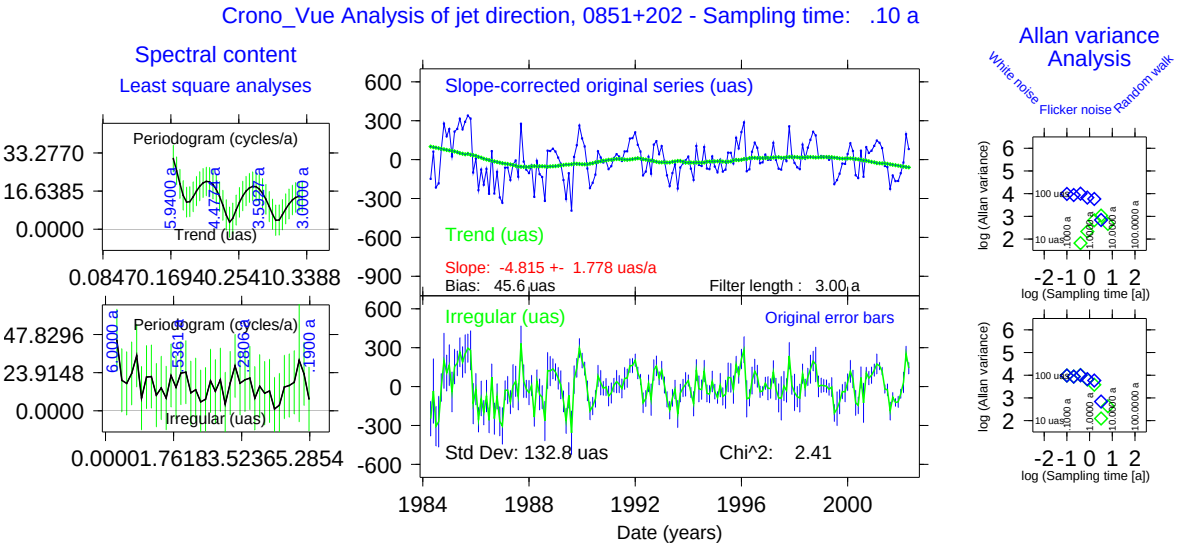

Fig. 14. Time series at 0.1-year intervals showing the apparent motion of source 0851+202 (OJ287) in the direction of maximum variance.

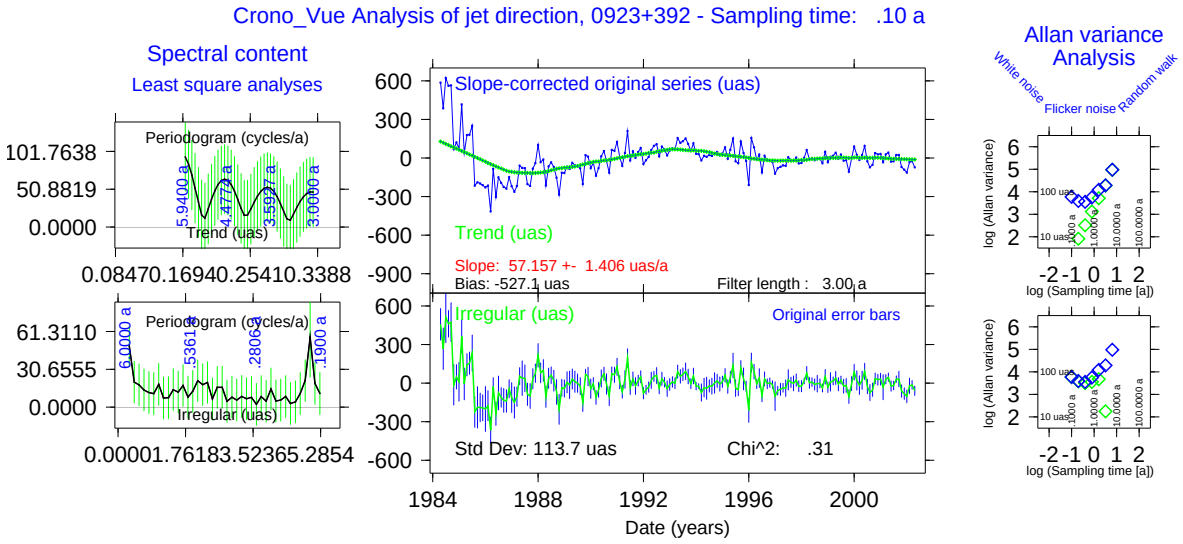

Fig. 15. Time series at 0.1-year intervals showing the apparent motion of source 0923+392 (4C39.25) in the direction of maximum variance.

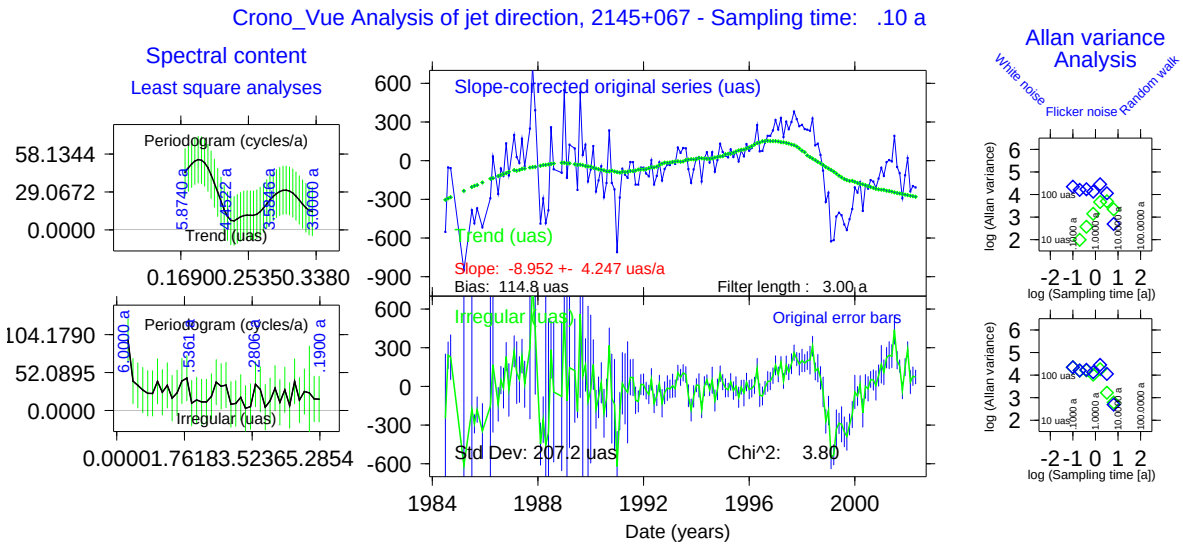

Fig. 16. Time series at 0.1-year intervals showing the apparent motion of source 2145+067 in the direction of maximum variance.

Table 4. Stability criteria for 362 well observed extragalactic sources, 1989.5-2002.4

No	Source	Alter.	Redsh.	Flux (Jy) 6 cm	11 cm	15 cm	Number sess	pts	R.A. cos(δ) AlSd μas	Drift μas/year	Declination AlSd μas	Drift μas/year	Stability criteria 1	2	3	4
1	0003 + 380		.23	.5		.6	12	8	32	-2 ± 20	15	-2 ± 11	d	1	1	1
2	0003 − 066		.35	1.6		1.7	492	12	110	-9 ± 8	177	30 ± 24	c	1	2	2
3	0007 + 171		1.60	1.2	.9		14	7	44	-66 ± 15	41	7 ± 31	d	1	4	
4	0008 − 264		1.09	.8		.6	12	9	19	-50 ± 13	64	101 ± 39	c		4	
5	0013 − 005		1.57	.8	.8		54	11	597	15 ± 4	70	4 ± 10	c	1	4	4
6	0014 + 813		3.39	.6		1.0	449	11	96	-7 ± 4	207	54 ± 11	d	1	4	4
7	0016 + 731		1.78	1.6		1.5	425	12	169	-26 ± 6	134	-15 ± 6	o	1	2	2
8	0019 + 058			.5	.5		27	9	26	-35 ± 6	112	-154 ± 32	o	1	4	
9	0026 + 346		.52			1.8	12	5	98	-393 ± 52	10	38 ± 26	o	4	4	
10	0048 − 097			1.9		1.3	1058	13	83	-5 ± 3	104	-7 ± 7	o	1	1	1
11	0056 − 001		.72	1.4		2.2	12	8	136	-262 ± 51	94	194 ± 90	c	3	4	
12	0059 + 581						932	11	158	2 ± 5	197	-26 ± 4	o	1	2	2
13	0104 − 408		.58	.9	.6		499	13	81	-4 ± 12	71	23 ± 13	o		1	1
14	0106 + 013		2.11	3.7		3.9	1280	13	69	6 ± 5	93	1 ± 9	o	1	1	1
15	0109 + 224			.8	.4		14	9	72	24 ± 25	30	13 ± 13	d	1	1	1
16	0111 + 021		.05				167	12	39	-16 ± 9	39	-3 ± 13	c	1	1	1
17	0112 − 017		1.37	1.2	1.4		49	10	192	68 ±117	79	58 ± 40	c	1	4	4
18	0113 − 118		.67	1.9	1.8		27	9	179	-31 ± 93	117	-313 ± 49	o	2	4	4
19	0119 + 041		.64	1.2		.9	1427	13	192	2 ± 11	161	-1 ± 7	c	1	2	2
20	0119 + 115		.57	1.0		1.8	387	11	45	4 ± 4	179	-34 ± 14	c	1	2	2
21	0133 + 476		.86	3.3		2.1	500	13	136	-14 ± 5	68	-12 ± 4	d	1	2	2
22	0134 + 329	3C48	.37	5.4	9.0		11	5	88	56 ±159	85	-299 ±189	o	4	4	
23	0146 + 056		2.35	1.2	.7		54	10	28	32 ± 15	89	63 ± 28	c	1	4	4
24	0149 + 218		1.32	1.1		1.4	43	9	107	-10 ± 13	104	30 ± 22	d	2	2	2
25	0159 + 723			.3	.3		19	7	37	-7 ± 26	84	-16 ± 41	d	1	1	1
26	0201 + 113		3.61	1.2		1.3	360	13	91	21 ± 7	131	-22 ± 16	c	1	2	2
27	0202 + 149		.41	3.1		3.2	516	13	174	-9 ± 7	228	49 ± 9	c	2	2	2
28	0202 + 319		1.47	1.0		1.6	40	11	55	-19 ± 10	41	-4 ± 11	d	2	1	1
29	0208 − 512		1.00	3.2	3.6		274	13	140	3 ± 17	127	-58 ± 21	o		4	4
30	0212 + 735		2.37	2.2		2.3	1264	12	196	36 ± 8	127	-27 ± 6	o	2	3	3
31	0215 + 015		1.72	.4	.4		23	9	173	34 ± 36	87	11 ± 18	d	1	1	1
32	0221 + 067		.51	1.0		1.4	45	9	85	20 ± 14	29	-44 ± 16	c	2	2	2
33	0224 + 671	4C67.05				1.2	40	7	74	20 ± 32	90	28 ± 37	d	1	1	1
34	0229 + 131		2.07	1.0		2.0	1946	13	105	-23 ± 3	125	-11 ± 4	c	1	2	2
35	0230 − 790		1.07	.8	.6		11	7	70	10 ±170	43	-129 ± 91	d		4	
36	0234 + 285		1.21	2.8	1.2		1085	12	49	11 ± 1	123	-5 ± 3	c	2	2	2
37	0235 + 164		.94	2.8		2.0	442	13	103	1 ± 4	121	-14 ± 5	d	1	2	2
38	0237 + 040		.98	.8		.8	22	8	56	8 ± 18	118	140 ± 45	c	1	4	4
39	0237 − 027		1.12	.6	.4		14	8	174	137 ±102	104	-209 ± 65	c	1	4	4
40	0237 − 233		2.22	3.2	5.3		13	7	52	-20 ± 62	78	22 ±140	o	3	1	
41	0238 − 084	NGC1052	.00	.9	.6		275	10	123	-87 ± 22	138	-38 ± 26	o	2	4	4
42	0239 + 108					1.8	83	12	78	28 ± 11	44	-62 ± 13	d	2	4	4
43	0248 + 430		1.31	1.2	1.0		13	7	84	-47 ± 25	115	122 ± 40	d	2	4	4
44	0256 + 075		.89	1.0		.7	38	8	95	26 ± 32	72	21 ± 55	d	1	1	
45	0300 + 470			2.2	1.8		716	12	166	-15 ± 9	296	36 ± 18	o	1	2	4
46	0302 − 623						18	6	81	59 ± 58	51	-17 ± 60	d		4	4
47	0306 + 102		.86	.7		1.3	30	9	96	40 ± 23	79	-37 ± 22	d	1	2	2
48	0308 − 611						80	8	133	17 ± 45	73	30 ± 26	d		2	2
49	0309 + 411		.14	.5		.6	12	6	13	-12 ± 8	69	22 ± 5	d	2	2	
50	0317 + 188						30	6	32	16 ± 15	56	-27 ± 41	c	1	1	

(continued on next page)

(Table 4. continued)

No	Source	Alter.	Redsh.	Flux (Jy) 6 cm	11 cm	15 cm	Number sess	pts	R.A. cos(δ) AlSd μas	Drift μas/year	Declination AlSd μas	Drift μas/year	Stability criteria 1	2	3	4
51	0319+121		2.67	1.5		1.4	20	10	35	-5 ± 20	51	40 ± 42	o	3	1	1
52	0332–403		1.45	2.6	1.9		11	7	129	-147 ± 30	212	-426 ± 55	o		4	
53	0333+321	NRAO140	1.26	2.0		2.3	80	10	72	-11 ± 13	67	-11 ± 10	o	3	1	1
54	0336–019	CTA26	.85	2.6		2.7	726	13	160	16 ± 8	279	-25 ± 12	c	1	2	2
55	0338–214		.05	.9	.8		29	7	101	-124 ± 77	126	-87 ± 71	o		4	4
56	0341+158						22	7	50	-39 ± 6	104	110 ± 82	c	1	4	
57	0342+147						32	10	59	-50 ± 11	176	-69 ± 37	d	1	4	4
58	0355+508	NRAO150				6.8	470	9	43	6 ± 16	88	-20 ± 28	o	3	1	1
59	0400+258		2.11	1.8		1.4	36	9	120	26 ± 15	85	46 ± 16	d	2	2	2
60	0402–362		1.42	1.9	1.0		344	13	38	-14 ± 9	57	-18 ± 16	o		2	2
61	0403–132		.57	2.9		4.0	11	6	23	-49 ± 6	49	88 ± 29	o	1	4	
62	0405–385		1.28	1.1		1.0	73	9	19	13 ± 26	44	97 ± 23	c		4	
63	0406+121		1.02	1.6	1.2		32	9	75	-29 ± 40	260	20 ±156	d	1	2	2
64	0406–127		1.56	.5	.6		16	7	79	-8 ± 3	159	69 ± 33	c	1	4	
65	0414–189		1.54	.8		1.0	11	6	125	113 ± 18	19	-43 ± 5	d	1	4	
66	0420+417					1.7	19	8	63	-36 ± 22	39	23 ± 24	c	2	1	
67	0420–014		.92	1.6		1.0	1247	11	228	-10 ± 12	222	-45 ± 12	o	1	3	3
68	0422+004			1.6		.8	18	8	48	-15 ± 26	98	61 ± 58	d	1	4	4
69	0422–380		.78	.8	.5		15	8	28	-29 ± 20	32	89 ± 28	d		4	
70	0425+048						16	7	34	52 ± 59	24	174 ± 38	c	3	4	
71	0430+052	3C120	.03	5.1		6.4	97	9	183	-50 ± 39	50	-18 ± 10	o	3	4	4
72	0430+289			.5	.4		33	5	27	30 ± 28	71	-4 ± 29	n		1	1
73	0434–188		2.70	1.1		1.3	92	12	82	56 ± 14	99	17 ± 37	o	1	4	4
74	0440+345						30	10	41	15 ± 5	148	72 ± 19	c	1	4	4
75	0440–003	NRAO190	.84	2.4	3.5		18	7	40	-61 ± 15	40	-95 ± 37	d	1	4	
76	0451–282		2.56	2.2		2.3	11	7	78	-48 ± 63	124	104 ±106	c		4	
77	0454+844		$\geq$ 1.34	1.4		1.3	58	11	139	-14 ± 13	116	-25 ± 17	d	1	2	2
78	0454–234		1.00	1.9	1.8		1600	13	136	7 ± 7	124	3 ± 6	o	1	2	2
79	0454–810		.44	1.4	1.2		20	7	65	-218 ± 85	29	113 ± 26	d		4	
80	0457+024		2.38	1.2		1.3	59	11	57	29 ± 19	66	-1 ± 30	d	1	1	1
81	0458–020		2.29	1.6		2.0	1256	13	211	-16 ± 7	200	-21 ± 7	c	1	3	3
82	0500+019		.58	2.0		2.0	16	9	223	-54 ± 16	317	246 ± 62	o	3	4	4
83	0502+049		.95	1.0		.6	11	6	4	9 ± 6	8	-9 ± 15	d	2	1	
84	0507+179		.42	.8		.7	42	12	120	-35 ± 22	95	-6 ± 23	d	2	2	2
85	0521–365		.05	8.9		11.5	90	11	488	261 ± 82	342	-446 ± 87	d		4	
86	0528+134		2.07	4.4	2.7		2546	13	469	-7 ± 8	198	4 ± 4	c	1	4	4
87	0528–250		2.77	.8	1.3		16	8	56	-18 ± 31	120	88 ±102	o		4	
88	0530–727						55	7	43	-13 ± 29	76	32 ± 47	d		1	1
89	0536+145						33	7	96	-18 ± 12	58	-74 ± 20	o	1	4	4
90	0537–286		3.10	1.2		1.0	19	9	90	74 ± 35	52	-59 ± 19	d		4	
91	0537–441		.90	4.0	3.8		360	13	109	39 ± 8	82	24 ± 11	o	1	2	2
92	0539–057		.84	1.5	1.3		12	8	50	63 ± 41	39	32 ± 88	d	1	4	
93	0544+273						34	7	70	-17 ± 21	163	-101 ± 39	d	1	4	4
94	0552+398		2.36	5.4		3.4	3039	13	129	-8 ± 1	148	-5 ± 2	c	1	2	2
95	0554+242						22	5	42	-112 ± 36	173	-99 ± 83	n		4	4
96	0556+238						245	12	95	-35 ± 12	131	-75 ± 17	d	1	4	
97	0600+177						11	6	100	-22 ± 39	98	-34 ± 42	c	1	1	
98	0602+673		1.97	1.1	.8		13	7	85	38 ± 12	66	-48 ± 6	c		2	2
99	0605–085		.87	2.7	3.0		27	9	42	-16 ± 17	57	-25 ± 35	c	1	1	1
100	0607–157		.32	3.1		1.0	22	9	109	-36 ± 26	63	19 ± 14	c	2	2	4

(continued on next page)

(Table 4. continued)

No	Source	Alter.	Redsh.	Flux (Jy) 6 cm	11 cm	15 cm	Number sess	pts	R.A. cos(δ) AlSd μas	Drift μas/year	Declination AlSd μas	Drift μas/year	Stability criteria 1	2	3	4
101	0615 + 820		.71	1.0		1.3	30	8	51	-9 ± 25	60	35 ± 18	d	1	1	1
102	0636 + 680		3.18	.5	.3		34	9	30	15 ± 7	64	-17 ± 8	d	1	2	2
103	0637 − 752		.65	6.2	4.5		277	13	247	-23 ± 21	109	16 ± 10	d		2	2
104	0642 + 449		3.41	.8		1.2	464	12	113	2 ± 6	69	-1 ± 3	d	1	1	1
105	0646 − 306		.46	1.1		.9	11	6	39	170 ± 42	41	172 ± 86	c	2	4	
106	0648 − 165						17	7	109	-30 ± 35	115	192 ± 53	d	1	4	4
107	0650 + 371		1.98	1.0		1.0	30	7	192	-249 ± 45	109	-202 ± 58	c	1	4	4
108	0657 + 172						114	12	88	-14 ± 7	85	-6 ± 7	c	1	1	1
109	0707 + 476		1.29	1.0		.8	13	7	150	-26 ± 8	165	45 ± 26	d	1	2	2
110	0716 + 714			1.1		.7	94	10	38	-12 ± 7	108	-33 ± 15	d	1	2	2
111	0718 + 7920718+793					1.0	476	10	78	23 ± 5	57	1 ± 4	d	1	2	2
112	0723 − 008		.13	2.3		2.1	27	8	163	45 ± 77	173	-94 ± 77	d	2	4	4
113	0727 − 115						2101	13	159	12 ± 4	165	16 ± 7	o	1	2	2
114	0735 + 178		≥ .42	2.0		2.0	486	12	377	-40 ± 25	180	-10 ± 12	o	1	4	4
115	0736 + 017		.19	1.9		2.9	43	11	234	4 ± 13	35	18 ± 13	c	3	2	2
116	0738 + 313		.63	2.5		1.9	22	9	144	-6 ± 2	80	-15 ± 2	d	1	2	2
117	0742 + 103					3.9	301	12	126	39 ± 13	129	-52 ± 13	o	1	4	4
118	0743 + 259					.6	18	9	176	-14 ± 71	122	122 ± 41	d	1	4	
119	0743 − 006		.99	1.3	1.0		24	9	116	-95 ± 31	289	-412 ± 45	o	1	4	
120	0745 + 241		.41	1.3	.7		111	10	57	-20 ± 9	47	-32 ± 6	d	2	2	2
121	0748 + 126		.89	2.2		2.0	20	7	24	8 ± 11	74	22 ± 38	c	2	1	1
122	0749 + 540		≥ .20	.6	.7		376	12	141	-27 ± 4	96	-4 ± 3	d	1	2	2
123	0754 + 100		.28	1.5	1.0		20	8	27	-28 ± 14	47	-11 ± 21	d	1	1	1
124	0804 + 499		1.43	2.1		1.3	768	13	101	6 ± 3	101	-5 ± 3	d	1	2	2
125	0805 + 410		1.42	.8		.7	240	11	67	-5 ± 7	53	4 ± 5	d	1	1	1
126	0808 + 019			.7		.4	28	8	199	86 ± 25	247	-228 ± 37	c	1	4	4
127	0814 + 425		.26	1.7		1.6	116	11	165	-82 ± 11	75	-11 ± 6	c	1	4	4
128	0818 − 128			.9		.9	18	7	86	29 ± 24	35	-11 ± 20	d	1	1	
129	0820 + 560		1.42	1.2		1.7	53	11	29	52 ± 4	27	4 ± 3	d	1	4	4
130	0821 + 394		1.22	1.0		1.9	14	8	19	-8 ± 6	41	-39 ± 14	d	2	1	1
131	0821 + 621		.54	.6	.3		12	6	218	-261 ± 35	90	38 ± 20	c		4	4
132	0823 + 033		.51	1.4		1.4	785	13	161	-21 ± 6	190	-17 ± 13	c	1	2	2
133	0826 − 373						16	9	53	-77 ± 13	24	-2 ± 22	d		4	
134	0827 + 243		.94	.9		1.3	62	10	108	-8 ± 13	162	47 ± 17	c	2	2	2
135	0828 + 493		.55	1.0		.5	14	8	16	0 ± 11	62	33 ± 44	d	1	1	1
136	0829 + 046		.18	.7		.7	14	7	123	-93 ± 34	133	111 ± 61	d	2	4	4
137	0839 + 187		1.27	1.2		2.2	21	10	140	52 ± 21	363	218 ± 85	d	3	4	4
138	0851 + 202	OJ287	.31	2.6	3.4		2756	13	224	9 ± 4	121	5 ± 3	c	1	2	2
139	0859 − 140		1.34	2.3		2.9	18	7	57	46 ± 31	62	36 ± 26	c	3	2	4
140	0906 + 015		1.02	.9		.8	25	9	55	-18 ± 39	58	-53 ± 79	c	2	4	4
141	0917 + 624		1.45	1.2		1.6	123	10	132	-34 ± 13	129	31 ± 11	d	1	2	2
142	0919 − 260		2.30	2.4		1.2	336	13	62	3 ± 22	137	21 ± 31	o	2	1	1
143	0920 + 390						44	7	95	-91 ± 16	63	-13 ± 21	c		4	4
144	0920 − 397		.59	1.5		2.1	88	12	62	-17 ± 15	140	-227 ± 59	c		4	4
145	0923 + 392	4C39.25	.70	7.6		4.2	2756	13	296	52 ± 3	153	-11 ± 2	o	1	4	4
146	0925 − 203		.35	.7	.8		17	6	47	20 ± 31	44	29 ± 40	c		1	
147	0945 + 408		1.25	1.8		1.7	14	9	64	-17 ± 16	66	-14 ± 11	d	2	2	1
148	0951 + 693	M81		.1		.5	65	9	127	3 ± 25	164	-10 ± 25	o		2	2
149	0952 + 179		1.48	.7		1.0	33	10	64	-38 ± 12	74	39 ± 23	d	3	2	2
150	0953 + 254	OK290	.71	1.8		1.3	530	13	284	38 ± 18	219	49 ± 15	o	1	3	3

(continued on next page)

(Table 4. continued)

No	Source	Alter.	Redsh.	Flux (Jy) 6 cm	11 cm	15 cm	Number sess	pts	R.A. cos(δ) AlSd μas	Drift μas/year	Declination AlSd μas	Drift μas/year	Stability criteria 1	2	3	4
151	0954+658		.37	1.5		.9	247	12	90	1 ± 8	113	-31 ± 17	d	1	2	2
152	0955+326		.53	.7		.7	13	8	70	0 ± 4	126	9 ± 6	d	2	1	1
153	0955+476		1.87	1.0		1.1	1049	11	329	-33 ± 4	119	2 ± 2	d	1	4	4
154	1004+141		2.71	.7		.8	262	13	145	16 ± 23	98	18 ± 13	o	2	2	2
155	1012+232		.56	1.1	.7		13	7	27	27 ± 19	53	13 ± 30	d	1	1	1
156	1014+615		2.80				19	7	225	-128 ± 47	50	-43 ± 8	c		4	4
157	1020+400		1.25	.9		1.2	15	10	219	-10 ± 2	35	-27 ± 6	d	1	3	2
158	1022+194		.83	.6		1.0	22	6	43	-12 ± 13	172	94 ± 61	c	2	4	
159	1030+415		1.12	1.1		.8	15	6	58	-122 ± 28	29	-53 ± 20	d	2	4	
160	1032–199		2.20	1.0	1.1		11	8	146	305 ± 42	196	-222 ± 76	d		4	
161	1034–293		.31	1.5		1.3	1081	13	113	-9 ± 7	138	8 ± 11	o	1	2	2
162	1038+064		1.26	1.3		1.6	48	11	74	-58 ± 17	119	125 ± 51	d	1	4	4
163	1038+528	1038+52*A*	.68	.7	.4		162	10	59	-13 ± 10	168	39 ± 24	d		2	2
164	1039+811		1.26	1.1	.9		37	11	41	4 ± 10	53	-3 ± 14	d	1	1	1
165	1044+719		1.15	.7		1.0	508	12	240	-19 ± 12	204	5 ± 12	c	1	2	2
166	1045–188		.60	1.1	.9		12	7	5	-13 ± 2	18	-34 ± 4	o	1	2	
167	1053+704		2.49	.7		.6	27	9	111	-1 ± 21	34	-20 ± 3	c	1	2	2
168	1053+815		.71	.8		.6	179	12	75	-6 ± 5	114	8 ± 6	d	1	1	1
169	1055+018		.89	3.4		2.9	258	12	125	-3 ± 11	95	13 ± 13	o	2	2	2
170	1057–797						249	13	120	-11 ± 11	162	-24 ± 12	d		2	2
171	1101+384		.03	.7		1.0	209	9	138	-36 ± 11	78	5 ± 11	c	1	2	2
172	1101–536						33	8	63	77 ± 8	136	139 ± 47	c		4	4
173	1104–445		1.60	2.0	1.8		203	12	122	-119 ± 19	87	70 ± 27	o		4	
174	1111+149		.87	.5	.6		20	9	35	-20 ± 21	50	46 ± 30	d	1	1	1
175	1123+264		2.34	.8		.7	129	9	71	-9 ± 24	52	6 ± 13	o	1	1	1
176	1124–186		1.05	1.6		.6	405	12	64	5 ± 7	52	-8 ± 7	c	1	1	1
177	1127–145		1.19	7.3	6.4		28	9	200	-84 ± 85	43	45 ± 27	c	2	4	4
178	1128+385		1.73	.8		.9	707	12	85	-13 ± 3	138	6 ± 6	d	1	2	2
179	1130+009					.3	28	12	120	43 ± 67	88	-11 ± 73	d	1	1	
180	1144+402		1.09	1.0		.9	120	12	88	5 ± 7	129	-40 ± 13	o	1	2	2
181	1144–379		1.05	2.2	1.1		393	13	65	1 ± 8	85	50 ± 12	c		4	2
182	1145–071		1.34	1.2		1.0	114	10	64	-27 ± 11	121	-2 ± 19	c	1	2	2
183	1148–001		1.98	1.9		2.5	21	9	86	-103 ± 50	74	-119 ± 52	c	3	4	
184	1150+812		1.25	1.2		1.2	60	10	75	13 ± 8	110	20 ± 9	d	2	2	
185	1156+295		.73	1.5		1.3	589	13	125	-16 ± 4	205	-2 ± 7	c	2	2	2
186	1213+350		.86	1.0		1.2	16	8	44	-58 ± 22	21	6 ± 13	d	1	4	4
187	1213–172					1.2	18	8	160	36 ± 10	347	-93 ± 44	c	1	4	
188	1216+487		1.08	1.1		.7	15	9	28	-1 ± 21	42	-2 ± 23	d	1	1	1
189	1219+044		.96	1.4		.6	836	11	32	2 ± 2	157	-10 ± 9	d	1	1	1
190	1219+285		.10	.7		1.5	18	9	84	15 ± 37	54	-24 ± 24	c	2	1	
191	1221+809			.5	.4		19	10	62	-36 ± 9	35	-18 ± 4	d	1	2	2
192	1222+037		.96	1.2		1.0	53	10	71	56 ± 21	56	-82 ± 27	c	2	4	4
193	1226+023	3C273B	.16	43.4	41.4		1012	9	101	-227 ± 58	48	-137 ± 21	o		4	
194	1226+373		1.51	.9	.2		13	7	162	17 ± 46	180	-69 ± 62	d	1	4	
195	1228+126	3C274	.00	71.9			407	12	90	-10 ± 7	118	2 ± 9	c	3	1	1
196	1236+077		.40	.7		.6	16	8	58	-1 ± 40	108	157 ± 56	d	1	4	4
197	1237–101		.75	1.5		1.6	21	6	31	6 ± 22	104	129 ± 21	c		4	
198	1243–072		1.29	.9		.7	31	7	77	-83 ± 12	90	-39 ± 71	c	1	4	
199	1244–255		.64	2.3		1.4	76	10	125	2 ± 30	48	-44 ± 14	c		2	4
200	1251–713						18	7	53	-51 ± 43	73	-123 ± 51	d		4	

(continued on next page)

(Table 4. continued)

No	Source	Alter.	Redsh.	Flux (Jy) 6 cm	11 cm	15 cm	Number sess	pts	R.A. cos(δ) AlSd μas	Drift μas/year	Declination AlSd μas	Drift μas/year	Stability criteria 1	2	3	4
201	1252 + 119		.87	.7		1.8	35	7	37	70 ± 25	32	-5 ± 29	d	1	4	4
202	1253 − 055	3C279	.54	15.3		11.8	223	11	202	195 ± 32	152	-72 ± 33	o	2	4	4
203	1255 − 316		1.92	1.4		1.6	144	11	77	65 ± 24	69	122 ± 23	c		4	4
204	1257 + 145					2.9	14	8	123	-181 ± 80	100	148 ± 74	d	1	4	
205	1300 + 580						197	9	89	-12 ± 6	45	-1 ± 5	o	1	1	1
206	1302 − 102		.29	.8		1.0	48	11	95	83 ± 16	109	120 ± 44	c	1	4	4
207	1308 + 326		1.00	1.5	1.6		1314	13	233	-3 ± 10	232	17 ± 10	d	1	2	2
208	1308 + 328		1.65	1.1			34	7	66	22 ± 17	127	72 ± 25	n		4	4
209	1313 − 333		1.21	1.1		1.2	177	11	35	-4 ± 10	132	-19 ± 50	c	1	1	1
210	1315 + 346	OP326	1.05	.3	.5		21	10	75	7 ± 10	53	-39 ± 17	c	1	1	
211	1334 − 127		.54	2.8		1.9	1670	13	183	-18 ± 6	108	-10 ± 6	o	1	2	2
212	1342 + 663		1.35	.8	.6		39	10	60	5 ± 13	84	-19 ± 17	d	1	1	1
213	1347 + 539		.98	1.0		.9	14	9	117	-117 ± 35	118	-32 ± 19	d	2	4	
214	1349 − 439		.05	.8	.5		21	9	27	-17 ± 42	30	33 ± 42	c		1	
215	1351 − 018		3.71	.8		.8	434	11	121	6 ± 8	111	34 ± 10	c	1	2	2
216	1354 + 195		.72	2.6		1.8	124	12	104	12 ± 12	107	16 ± 18	o	2	2	2
217	1354 − 152		1.89	.8		1.2	91	10	378	-8 ± 68	430	82 ±116	c	1	4	4
218	1357 + 769						861	11	98	-1 ± 3	116	5 ± 2	c	1	1	1
219	1402 + 044		3.21	.7		.6	41	8	253	17 ± 46	201	-34 ± 71	c	1	2	2
220	1404 + 286	OQ208	.08	2.9		1.7	1156	12	39	2 ± 2	139	47 ± 5	o	1	2	2
221	1406 − 076		1.49	.8		1.3	31	10	32	-9 ± 12	33	31 ± 17	c	1	1	
222	1413 + 135		.25	1.2		.9	36	12	81	19 ± 12	59	36 ± 16	o	3	2	2
223	1418 + 546		.15	1.1		1.0	356	12	129	-7 ± 5	109	9 ± 4	d	2	2	2
224	1424 − 418		1.52	2.2		2.2	296	13	82	-23 ± 12	125	-8 ± 23	o		2	2
225	1435 + 638		2.07	.8		1.6	15	8	51	54 ± 23	40	-4 ± 34	d	3	4	4
226	1442 + 101	OQ172	3.54	1.1		2.0	30	9	156	31 ±103	103	9 ± 62	d	3	2	2
227	1448 + 762		.90	.7		1.0	21	8	45	-72 ± 31	89	-41 ± 28	d	1	4	4
228	1451 − 375		.31	1.8		1.4	114	11	103	-34 ± 17	107	-22 ± 49	c		2	2
229	1451 − 400		1.81	.6	.7		27	7	133	-3 ± 57	78	24 ± 49	c		1	1
230	1458 + 718	3C309.1	.90	3.8		6.9	18	9	69	36 ± 18	132	-188 ± 33	o	3	4	4
231	1459 + 480					.5	12	7	20	25 ± 12	20	20 ± 17	d	1	2	2
232	1502 + 106		1.83	2.5		2.0	567	10	132	-25 ± 14	45	17 ± 3	o	1	2	2
233	1504 − 166		.88	2.8		2.2	29	6	90	16 ± 76	80	11 ± 55	c	1	1	1
234	1508 + 572		4.30	.3			51	7	80	-52 ± 15	109	-37 ± 22	c		4	4
235	1510 − 089		.36	4.4		3.1	315	11	166	-4 ± 13	127	-17 ± 12	o	1	2	2
236	1511 − 100		1.51	1.2		.9	19	8	210	-97 ± 31	90	-4 ± 57	c	1	4	
237	1514 + 197		1.07	.5		.5	12	8	37	-8 ± 5	62	28 ± 10	d	1	1	
238	1514 − 241		.05	1.9		1.9	215	10	96	-31 ± 14	69	6 ± 22	c		1	2
239	1519 − 273			1.8		1.0	183	11	112	-11 ± 10	110	-8 ± 11	c		2	2
240	1538 + 149		.61	2.0		1.5	35	8	133	-24 ± 38	165	23 ± 49	d	1	2	2
241	1546 + 027		.41	1.1		.8	41	11	96	22 ± 16	154	12 ± 57	c	1	2	2
242	1547 + 507		2.17	.7	.7		14	6	28	45 ± 18	28	31 ± 20	d	3	2	1
243	1548 + 056		1.42	2.2		2.3	216	11	83	-33 ± 12	104	125 ± 21	o	2	4	4
244	1557 + 032		3.89	.5	.5		27	6	174	-12 ± 43	355	35 ±152	c		4	4
245	1600 + 335					2.7	16	6	213	21 ± 12	61	38 ± 12	d	1	2	2
246	1604 − 333					.6	20	8	48	56 ± 50	110	22 ± 71	d		4	
247	1606 + 106		1.23	1.4		1.0	1211	13	190	21 ± 4	195	1 ± 5	d	1	2	2
248	1610 − 771		1.71	5.6	3.8		260	13	155	36 ± 29	229	10 ± 28	o		2	2
249	1611 + 343		1.40	2.3	2.4		1055	13	119	-11 ± 2	182	14 ± 5	c	1	2	2
250	1614 + 051		3.22	.9		.6	117	10	72	15 ± 13	104	-25 ± 28	c	1	2	2

(continued on next page)

(Table 4. continued)

No	Source	Alter.	Redsh.	Flux (Jy) 6 cm	11 cm	15 cm	Number sess	pts	R.A. cos(δ) AlSd μas	Drift μas/year	Declination AlSd μas	Drift μas/year	Stability criteria 1	2	3	4
251	1622 − 253		.79	2.2	2.3		1246	13	89	-3 ± 5	82	-18 ± 7	o	1	1	1
252	1622 − 297		.81	1.9		2.2	41	9	72	18 ± 43	58	-22 ± 44	c		1	1
253	1624 + 416		2.55	1.6		1.5	31	10	78	7 ± 19	118	-7 ± 30	d	2	1	1
254	1633 + 382	1633+38	1.81	4.1		2.1	433	11	146	15 ± 12	128	5 ± 12	o	1	2	2
255	1637 + 574		.75	1.8		1.4	258	12	102	6 ± 10	123	17 ± 19	d	1	2	2
256	1638 + 398	NRAO512	1.67	1.2		1.1	814	12	169	-11 ± 8	115	23 ± 4	o	1	2	2
257	1641 + 399	3C345	.59	5.7		7.6	1087	10	335	85 ± 44	210	75 ± 9	o	1	4	4
258	1642 + 690		.75	1.4		1.7	146	11	86	4 ± 5	64	23 ± 5	d	2	2	2
259	1652 + 398	DA426	.03	1.3	1.5		207	11	57	-2 ± 6	89	34 ± 10	c	2	2	2
260	1655 + 077		.62	1.6		1.6	18	9	62	-23 ± 18	63	28 ± 38	c	3	1	1
261	1656 + 053		.88	1.4		1.6	45	9	1304	205 ± 45	294	22 ± 6	c	2	4	4
262	1657 − 261					1.1	30	10	39	43 ± 16	97	45 ±106	c		1	
263	1705 + 018		2.58	.5	.5		42	9	48	15 ± 10	48	85 ± 16	d	1	4	4
264	1706 − 174						37	11	66	-49 ± 36	73	-52 ± 53	d	1	4	
265	1717 + 178			.9		1.0	15	8	83	25 ± 21	31	-6 ± 16	o	1	1	1
266	1725 + 044		.29	.9		.8	15	11	81	43 ± 23	147	-41 ± 75	d	1	2	4
267	1726 + 455		.71	.6	.7		755	11	176	-17 ± 7	89	14 ± 3	d	1	2	2
268	1730 − 130	NRAO530	.90	4.2	4.9		599	11	90	20 ± 12	144	71 ± 26	o	2	4	4
269	1732 + 389		.98	1.1	.7		41	7	95	9 ± 4	129	-1 ± 16	c	1	1	4
270	1738 + 476		.32	.9		.9	18	9	46	-41 ± 8	28	5 ± 10	c	1	2	2
271	1739 + 522		1.38	2.0	1.9		1366	13	303	-3 ± 6	344	-1 ± 7	c	1	4	4
272	1741 − 038		1.06	2.3		5.6	2158	13	212	-18 ± 4	146	16 ± 4	o	1	3	3
273	1743 + 173		1.70	.9		.9	29	8	116	-36 ± 17	264	25 ± 12	d	1	2	4
274	1745 + 624		3.89	.6	.6		411	10	138	3 ± 9	103	-10 ± 7	d	2	2	2
275	1749 + 096		.32	2.5		1.1	1545	13	189	5 ± 4	203	-3 ± 6	c	1	2	2
276	1749 + 701		.77	1.1		1.1	20	6	36	63 ± 16	76	-42 ± 18	d	2	4	4
277	1751 + 288					1.1	16	6	17	25 ± 9	24	-45 ± 29	o	1	2	
278	1758 + 388		2.09	.9		.6	24	8	97	10 ± 17	124	-61 ± 15	c		4	4
279	1800 + 440		.66	1.0		.8	12	6	56	-79 ± 23	24	-60 ± 9	d	1	4	
280	1803 + 784		.68	2.6		2.6	1942	13	199	-3 ± 3	152	0 ± 3	c	1	2	2
281	1806 + 456		.83	.7		.5	12	7	92	-77 ± 52	32	-32 ± 15	c		4	
282	1807 + 698	3C371	.05	1.7		3.1	249	13	71	12 ± 3	84	7 ± 4	c	2	2	2
283	1815 − 553						145	13	103	33 ± 39	102	23 ± 24	o		2	2
284	1821 + 107		1.36	1.2	.9		19	8	39	47 ± 26	34	36 ± 29	c	1	2	
285	1823 + 568		.66	1.7		1.6	164	11	98	-1 ± 8	93	23 ± 8	d	1	1	1
286	1830 + 285		.59	1.0		1.3	11	7	62	5 ± 23	27	3 ± 20	d	2	1	1
287	1831 − 711		1.36	1.1	1.3		19	8	102	151 ± 39	9	3 ± 8	c		4	4
288	1842 + 681		.47	.9		1.2	12	8	58	37 ± 22	60	44 ± 17	d	1	2	2
289	1845 + 797	3C390.3	.06	4.5		7.3	29	11	170	65 ± 57	187	26 ± 55	d	2	4	4
290	1849 + 670		.66	.6	.9		121	7	31	-31 ± 8	74	63 ± 6	d	2	4	4
291	1856 + 737	1856+736	.46	.4	.4		13	7	36	37 ± 12	48	-69 ± 10	d	1	4	
292	1901 + 319	3C395	.63	1.8		3.1	28	10	184	-67 ± 28	119	68 ± 25	o	3	4	4
293	1908 − 201					2.3	387	12	60	0 ± 8	172	-25 ± 18	c		2	2
294	1920 − 211						63	10	124	10 ± 26	197	53 ± 49	c		4	2
295	1921 − 293		.35	14.3	4.6		1358	13	123	1 ± 7	185	-37 ± 16	o	1	2	2
296	1923 + 210						97	10	59	-42 ± 18	47	-30 ± 12	c	2	2	2
297	1928 + 738		.30	3.3		3.0	129	11	99	-20 ± 10	170	-11 ± 16	o	2	2	2
298	1933 − 400		.96	1.4	1.2		26	10	33	5 ± 11	34	-33 ± 26	c		1	
299	1936 − 155		1.66	.8		1.3	46	9	66	17 ± 18	109	36 ± 30	c	1	2	2
300	1937 − 101		3.79	.8		.9	16	9	170	-17 ± 20	43	-31 ± 20	c	1	2	2

(continued on next page)

(Table 4. continued)

No	Source	Alter.	Redsh.	Flux (Jy) 6 cm	11 cm	15 cm	Number sess	pts	R.A. cos(δ) AlSd μas	Drift μas/year	Declination AlSd μas	Drift μas/year	Stability criteria 1	2	3	4
301	1947+079		2.70	.7		.5	28	6	112	87 ±279	175	935 ±239	n		4	4
302	1954+513		1.22	1.6		1.4	43	10	40	3 ± 10	45	-18 ± 12	d	1	1	1
303	1954–388		.63	2.0		1.0	373	11	56	12 ± 10	88	-34 ± 20	d		2	2
304	1958–179		.65	2.7		1.1	839	13	98	4 ± 4	90	2 ± 6	o	1	1	1
305	2000–330		3.78	1.0		1.1	21	9	85	-125 ± 56	107	27 ±155	d		4	
306	2007+777		.34	1.3		1.2	241	11	303	45 ± 13	56	3 ± 3	o	1	4	4
307	2008–159		1.18	.9		.6	84	11	88	15 ± 15	139	-72 ± 33	o	1	4	
308	2021+317						13	8	35	-35 ± 24	42	16 ± 24	d	1	1	
309	2029+121		1.22	1.3		1.1	20	8	34	-10 ± 13	38	-54 ± 30	d	1	4	4
310	2037+511	3C418	1.69	3.8		5.0	353	12	54	0 ± 3	45	1 ± 3	d	3	1	1
311	2037–253		1.57	.7		.9	11	6	66	184 ± 19	63	-149 ± 29	c		4	
312	2052–474		1.49	2.5	3.0		70	12	106	-22 ± 31	111	-22 ± 49	d		2	4
313	2059+034		1.01	1.4		.6	12	10	48	-32 ± 8	63	-13 ± 20	d	1	2	4
314	2106–413		1.05	2.3	2.1		22	9	123	79 ± 28	59	-21 ± 25	d		4	
315	2109–811						14	5	18	-50 ± 30	78	152 ±148	d		4	
316	2113+293		1.51	1.5		1.1	139	11	61	-8 ± 5	371	15 ± 34	d	1	3	3
317	2121+053		1.94	3.2		2.5	851	13	397	78 ± 10	73	-1 ± 3	o	1	4	4
318	2126–158		3.28	1.2		.9	180	12	96	6 ± 13	70	-74 ± 15	c	1	4	4
319	2128–123		.50	2.0		1.7	700	12	249	37 ± 27	234	20 ± 47	o	2	2	2
320	2131–021		1.28	2.1		2.2	15	8	19	-63 ± 4	22	99 ± 16	c	1	4	
321	2134+004	2134+00	1.93	11.5		6.5	909	13	70	-38 ± 18	94	-40 ± 26	o	1	2	2
322	2136+141		2.43	1.1		1.2	278	12	122	24 ± 9	49	-19 ± 5	d	1	2	2
323	2143–156		.70	.5		1.0	18	9	84	17 ± 17	213	-55 ±109	d	2	4	
324	2144+092		1.11	1.0		.8	24	9	507	35 ± 9	142	-29 ± 15	c	1	4	
325	2145+067		1.00	4.4		3.1	1696	13	439	-5 ± 14	180	22 ± 7	d	1	4	4
326	2149+056		.74	1.0		1.1	40	12	419	-72 ± 52	222	-46 ± 70	c	1	4	4
327	2149–307	2149–306	2.35	1.3		1.4	16	6	112	-21 ± 50	90	-4 ± 53	o		1	
328	2150+173			1.0		1.1	21	6	131	-57 ± 50	82	-30 ± 34	d	2	4	4
329	2155–152		.67	1.7		1.8	61	10	231	76 ± 67	166	193 ± 67	o	1	4	4
330	2200+420	VR422201	.07	2.9		4.2	955	12	134	-10 ± 6	268	0 ± 10	o	1	2	2
331	2201+315		.30	2.8		2.0	305	13	167	11 ± 8	296	32 ± 12	o	1	2	2
332	2209+236					.7	18	11	69	42 ± 22	31	15 ± 12	d	1	2	2
333	2210–257		1.83	.8		.9	11	6	80	43 ± 11	71	-61 ± 15	c		4	
334	2216–038		.90	1.6		1.6	441	12	94	4 ± 8	211	24 ± 30	o	1	2	2
335	2223–052	3C446	1.40	4.1		5.2	248	9	165	36 ± 15	206	-73 ± 23	c	3	4	4
336	2227–088		1.56	1.4		1.3	61	11	153	52 ± 20	67	-63 ± 19	c	1	4	4
337	2229+695			.8	.6		18	9	82	-98 ± 36	59	-12 ± 25	d	1	4	4
338	2230+114	CTA102	1.04	4.0	4.9		158	12	185	21 ± 10	77	-18 ± 7	o	2	2	2
339	2232–488		.51	.9	.8		13	6	41	116 ± 46	44	-104 ±145	d		4	
340	2233–148		$\geq$ .61	.6	.5		18	9	72	77 ± 35	31	-97 ± 36	c	1	4	
341	2234+282		.80	1.1		.9	1689	13	384	-73 ± 9	264	-45 ± 6	c	1	4	4
342	2243–123		.63	2.7	2.7		369	12	113	26 ± 11	350	-88 ± 46	o	1	4	4
343	2245–328		2.27	.6	2.0		31	10	44	70 ± 20	58	-84 ± 45	c		4	
344	2251+158	3C454.3	.86	10.0		10.5	1067	10	296	-222 ± 58	73	5 ± 28	o		4	4
345	2253+417		1.48	1.0		1.5	40	9	48	-21 ± 11	78	42 ± 23	c	1	2	2
346	2254+024		2.09	.5	.5		23	9	116	71 ± 54	87	-118 ± 62	c	1	4	4
347	2254+074		.19	.5		.9	20	9	79	-69 ± 14	27	-16 ± 7	d	1	4	
348	2255–282		.93	2.1	1.4		886	13	124	-3 ± 9	100	-15 ± 11	o	2	2	2
349	2318+049		.62	1.0	1.2		125	11	103	12 ± 19	48	12 ± 28	c	1	1	1
350	2319+272		1.25	1.1		1.1	27	10	282	32 ± 42	176	88 ± 26	d	1	4	4

(continued on next page)

(Table 4. continued)

No	Source	Alter.	Redsh.	Flux (Jy) 6 cm	11 cm	15 cm	Number sess	pts	R.A. cos(δ) AlSd μas	Drift μas/year	Declination AlSd μas	Drift μas/year	Stability criteria 1	2	3	4
351	2320 − 035		1.41	.4		.8	66	11	79	40 ± 22	101	-92 ± 50	c	2	4	4
352	2326 − 477		1.31	2.1	2.4		28	7	141	-79 ±157	28	-69 ± 57	d		4	
353	2328 + 107		1.49	1.0		1.0	13	6	16	32 ± 20	53	115 ± 66	c	2	4	
354	2329 − 162		1.15	1.9		1.2	11	5	28	100 ± 27	37	-48 ± 40	d	2	4	
355	2331 − 240		.05	.9		.9	22	9	161	-102 ± 57	113	43 ± 54	c		4	
356	2335 − 027		1.07	.6		.6	28	10	74	14 ± 36	107	-14 ± 80	c	1	1	
357	2337 + 264					1.0	15	9	147	271 ± 44	197	308 ± 91	o	3	4	4
358	2344 + 092	2344+09A	.67	1.4		1.9	27	11	412	169 ± 94	507	203 ±162	c	2	4	4
359	2345 − 167		.58	3.5	4.1		130	10	147	16 ± 32	86	-94 ± 32	o	1	4	
360	2351 + 456		1.99	1.5	1.4		28	8	36	-15 ± 20	29	24 ± 20	o	2	1	2
361	2355 − 106		1.62	1.6	.5		139	11	161	6 ± 20	175	17 ± 40	c	1	2	2
362	2356 + 385		2.70	.7		.5	206	7	73	41 ± 4	141	-82 ± 11	c		4	4

Maintenance of the link to Hipparcos

N. Zacharias

U.S. Naval Observatory (USNO), Washington D.C., USA

Abstract. The optical wavelength astrometric reference frame is currently based on observations made by the Hipparcos astrometric satellite. Unfortunately, since the Hipparcos Celestial Reference Frame (HCRF) is comprised of bright stars which are sparsely distributed on the sky, the frame often is inappropriate for astronomical and astrometric programs requiring a denser distribution of faint stars. Thus, significant effort has been channeled into the densification of the HCRF. We discuss optical reference frame densification programs and the maintenance of the link between these programs and the HCRF.

1 Introduction

Following IAU resolution B1.2 (24th General Assembly, Manchester, 2000) only Hipparcos stars without known multiplicity (flags C,G,O,V,X) are to be used for astrometric reference frame link and densification work. This subset of Hipparcos stars defines the Hipparcos Celestial Reference Frame (HCRF). However, in many cases as mentioned below, Hipparcos stars are too bright and too sparse to be used as reference stars directly. Almost all current densification projects rely on the Tycho-2 Catalogue (Høg et al., 2000), which is on the HCRF (within its limits).

The Tycho-2 actually involves 2 aspects. Positions near the central Hipparcos epoch (1991.25) are based on the Hipparcos/Tycho space mission data (ESA 1997). The accuracy of densification catalogs here depend on how successful the Hipparcos Catalogue and the Tycho data have been put on the same system, which is believed to be on the sub-mas level. The Tycho-2 proper motions on the other hand have been derived from a combination of many ground-based, early epoch catalogs, which have been put onto the HCRF as good as possible before deriving the proper motions. Particularly at the faint end, systematic errors are possible. The projects discussed here are not yet ready to externally assess the link between HCRF and Tycho-2. However, some projects have the potential to allow such an evaluation in the near future.

Over 10 years after the successful Hipparcos mission a first attempt was made to improve upon the original link between the HCRF and the extragalactic ICRF (Bobylev et al., 2004). The possible error in the alignment between the 2 systems increases with time, approaching about 3 mas estimated standard error per axis at the 2005 epoch. The ongoing USNO extragalactic link program has the potential to externally test the HCRF to ICRF link. Observations were completed by end of 2004 and reductions are in progress. First results were presented at the Lowell astrometry meeting (Zacharias & Zacharias, 2005).

For the Hipparcos system maintenance issue in a broad sense, several observational programs are ongoing. These fall into 3 categories: 1) densification of the reference frame at optical wavelengths, 2) extension of the Hipparcos frame to infrared (IR) wavelengths, and, 3) critical check on the radio to optical reference frame link itself.

An overview and the status of these projects is given below. Much is work in progress without results on reference frame issues at this time.

2 Densification

An overview is given in the IAU reviews about ground-based (Zacharias, 1998) and space-based (Röser 1998) densification programs. There is currently no astrometric space mission close to a launch date.

Table 1 gives an overview of the ground-based densification programs. All except the 2MASS project (see below) are at optical wavelengths. The meaning of the column "type" is: S = astrometric program but selected area in the sky only, A = all-sky astrometric, and G = general survey, no emphasize on astrometry. The number of stars in each catalog is given in millions (M). The quoted positional errors are 1 sigma estimated external errors per coordinate. When a range is given, the errors depend mainly on the magnitude. Release years beyond 2005 are estimates.

NOMAD is the Naval Observatory Merged Astrometric Dataset (Zacharias et al. 2004). For each star "the best" astrometry and photometry is picked from various catalogs including Hipparcos, Tycho-2, UCAC, USNO-B, and 2MASS. Cross-references are given in NOMAD but not all columns from the original catalogs are copied into NOMAD. NOMAD is not a compiled catalog. Although all catalogs merged into NOMAD are on the ICRF within their limitations, systematic differences between individual catalogs do exist. The original catalog positions merely have been copied into NOMAD. Figure 1 shows an example for the UCAC to USNO-B differences, most of which can be attributed to the USNO-B.

2.1 UCAC

A major program for the densification of the optical reference frame is the UCAC project (USNO CCD Astrograph Catalog). This all-sky survey gives 20 mas positions for stars in the about 10 to 14 mag range, with a limiting magnitude of about R=16. The first release (UCAC1) was published in March 2000 (Zacharias et al., 2000), containing positions and proper motions of 27 million stars on the Hipparcos System (HCRF). Reductions of the UCAC1 positions rely on the original Tycho Catalogue (Tycho-1). UCAC1 proper motions of bright stars ($R \leq 12^m$) utilize mainly Astrographic Catalogue (AC2000) data (Urban et al., 1998), and faint stars the USNO A2 (Monet, 1998).

In September/October 2001, the astrograph was relocated from CTIO (Chile) to the Naval Observatory Flagstaff Station (NOFS) in Arizona. All sky observations were completed in May 2004. The last Kitt Peak 0.9m run for the extragalactic link program was performed in December 2004 with parallel observing at the astrograph.

The second data release (UCAC2) includes observations up to mid December 2002. Contrary to UCAC1 the UCAC2 positions are based on the Tycho-2 catalog and improved proper motions are provided utilizing a part of recent re-measures of the AGK2 plates performed on the USNO Washington StarScan measuring machine, as well as PMM remeasures of the NPM and SPM data. The UCAC2 contains over 48 million stars, covers 86% of the sky and was released at the 2003 IAU in Sydney (Zacharias et al., 2004).

For the final UCAC3 the pixel raw data will be re-reduced to achieve a higher completeness and improve on astrometric and photometric reductions. The over 1200 tapes (4.5 TB) are being loaded to RAID disk arrays; however, UCAC3 will not be ready before 2006.

Table 1. Important, recent catalogs for astrometry.

Name of catalog	mag. range	bandpass (approx.)	number of stars	pos.err. (mas)	type	release year	comment
ACR-2	10–17.5	R	1.2 M	26– 60	S	1999	equator. areas
M2000	– 17	V	2.3 M	35–100	S	2001	+11 to +18 decl.
CMC12	9 – 17	r'	6.3 M	36–113	S	2002	−3 to +3 decl.
CMC13	9 – 17	r'	many	35–100	S	2003	+3 to +30 decl.
UCAC1	8 – 16	579-643	27 M	25– 70	(A)	2000	−90 to −15 decl.
UCAC2	8 – 16	...	48 M	20– 70	(A)	2003	−90 to +40 decl.
UCAC3	8 – 16	...	70 M	20– 70	A	2006	all sky
GSC-2.2	12 – 20	B,V	456 M	300	G	2002	posit., photom.
USNO-A2	12 – 20	...	526 M	200	G	2001	posit., photom.
USNO-B	12 – 20	...	1000 M	200	G	2002	incl. proper motions
SDSS	15 – 23	u,b,v,r,z	many	50–150	G	2003	about 5000 sq.deg
2MASS		J,K,H	471 M	60–100	G	2003	infrared survey
NOMAD	-1 – 20	B,V,R,J,H,K	1100 M	10–200	A	2005	merged data set

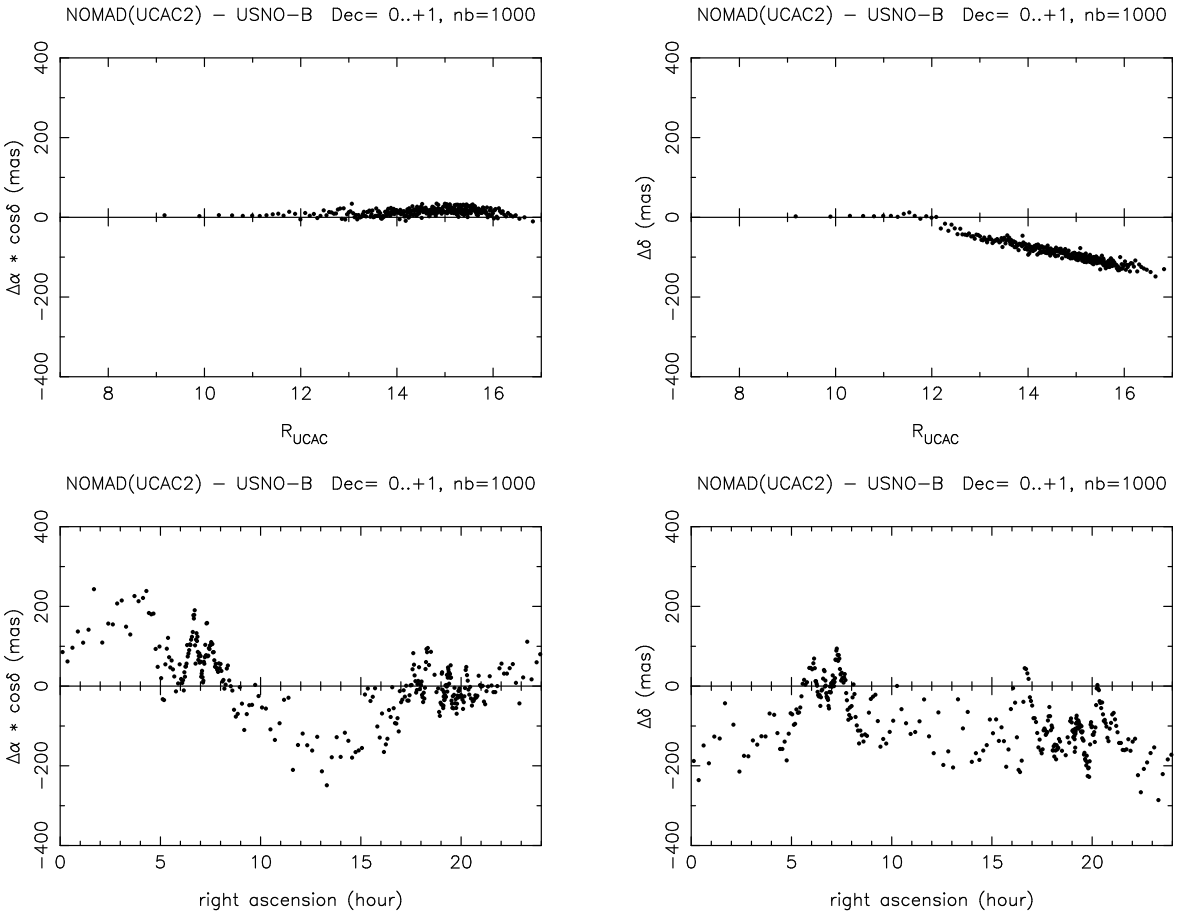

Fig. 1. UCAC2 minus USNO-B systematic position differences. Examples are shown as a function of magnitude and right ascension.

2.2 Other densification projects

Other major densification projects are the CMC, M2000 and ACR. The Carlsberg Meridian Circle (CMC12 and CMC13) program, is a joint effort of institutes from Denmark, UK, and Spain. The declination zone −3 to +30 degree has been observed in drift-scan mode with a re-furbished transit circle instrument (Evans, Irwin &Helmer, 2002). A northern extension is being observed. A similar project, the M2000 catalog has been produced by the Bordeaux Observatory for the +11 to +18 degree zone (Ducourant et al. 2002). The second release of the Astrometric Calibration Regions (ACR) obtained from the Flagstaff Astrometric Scanning Transit Telescope (FASTT) are available since a few years (Stone, Pier & Monet, 1999). All these projects use Tycho stars to link to the Hipparcos system.

The Sloan Digital Sky Survey (SDSS) concluded its deep 5-band photometric survey in areas around the galactic north pole. Astrometry is tied to the HCRF via Tycho-2 and preliminary UCAC positions, where available. When using UCAC data, the SDSS positions are more accurate than using Tycho-2 stars by a factor of about 2 due to the high accuracy and density of UCAC.

World wide web links for all mentioned projects are provided in Table 2. Most projects are ongoing and only preliminary data are available now. A comparison between the UCAC1 and Tycho-2 has been published (Zacharias et al. 2000). The current, astrometric, ground-based catalogs have mainly systematic errors as a function of magnitude, typically on the 20 to 30 mas level. Variations as a function of color as well as location in the sky (mainly zonal, declination dependent) are also possible. A detailed comparison between the various position catalogs is planned in the near future.

Table 2. World wide web links to densification projects.

Project	link
ACR-2	ftp.nofs.navy.mil /pub/outgoing/calibregions
M2000	www.obs.u-bordeaux1.fr/m2a/soubiran/equipe/JF/M2000/m2000.htm
CMC12,13	www.ast.cam.ac.uk/ dwe/SRF/cmc12.html
UCAC	ad.usno.navy.mil/ucac
GSC-2.2	www-gsss.stsci.edu/gsc/gsc2/GSC2home.htm
USNO A,B	www.nofs.navy.mil/projects/pmm/
SDSS	www.sdss.org
2MASS	www.ipac.caltech.edu/2mass/
NOMAD	www.nofs.navy.mil/nomad

3 IR observations

3.1 2MASS

The major program to extend the Hipparcos frame into wavelengths other than optical or radio is the 2-micron All Sky Survey (2MASS) project. IR photometry (J,H,K) has been obtained with 2 identical telescopes (north, south) for over 400 million point sources. The astrometry is on the HCRF and the average error per catalog position coordinate is around 80 mas with much smaller systematic (zonal and magnitude dependent) errors.

In 2001, pre-release 2MASS data was obtained by USNO from R. Stiening (private communication) and a comparison with UCAC positions was made. Overall a very good agreement was found, with largest systematic position differences being 50 mas. The results helped to better understand systematic errors in the 2MASS data and lead to improvements in the reduction pipeline. For the final release a significant improvement in the accuracy of 2MASS positions was achieved, with similar random errors in positions as reported on the preliminary data (Zacharias et al., 2005).

End of 2002 new, preliminary 2MASS data were received and compared to preliminary UCAC2 positions. Observations for both projects were obtained almost at the same epoch. The 2MASS data is strictly reduced with Tycho-2 data for reference stars, as is UCAC2. Thus for stars not in Tycho-2 (mainly R $\geq$ 12) the UCAC2–2MASS differences are truly external. Some results are presented in Figures 2 and 3. Systematic errors as a function of magnitude are small except for the critical link area around 9 to 11th magnitude. There are also significant variations as a function of location in the sky and color of the stars (Figure 3). Note, the systematic differences are highlighted in these plots due to binning of a large number of stars. The average precision of a single star is about 20 to 70 mas in UCAC2 and 60 to 100 mas in 2MASS, while the systematic errors are only on the 10 to 20 mas level.

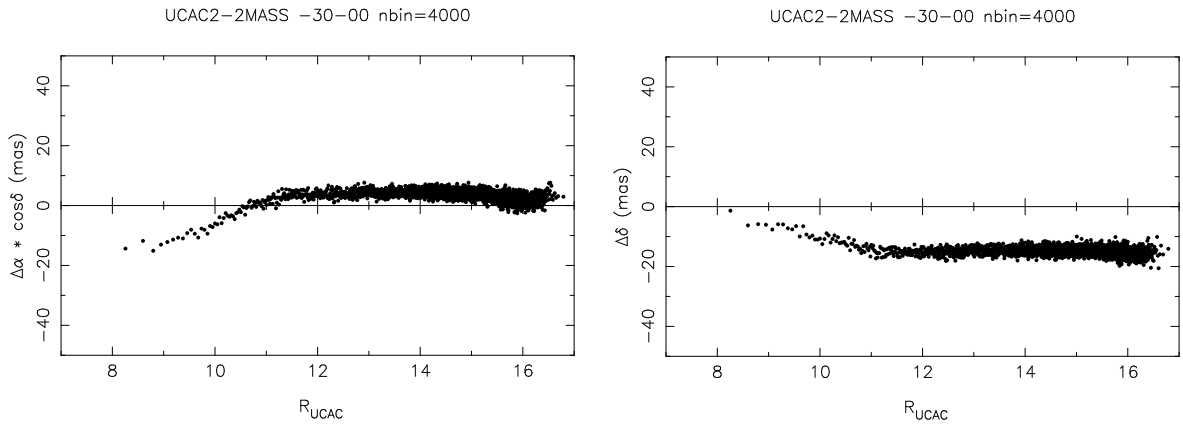

Fig. 2. Sample comparison between UCAC2 (optical) and 2MASS (IR) pre-release positions. Position differences for stars in the −30 to 0 degree declination range are shown as a function of UCAC red magnitude. Each dot represents the mean over 4000 stars to highlight systematic differences.

3.2 Other efforts

At the 1.55m Strand telescope in Flagstaff, test observations were performed with a large format (1k chip) IR detector of selected extragalactic link sources. Currently optical observations are being performed with an even larger field of view (2k detector) and lower noise characteristics.

As far as other wavelengths are concerned, radio observations are usually tied directly into the ICRF. X-ray and Gamma-ray observations are being linked to dense optical catalogs like the USNO A and B, thus are typically on the 200 mas level if an optical identification can be made at all.

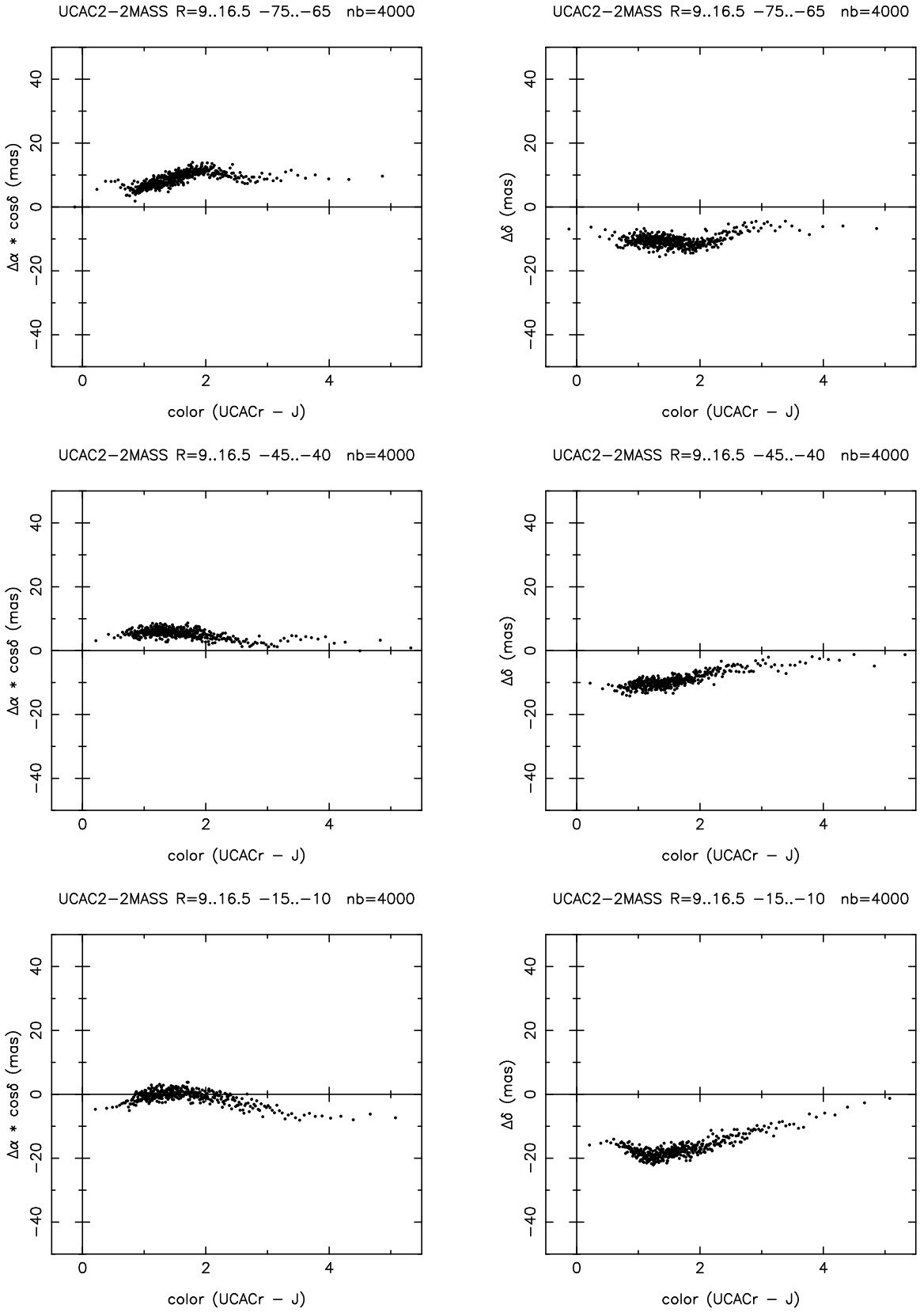

Fig. 3. Similar to the previous figure for UCAC−2MASS position differences (RA on the left, Dec on the right) are shown as a function of color. The data are split into declination zones (top to bottom), showing a clear variation with area in the sky.

4 Radio–optical extragalactic link program

A comprehensive extragalactic link program is part of the UCAC project. The goal is to eventually provide a link between the ICRS and the UCAC, independent of HCRF (using block adjustment procedures) and then quasi externally assess the HCRF-ICRF link accuracy. As a first step traditionally reduced CCD frames provide optical positions of ICRF counterparts supposedly on the HCRF, using Tycho-2 and UCAC anonymous secondary reference stars in a 2-step procedure. Preliminary results from a subset of the data were published (Assafin et al., 2003; Zacharias & Zacharias, 2005).

The Assafin et al. paper is based on optical positions of about 120 ICRF sources which were obtained in 3 observing runs at CTIO and KPNO during 2001, supplemented with some observations by the 1.6-meter LNA (Brazil) of optically faint targets. It uses the UCAC2 general-survey as reference stars.

The Zacharias & Zacharias paper is the first to utilize the special USNO astrograph observations performed in parallel with the deep CCD imaging. Advantages of this approach are:

same bandpass of astrograph and deep CCD frames (579–643 nm): minimizing differential refraction effects of the atmosphere

simultaneous observations of astrograph and deep field observations to avoid problems with unknown proper motions of anonymous secondary stars used to link the data

extra observing at the astrograph provides much higher precision of star positions than regular UCAC survey data alone

east and west of pier observations with the astrograph of ICRF fields provide good calibration of systematic errors to enhance the astrometric accuracy beyond the general UCAC survey data

The goal of this project is to improve the accuracy of the HCRF to ICRF link by a factor of 2 beyond what has been obtained initially with the Hipparcos and ground-based effort. This observational program was completed by end of 2004 and a total of about 500 ICRF sources (including extensions 1 and 2) are likely to show measurable optical counterparts on our deep CCD imaging data, covering both the northern and southern hemisphere.

5 Future Developments

The late Christian de Vegt envisioned a next generation, dedicated, astrometric survey telescope (de Vegt, Laux, & Zacharias, 2003; Laux & Zacharias, 2005). The USNO Robotic Astrometric Telescope (URAT) project is based on this design (Zacharias, 2005). The 0.85 m aperture 3.6m focal length planned instrument has a 4 degree field of view. The goal is to obtain positions of stars on the 5 to 10 mas level for the 14 to 18 mag range with a limiting magnitude of about 20. A direct tie to the defining ICRF sources would be possible. Narrow bandpass observations will also allow to access Hipparcos stars. Funds have been secured for the detector development (large-format, monolithic chip), and optical design studies are in the final stages.

Space-based projects of relevance for astrometry are the NASA Space Interferometry Mission (SIM, planet quest), the ESA GAIA mission and

NASA roadmap study Origins Billions Star Survey (OBSS) (Johnston et al., 2004). However, none have lauch dates before 2010.

References

Assafin, M., et al. 2003, AJ, 125, 2728

Bobylev, V. V., et al. 2004, Astronomy Letters, 30, 848

de Vegt, C., Laux, U., Zacharias, N. 2003, A dedicated 1-meter telescope for high precision astrometric sky mapping of faint stars, in "Small Telescopes in the New Millenium II. The Telescopes We Use." ed. T. Oswalt, Kluwer Acad. Publ. p.255

Ducourant, C. et al. 2002, A&A 376, 325

ESA, The Hipparcos and Tycho Catalogues, 1997, European Space Agency, publication SP-1200

Evans, D. W., Irwin, M. J., & Helmer, L. 2002, A&A 395, 347

Høg, E., et al., 2000, Astron.& Astroph. 355, L27

Johnston, K. J., et al., 2004, BAAS, 36, 1342, abstract 5.11, "The Origins Billion Star Survey"

Laux, U. & Zacharias, N., 2005, ASP Conf. Ser. 338, p. 106, Eds: P. K. Seidelmann & A. K. B. Monet, San Francisco

Monet, D. G. 1998, BAAS 30, 4, 1427

Extension of the optical reference frame: space based, in Highlights of Astronomy, Vol. 11A, p. 304, ed. J. Andersen, Kluver Acad. Publ.

Stone, R., Pier, J. R., & Monet, D. G. 1999, AJ, 118, 2488

Urban, S. E., Corbin, T. E., Wycoff, G. L., Martin, J. C., Jackson, E. S., Zacharias, M. I., & Hall, D. M., 1998, AJ, 115, 1212

Zacharias, N. 1998, Extension of the optical reference frame: ground based, in Highlights of Astronomy, Vol. 11A, p. 300, ed. J. Andersen, Kluver Acad. Publ.

Zacharias, N., Urban, S. E., Zacharias, M. I., Hall, D. M., Wycoff, G. L., Rafferty, T. J., Germain, M. E., Holdenried, E. R., Pohlman, J. W., Gauss, F. S., Monet, D. G., & Winter, L., 2000, UCAC1 paper, AJ, 120, 2131 (Oct. 2000)

Zacharias, N., Urban, S. E., Zacharias, M. I., Wycoff, G. L., Hall, D. M., Monet, D. G., & Rafferty, T. J., 2004, AJ 127, 3043 (May) "The Second US Naval Observatory CCD Astrograph Catalog (UCAC2)"

Zacharias, N., Zacharias, M. I., Urban, S. E., & Høg, E., 2000, Comparing Tycho-2 astrometry with UCAC1, AJ, 120, 1148

Zacharias, N., Monet, D. G., Levine, S. E., Urban, S. E., Gaume, G. L., & Wycoff, G. L., 2004, BAAS 36, 1418, abstract 48.15

Zacharias, M. I. & Zacharias, N., 2005, ASP Conf. Ser. 338, p. 184, Eds: P. K. Seidelmann & A. K. B. Monet, San Francisco

Zacharias, N., 2005, ASP Conf. Ser. 338, p. 98, Eds: P. K. Seidelmann & A. K. B. Monet, San Francisco

Zacharias, N., McCallon, H. L., Kopan, E., & Cutri, R. M., 2006 Extending the ICRF into the Infrared: 2MASS−UCAC Astrometry in Proceedings of IAU XXV (2003) JD16, eds. R. Gaume, D. McCarthy, J. Souchay, USNO publication, in press

Astro-photometric properties of the ICRF with respect to catalogues of quasars

J. Souchay, A. M. Gontier, and C. Barache

Observatoire de Paris, SYRTE, 61, av. de l'Observatoire, 75014 Paris, FRANCE

Abstract. After carrying out a cross-identification of the objects belonging both to the ICRF catalogue and to the most complete catalogue of quasars at optical wavelengths, (Véron-Cetty and Véron, 2003) we show some photometric as well as astrometric properties of the cross-identified objects (roughly 67% of the sample), comparing these properties to the general ones concerning the whole set of quasars.

1 Introduction

Since 1998, January 1st., the International Celestial Reference Frame (ICRF), consisting in a set of coordinates of extragalactic radio-sources, has been adopted by the IAU General Assembly (Kyoto, 1998) as the materialization of the International Celestial Reference System (ICRS), and must be considered by the entire astronomical community, as the conventional celestial reference frame. Despite that fact, rather few studies were devoted to the intrinsic properties of the objects of the ICRF obtained from other recent catalogues, and more specifically from catalogues of quasars obtained at optical and infrared wavelengths. This is one of the main purposes of this paper.

Moreover, in the prospect of a future densification of the ICRF, an increasing number of sources detectable from radio observations, and thus subject to possible VLBI observations, will undoubtedly be chosen as candidates to represent quasi-inertial directions in space, as it is the case at present for the 212 defining sources of the ICRF. Therefore it is interesting to evaluate the potential astrometrical improvements which should be brought by this densification, in particular concerning the sky coverage. This study is all the more interesting that in a reasonable future, with the arrival of space missions as GAIA, scheduled in the next decade, very accurate astrometric measurements of quasars and active galactic nuclei will be possible at optical wavelengths. Then the possibility of defining the new ICRF through the intermediary of the positioning of thousands of extragalactic objects, will certainly be seriously taken into account. Thus as an informative study, we consider here the total number of quasars detected today (Véron-Cetty and Véron, 2003), i.e. more than 48 000 objects, and their particularities, in the scope of such a future prospect, and in comparison with the present ICRF.

2 Generalities about quasars

Quasars are known for roughly 40 years now. The discovery of the first quasar was done in 1963, when Hazard, Mackey and Shimings, using the new technique of occultation of radiosources, got the position of the object named 3C273, with an extraordinary precision (at this epoch) of 1". Then Maarten Schmidt, working at Palomar Mount, identified 3C273 with an object of stellar aspect. The perfect correspondence between the optical and the radio positions let no doubt for the identification. The spectra obtained by M. Schmidt showed a series of emission lines, whose some were characteristics of the atom of hydrogen, all of them being

shifted toward lower wavelengths. Supposing that the other spectral lines were shifted with the same relative amount, Schmidt could identify by extrapolation well known ones, as the oxygen and the magnesium. Then he could measure the redshift $z = 0.158$.

Because of their astrometric and intrinsic physical properties, quasars must be considered as exceptional objects. Being the most powerful objects known in the universe today, their large redshifts suggest that they are very distant and that they were carried along with the expansion of the universe, even if these redshifts might arise from other phenomena as that related to the Hubble law. This is still subject to some debate. Presently most astronomers consider also that the question of what could generate such a tremendous power is solved, thus involving the presence of a supermassive black hole, located in the center of a previous galaxy, and attracting the surrounding matter. The mass of the central black hole may be a billion or more times the mass of the Sun, and the brightest quasars shine more powerfully than a thousand galaxies as ours.

With the exception of radio emission, which is often extended, the vast energy output of the quasars is concentrated into a very small area, which give them a quasi ponctual aspect, thus giving birth to their naming, "quasar" for "quasi stellar source". Fundamental characteristics can be found in their spectra, characterized by strong, broad and redshifted emission lines for wavelengths ranging in the optical and UV parts, together with a flat and often blue continuum from far infrared to X-ray.

Quasars' data are coming from a large variety of sources each of them having its own resolution and energy range. X-ray observations, characterized by a low resolution of the detectors necessitating an appropriate post-reduction with a standard software (IRAF, MIDAS), are done from satellites, as EXOSAT, ROSAT, ASCA, *Einstein*. For infra-red and optical wavelengths, spectal data, i.e. determination of the fluw w.r.t. the wavelength, can be obtained from ground-based telescopes, with radius at least 4 meters, because of the large magnitude of the quasars. Nevertheless, ground based telescopes of the order of 1 meter enable to carry out photometric data, as a magnitude in the usual UBVRIJHJK color range. The IRAS database provides far infrared data of the quasars, as a flux for each specific band filter, whereas radio telescopes enable to measure fluxes or brightness temperatures in specific frequency bands.

As soon as in 1971, i.e. less than 10 years after the discovery of the quasars, the first catalog of these exotic objects was published. It contained 202 objects (De Veny et al., 1971). Then, various observational programs lead to important increase of known quasars. All the observed ones were gathered on a regularly basis by Véron-Cetty and Véron, in ESO Scientific Reports (1984, 1985, 1987, 1989, 1991, 1993, 1996, 1998, 2000). In order to identify a quasar from any other object, Véron-Cetty and Véron (2001, 2003) have defined a quasar as a starlike object, or an object with a starlike nucleus with broad emission lines, brighter than magnitude $M_B = -23$. This last magnitude is estimated through a law involving the apparent magnitude m, the distance D, and corrective factors k and $\Delta m(z)$ (Véron-Cetty and Véron, 2001):

$$M = m + 5 - 5\log D - k + \Delta m(z) \tag{1}$$

Where the distance D is defined itself from the Hubble's law:
$D = c/H_0 \times A$

A being the photometric distance (Terrell, 1977) given by:

$$A = z\left[1 + \frac{z(1-q_0)}{\sqrt{1+2q_0z}+1+q_0z}\right] \tag{2}$$

In the equation above, k is dependent on the redshift, in the form: $k = -2.5\log(1+z)^{1-\alpha}$ and Δm is a correction to k as determined by this last equation, taking into account the spectral profile of the quasars.

In figure 1 we show the total number of quasars as recorded in the Véron-Cetty and Véron's publications, with respect to the year of publication. We can note that this number has dramatically increased in the recent years, showing an exponential type curve. This is due to the upcoming of new programs, as the 2dF (2 degrees field) QSO Redshift Survey (Crooms et al., 2000) as well as the SDSS (Sloan Digital Sky Survey) (Richards et al., 2001).

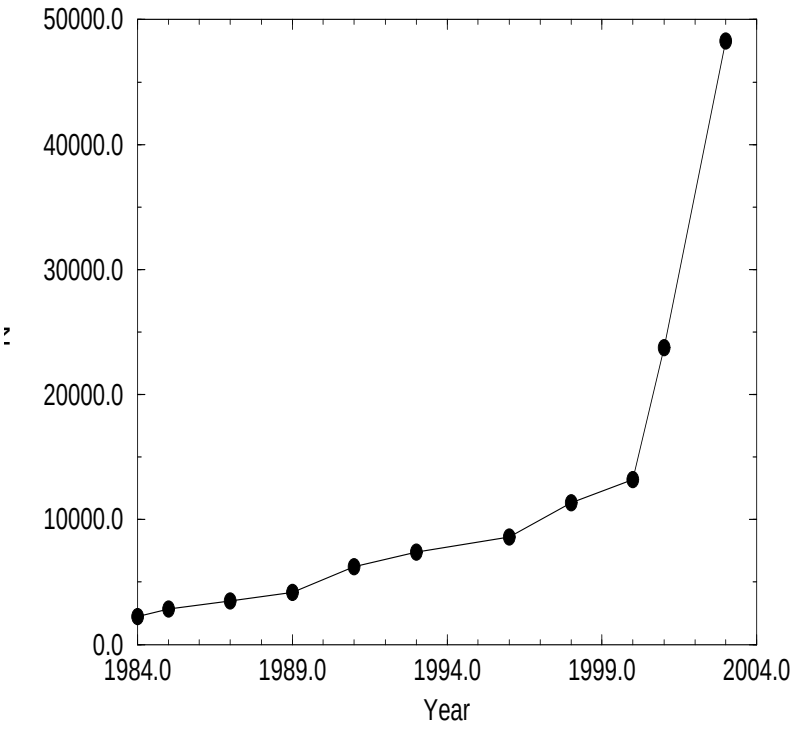

Fig. 1. Number of quasars recorded by Véron-Cetty and Véron since 1984 until 2003 in their various publications.

A first release of the 2dF QSO redshift Survey has almost doubled the number of known quasars (Véron Cetty and Véron, 2001). This release consisted in a catalog comprising more than 10 000 QSO's covering an effective area of 290 $\deg^2$. Their detection was based on single spectroscopic observations at the AAT (Anglo Australian Telescope). All the objects have their magnitude b_j included in the range $18.25 < b_j < 20.25$. In the second release, the total 2dF survey area is 740 deg^2, arranged in two $75^\circ \times 5^\circ$ declination strips centered on $\delta = -30^\circ$ and $\delta = 0^\circ$. These strips extend respectively from $\alpha = 21^h40^{mn}$ to $\alpha = 3^h15^{mn}$ and from $\alpha = 9^h50^{mn}$ to $\alpha = 14^h50^{mn}$

3 Cross-identification between ICRF and catalogues of quasars

The last version of the Véron-Cetty and Véron catalogue (Véron-Cetty and Véron, 2003), quoted as VCV2003 in the following, contains in addition to the anterior version the objects recorded in the second release of the 2dF quasar catalogue, and of the first part of the SLOAN catalogue. Therefore, it has almost doubled the number of known quasars whereas the number of active nuclei has also considerably increased: at total it contains 48 921 quasars, 876 B LAC objects, and 15 069 active galaxies, whose a majority, 11 777 ones, i.e. 78%, are Seyfert galaxies. Like the previous edition, the VCV2003 catalogue includes position at J2000.0, redshift and U,B,V photometry. When available, flux densities, expressed in Jy, at 6 cm and 11 cm are given, but in fact a very small proportion of objects have been observed at radio wavelengths: only 2850 quasars have been recorded at 6 cm (5.8 %) and only 1 418 (2.9 %) at 11 cm, nearly all of these last ones (1411 objects) have been observed in the two radio bandwidths.

Recall that the present access to the ICRS in radiowavelengths is given by the 667 extragalactic radio sources in ICRF-Ext.1 (IERS, 1999). In this extended version of the ICRF, four categories of sources are considered: defining sources, candidate sources, sources quoted as "other sources", and new sources. The first category designate 212 very stable sources whose coordinates are so stable that they have conventionally been fixed: their coordinates remain unchanged with respect to the first realization of the frame and they materialize the ICRF (Arias et al., 1995; Ma et al., 1998). The second category designates 294 sources which might be chosen as defining ones because they seem to be stable, but they need more observations to conclude about their astrometric quality. The "other" sources are useful to the densification of the frame, but do not present enough garantee of astrometric stability to be ranged in one of the two first categories. At last, a new category was added in the ICRF-Ext.1 catalogue with a set of 59 new sources which were previously not observed in the ICRF.

In table 1 we indicate the number of cross-identified objects between the ICRF and two catalogues of quasars, the PKS and the VCV2003 catalogues. We can remark that a large proportion of ICRF objects are not belonging to the VCV2003 catalogue: 38 % for the defining sources, 46 % for the candidate sources and 32 % for the other sources.

Thanks to the cross-identified objects above between the ICRF and the VCV2003 objects, it is possible, in the following, to compare the general characteristics of the ICRF (redshifts, magnitudes, flux) with respect to all the other extragalactic objects belonging to the VCV2003 catalogue.

4 Photometric properties of the ICRF quasars

In figures 2 and 3, we present respectively the histogramms of the V magnitudes of the 48921 quasars recorded in the VCV2003 catalogue, and those of the 128 cross-identified ICRF defining sources.

We can remark that a large majority of these last ones (rouhghly 75 %) are included in the range $16.5 < V < 19.5$, whereas the same percentage in the VCV2003 objects concerns the range $18.5 < V < 21.0$. From that we can assert that ICRF selected objects are globally bright objects in

Table 1. Number of quasars cross-identified between recent catalogues (Véron Cetty and Véron, 2003, PKS catalogue) and the three categories of objects used in the construction of the ICRF: defining, candidate and other sources. Three different angular thresholds have been chosen for the cross-identification: 2", 3", and 4".

Catalogue	Threshold (")	Defining ICRF	Candidate ICRF	Other ICRF
Véron Cetty	4	132/212	160/294	69 /102
and Véron, 2003		(62.2%)	(54.4%)	(67.6%)
rms(") α/δ		0.82/0.73	0.91/0.75	0.69/0.66
Véron Cetty	3	132/212	160/294	69 /102
and Véron, 2003		(62.2%)	(54.4%)	(67.6%)
rms(") α/δ		0.82/0.73	0.91/0.75	0.69/0.66
Véron Cetty	2	128/212	152/294	69 /102
and Véron, 2003		(60.3%)	(51.7%)	(67.6%)
rms(") α/δ		1.23/0.65	1.29/0.68	1.09/0.66
PKS	4	58/212	114/294	43 /102
		(27.4%)	(38.8%)	(42.1%)
rms(") α/δ		0.82/0.78	0.80/0.76	0.77/0.73
PKS	3	58/212	114/294	43 /102
		(27.4%)	(38.8%)	(42.1%)
rms(") α/δ		0.82/0.78	0.80/0.76	0.77/0.73
PKS	2	55/212	107/294	43/102
		(25.9%)	(36.4%)	(67.6%)
rms(") α/δ		0.67/0.65	0.70/0.68	0.81/0.73

optical wavelengths in comparison with the average. From the comparison between the two histogramms we can add that the proportion of the quasars among the brightest ones ($15 < V < 17$) chosen to build up the ICRF is comparatively much higher than in the VCV catalogue. Nevertheless, at the other extremity of the histogramm, the presence of very faint ICRF sources, with $V > 20$, indicates that their faintness at optical wavelengths does not seem to be a handicap for their astrometric quality, which depends essentially on the quality of their emission at radio wavelengths.

In figures 4 and 5, we show the histogramms of the same kind of study as above, but at the 6 cm wavelength. Notice that in comparison VLBI observations are generally performed at X band (3,6 cm; 8.46 Ghz) and S band (13 cm; 2.3 Ghz). Paradoxally, the feature is quite different here: whereas in the VCV2003 catalogue, the number of sources is steadily increasing for a flux at 6 cm, where a peak is observed, then slightly and gradually decreasing after, the selected cross-identified ICRF sources have been chosen in a large proportion (roughly 80 %) in the range between 0.5 Jy and 1.5 Jy.

As the redshifts of quasars is directly related to their distance by the intermediary of Hubble's law, it appears interesting to plot the V-magnitude of theses objects, which in some extent should depend also on the distance, with respect to their redshift. This is properly done in figure 6, both for the VCV2003 recorded objects (in dots) and for the ICRF quasars belonging also to this last catalogue (in large full circles).

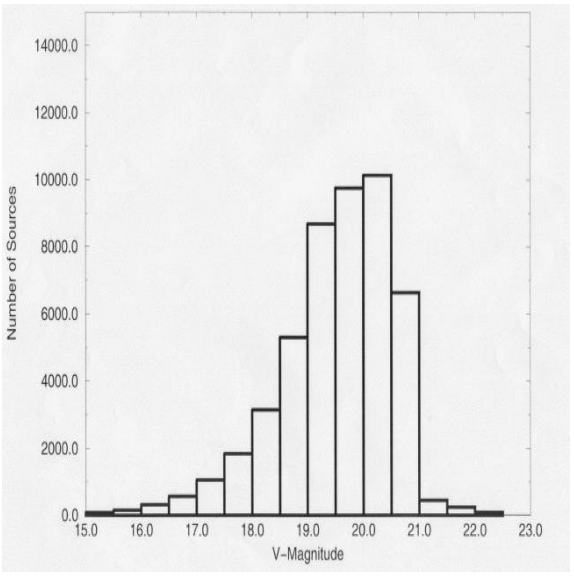

Fig. 2. Histogramm showing the number of quasars of VCV2003 catalogue with respect to their V-magnitude.

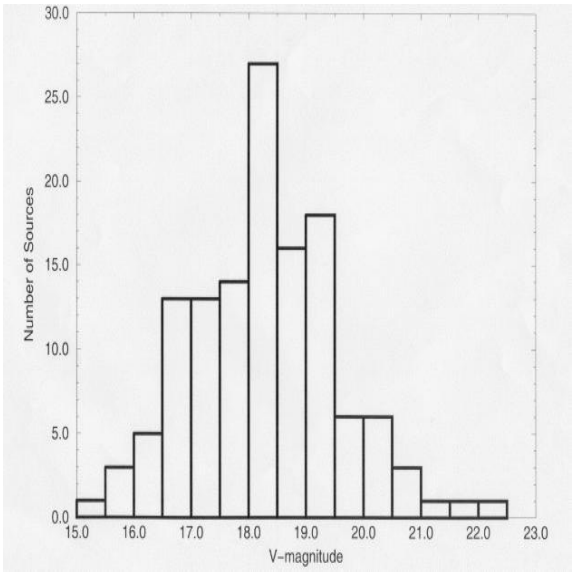

Fig. 3. Histogramm showing the number of defining sources of the ICRF cross-identified with VCV2003, with respect to their V-magnitude.

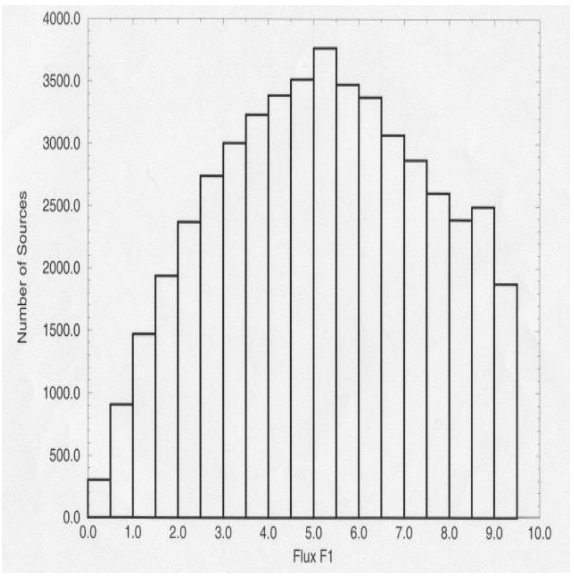

Fig. 4. Histogramm showing the number of quasars of VCV2003 catalogue with respect to their S-band flux (6 cm).

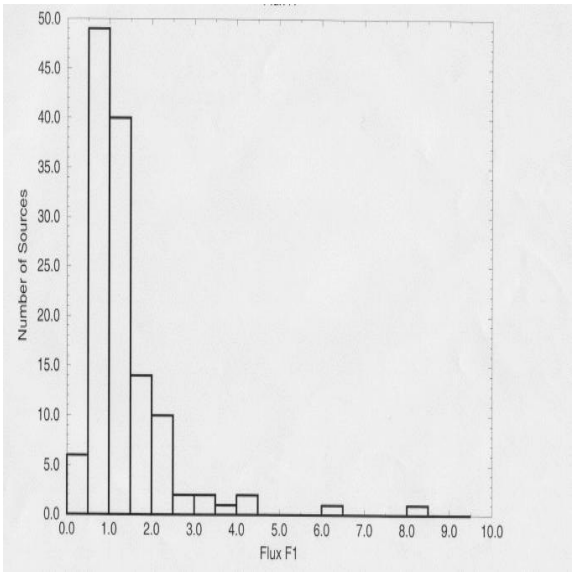

Fig. 5. Histogramm showing the number of defining sources of the ICRF cross-identified with VCV2003, with respect to their S-band flux (6 cm).

We can observe at the left part of the figure, that for a given redshift, there is well defined threshold for the upper limit in V. In opposite, this means that for a given redshift, i.e. at a given distance, it is not possible to find a quasar fainter than this magnitude threshold. As a consequence a very well defined limiting curve can thus be described, above which, no quasar can be found (in fact we can detect the presence of 3 quasars in this forbidden zone). Indeed, notice that this might be due to the definition of a quasar itself given by equations (1) and (2).

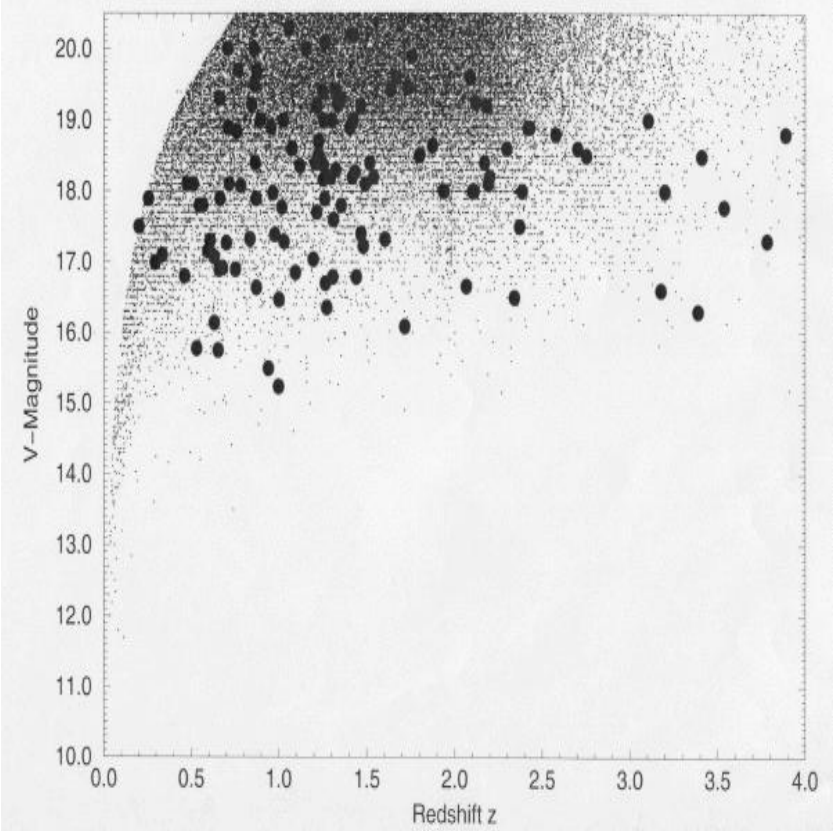

Fig. 6. Curve showing the V-magnitude of quasars of the VCV2003 catalogue (dots) and of the ICRF defining sources cross-identified with this last catalogue, with respect to their redshift.

5 About the sky coverage of the ICRS quasars and other catalogues

Although the ICRF catalogue has been adopted as the reference and conventional one since 1998, and despite its very high astrometric quality, its sky coverage is fairly poor, which is obviously due to the small number of objects: 212, if we take into account only the defining sources, 667 (for the ICRF-Ext.1) when considering also the candidate sources, the other sources, and the new sources. Indeed, the primary realization of the ICRS (International Celestial Reference System) at optical wavelengths has been carried out by the position of roughly 100 000 stars of the Hipparcos catalogue, and at a larger and less accurate extent by the 3 millions objects of the Tycho catalogue.

Here we focus our study on the intrinsic sky coverage of the ICRF and other quasar's catalogues, which will be measured in the following way: we select points of the celestial sphere separated by equal intervals, that is to say one degree in right ascension α and also in declination δ. Then for each of the points selected, we calculate the closest object of the selected catalogue we want to study. We must pay attention to the fact that the points are not regularly located on the sphere, but we choose such a repartition for reasons of commodity.

Figures 7 and 8 represent respectively in bi-dimensional coordinates (α, δ) the zones of the celestial sphere in white, for which the closest

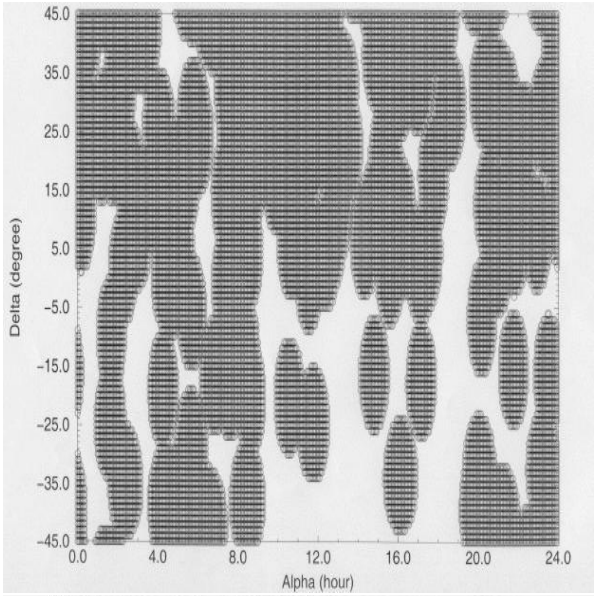

Fig. 7. Plot in black of the zones of the sky ($-45° < \delta < 45°$ for which the lowest distance to a defining source of the ICRF catalogue is less than 10°.

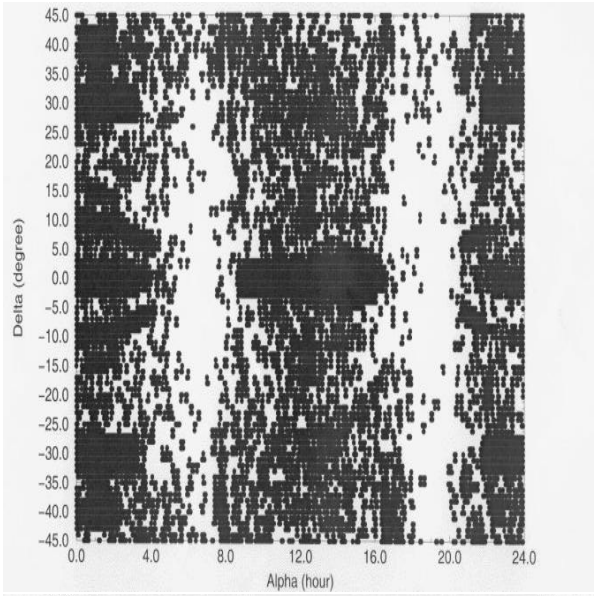

Fig. 8. Plot in black of the zones of the sky ($-45° < \delta < 45°$ for which the lowest distance to a defining source of the ICRF catalogue is less than 15°.

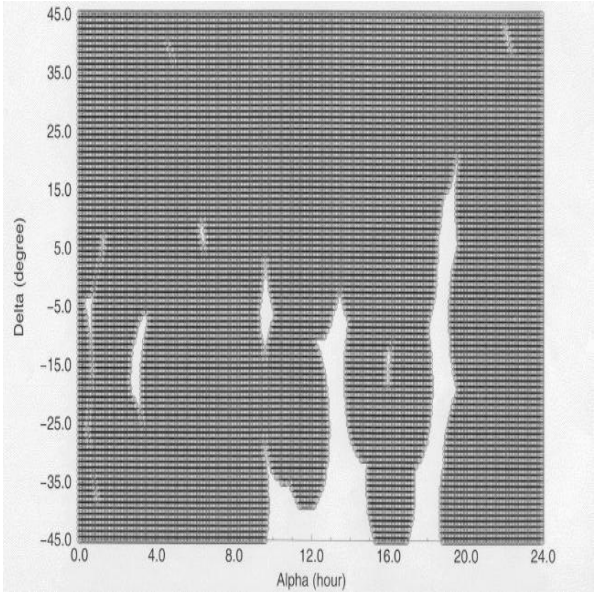

Fig. 9. Plot in black of the zones of the sky ($-45° < \delta < 45°$ for which the lowest distance to a quasar of the VCV2003 catalogue is less than 1°.

distance to an ICRF defining quasar is respectively larger then 10°, and larger than 15° (on the opposite the black zones correspond to points for which the closest defining ICRF quasar is at an angular distance respectively less than 10° and 15°). The study has been limited to zones for which $-45° < \delta < 45°$ in order to avoid distorsion at the high declinations (for which one degree separating two points in right ascension correspond to a very small angular distance). Obviously, the two figures show that the sky coverage is more deficient in the south hemisphere than in the north one, for wich the zones of depletion covers a considerably smaller surface. Moreover we have only considered here the 212 defining sources of the ICRF catalogue. The same kind of study we be done in the near future when considering the 667 extragalactic objects of the ICRF-Ext.1.

In figure 9 we present the same kind of study as above, but with the 48 291 quasars of the VCV2003 catalogue and an angular distance considerably smaller (1°). We can observe that a major part of the sky is covered by the recorded quasars at this level of angular distance, except two depletion zones covering respectively the intervals roughly from 5^h and 8^h and from 17^h to 20^h. These two zones correspond more or less to the presence of the galactic plane (the Milky Way) through which no extragalactic object can be easily observed.

6 Conclusion

In this paper we have carried out the cross-identification of the ICRF, constructed starting from observations at radio wavelengths, with VCV2003 (Véron-Cetty and Véron, 2003) which is the denser catalogue of quasars presently available, at optical wavelengths. Only a little more than 60% of the ICRF defining sources are belonging to the two catalogues. Nevertheless these common identifications enabled us to point out some general properties of the ICRF quasars, with respect to the general properties (magnitude, redshift flux at 6 cm) established statistically from the large set (48 291 objects) of the VCV2003 catalogue. In a second part we have compared the sky coverage of the ICRF catalogue and of the VCV2003. We have shown that whereas in the first case some zones of the sky are not covered at the angular distance of 15°, in the second case a large part of the sky is close to a quasar at the angular distance of 1°. No doubt that with the increasing number of quasars detected at an exponential level, it will be possible to improve drastically the astrometric measurements for the whole sky in the near future, and of course with the up-coming of the GAIA space mission which will be maybe able to detect around 500 000 quasars. This study is a first step to a more complete and detailed one, focused on the various photometric and spectral properties of the ICRF quasars but also of the BL LAC objects and Active Galaxies which belong in some significant proportion to the ICRF-Ext.1 catalogue.

References

Arias, E. F., Charlot, P., Feissel, M., Lestrade, J. F.: 1995, *Astron. and Astrophys.* 303, 604

Crooms, S. M., Smith, R. J., Boyle, B. J. et al., 2001, *MNRAS* 322, L29

De Veny, J. B., Osburn, W. M., James, K., 1971, *PASP* 83, 611

IERS Annual Report 1999 Eds. Obs. Paris
Richards, G. T., et al. 2001, *Astron. J.* 121, 2308
Terrell, J., 1977, *Am. J. Phys.* 45, 869
Véron-Cetty, M. P., Véron, P., 2001, *Astron. and Astrophys.* 374, 92
Véron-Cetty, M. P., Véron, P., 2003, *Astron. and Astrophys.* 412, 399

Tying the dynamical and extragalactic reference frames via millisecond pulsars

M. Feissel-Vernier[1] and I. Cognard[2]

[1] *Observatoire de Paris/CNRS UMR8630, 61 Av. de l'Observatoire, 75014, Paris, France and Institut Géographique National/LAREG*
[2] *CNRS/Laboratoire de Physique et Chimie de l'Environnement, 34 Avenue de la Rercherche Scientifique, 45071 Orléans, France*

Abstract. This chapter recalls the basic principles of the method for tying the solar system dynamical reference frame to the extragalactic ICRF. It summarizes the set of fiducial objects currently available for implementing the method. Its expected precision makes it a prospective competitor to the classical LLR-based tie, which accuracy was recently brought to the sub-milliarcsecond level.

1 Introduction

The co-existence of high precision celestial frames based on either the kinematics of extragalactic objects observed with VLBI, e.g. the International Celestial Reference Frame (ICRF), or the dynamics of the solar system, e.g. ephemerides of the Earth-Moon-planetary system, makes it necessary to maintain the tie between these frames, using some celestial bodies as transfer objects.

The current way of tying the dynamical and extragalactic reference frames is the well established method that uses the planet Earth has the transfer fiducial object: Lunar Laser Ranging (LLR) Earth orientation measurements, that are relative to a reference frame tied to the solar system, are compared with the VLBI ones, that are related to the ICRF. Folkner et al. (1994) estimated the tie with a 3 milliarcseconds (mas) precision. Progress in LLR observing precision and refinement in the modelling of the Earth-Moon system recently improved the precision by an order of magnitude (Chapront et al. (2002, 2003).

Other candidate fiducial bodies are fast rotating pulsars. The timing observation of their pulses allow to relate their motion in the Galaxy to the Earth's orbit in the solar system, while this same motion relative to background ICRF objects can be measured with VLBI differential observation. The method has been shown to be precise at the sub-milliarcsecond level.

2 Millisecond pulsars

A pulsar is an extremely dense and small neutron star believed to have been born as a result of a supernova, or explosion of a large star from a class ten or more times the mass of the sun. Pulsars emit beams of radio waves that have been focused by the stars' extremely strong, approximately dipolar magnetic fields. These signals are analogous to rotating lighthouse beams periodically sweeping across the universe.

All pulsars are slowing down their rotation rates as part of their aging process. After a few million year, old pulsars turn off; but if they are part of a binary (two-star) system, they may be reborn as millisecond pulsars. Absorbing energy and momentum relinquished by their dying partner, they spin up to rates as fast or faster than newborns. In general,

they rotate hundreds of times more rapidly than their younger relatives and slow down at a much lower rate. This combination of characteristics sets millisecond pulsars apart as a distinct class whose emissions are so regular that their pulses can be averaged to create a most accurate clock, used by researchers studying a variety of problems including general relativity theory.

As the name suggests, millisecond pulsars have pulse periods that are in the range from one to ten milliseconds. The first millisecond pulsar, designated PSR 1937+21, was discovered by Backer et al. (1982) using the Arecibo telescope. Its pulse period of 1.6 milliseconds; its mass is about 1.4 solar masses.

3 Frame tie using millisecond pulsars

Millisecond pulsars, by virtue of their relatively stable rotations and sharp pulses of nearly point-source radio emission, can be used to tie Earth-orbit-oriented reference frames to Earth-spin-oriented reference frames with unprecedented accuracy through a combination of timing and VLBI measurements.

We quote Bartel et al. (1986), who " determined the coordinates of PSR B1937+21 relative to those of the extragalactic source 1923+210, whose coordinates in a quasi-inertial extragalactic reference frame have a standard error of about 0.1 mas. They agree within the root-sum-square standard errors with those determined via VLBI by Petit (1994) and Dewey et al. (1996) and with those yielded by the application of the rotation of an indirect frame tie of Folkner et al. (1994) to the pulse-timing positions obtained by Kaspi et al. (1994) with JPL's DE200 ephemeris."

When applied on a set of well distributed pulsars, this method is expected to provide a frame tie at the level of tens of microarcseconds (μas). A few pulsar VLBI observing programs are run, see, e.g., Campbell (2001), Sekido et al. (1999).

4 Millisecond pulsars timing campaigns

Timing campaigns are run by several groups or consortia at a set of observatories. They are listed hereafter in approximate order of record length.

- Jodrell Bank: about 500 pulsars are monitored.[1]
- Parkes: several hundred pulsars are monitored.[2]
- Arecibo: many groups are using this telescope but telescope time is expensive and not so many pulsars are regularly observed.[3]
  - Princeton: for binary Nobel pulsar PSR B1913+16 and a handful of millisecond ones.[4]
  - Penn State University.
  - UC Berkeley
  - Caltech

[1] See http://www.jb.man.ac.uk/∼pulsar/
[2] See http://www.atnf.csiro.au/research/pulsar/
[3] See http://www.jb.man.ac.uk/∼drl/ao2002/
[4] See http://pulsar.princeton.edu/

– Paris Observatory's Nançay station. As an example, table 1 summarizes the existing pulsar timing series at Nançay. See Lestrade et al. (1999).
– Effelsberg: about 10 pulsars are monitored (Lang et al., 2000; Wolcsczan et al., 2000).
– Torun: 88 slow pulsars are monitored once a week (Lewandowski et al., 2000).
– Urumqi: about 100 pulsars are monitored (Wang et al., 2000).
– Kalyazin: 8 pulsars are monitored 2-3 days per month (Doroshenko et al., 2000; Potapov et al., 2003).
– Kashima: see Hanado et al. (2002).

Table 1. Current Nançay pulsar timing series. Another group of pulsars is also observed, but their timing results are not finalized. Those are 0030+04, 1257+12, 1516+02A, 1518+49, 1534+12, 1802-07, 1804-27, 1820-30, 1951+32, 2127+11A.

Pulsar		Period (ms)	Start date
B0244+60		217.093	Jul 1998
B0613-02		3.061	Dec 1998
B0751+18		3.478	May 1999
B1012+53		5.255	Feb 1999
B1022+10		16.452	Avr 1999
B1620-26	J1623-2631	11.075	Dec 1996
B1640+22	J1640+2224	3.163	Feb 1999
B1643-12		4.621	Mar 1996
B1713+07		4.570	Feb 1996
B1730-23		8.122	Dec 1998
B1744-11		4.074	Feb 1999
B1821-24	J1824-2452	3.050	Mar 1989
B1937+21	J1939+2134	1.557	Dec 1988
B2043+27		96.130	Dec 1998
B2051-08		4.508	Avr 1999
B2124-33		4.931	Feb 1999
B2145-07		16.052	Jul 1999
B2238+58		139.935	Dec 1998

5 Reference ICRF radio sources

Table 2 gives a preliminary list of ICRF objects close enough to pulsars with rotation periods shorter than 0.5 second, to can be used as reference objects for differential VLBI observation of these pulsars.

Table 3 gives statistics on 24 out of the 34 ICRF reference sources of table 2, based on all VLBI observations over 1989.5-2002.4: standard deviation of the source coordinates based on one session and estimated linear drift. The remaining 10 sources (0459-753, 1129-580, 1329-665, 1334-649, 1352-632, 1600-445, 1729-373, 1748-253, 1932+106, 1955+343) were observed in only one or two sessions over this time span. Their stability cannot be qualified with the currently available data.

Table 2. ICRF extragalactic radio sources closer than 1.5 degrees from pulsars with rotation periods shorter than 0.5 second. The pulsar names are J2000 IAU names.

IERS name	Nearby pulsar(s)	Per. (sec)	Dist. (kPc)	Flux (mJy) 1.4GHz	.4GHz
0219+428	0218+4232	.002	5.85		
0252-549	0255-5304	.448	1.15	17.0	3.0
0355+508	0357+5236	.197	4.72	12.0	1.9
0426+273	0435+27	.326	3.43		
0430+289	0435+27	.326	3.43		
0437-454	0437-4715	.006	.14	600.0	90.0
0451-282	0448-2757	.450	1.55	2.7	1.2
0459-753	0455-6947	.320	49.40	.6	
0831-445	0835-4510	.089	.50	5000.0	1100.0
1048-313	1045-3033	.330	4.17	13.0	
1101-536	1057-5226	.197	1.53	80.0	
1105-680	1112-6613	.334	19.29	19.0	
1129-580	1126-6054	.203	8.05		1.2
1252+119	1300+1240	.006	.62	20.0	1.0
1313-333	1321-3509	.458	1.25	7.0	
1329-665	1327-6301	.196	6.50		3.4
1334-649	1340-6456	.379	1.93	9.0	1.1
	1341-6220	.193	8.66		2.0
1352-632	1357-6228	.456	6.90		6.0
	1359-6038	.128	5.91	105.0	7.0
1600-445	1559-4438	.257	1.63	110.0	40.0
1622-253	1623-2631	.011	1.80	15.0	1.1
1639+230	1635+2418	.491	2.09	9.1	.4
	1640+2224	.003	1.18		
1729-373	1733-3716	.338	3.45		2.6
	1737-3555	.398	2.25		.5
1741-038	1743-0337	.445	1.79	3.1	.5
1748-253	1748-2446A	.012	7.10		2.5
	1748-2446B	.443	3.91		.3
	1757-2421	.234	3.50	20.0	7.1
1817-254	1824-2452	.003	5.50	40.0	1.8
1901+319	1900+30	.602	4.56		
1923+210	1924+2040	.238	10.74	4.0	
1926+087	1933+07	.437	8.94		
1929+226	1932+2220	.144	9.80	7.8	1.2
1932+106	1932+1059	.227	.17	303.0	41.0
1932+204	1932+2020	.268	9.14	29.0	1.2
	1939+2134	.002	3.60	240.0	16.0
1955+335	1952+3252	.040	2.50	7.0	1.0
1955+343	1952+3252	.040	2.50	7.0	1.0
2005+403	2013+3845	.230	13.09	26.0	6.4
2134+004	2139+00	.312	2.97		

Table 3. Stability statistics of the reference ICRF extragalactic radio sources. Quality column: sources marked ** are well observed and stable, those marked @@ are well observed and unstable (Feissel-Vernier, 2003). Sources marked * are considered stable and those marked @ are considered stable although they were not frequently observed over the same time span.

IERS name	Quality	IVS alias	Standard error $\alpha \cos\delta$ (mas)	Standard error δ (mas)	Apparent linear drift $\alpha \cos\delta$ mas/year		Apparent linear drift δ mas/year	
0219+428	*		.076	.090	.014	± .057	.000	± .055
0252-549	@	4C67.05	.207	.310	.174	± .095	-.024	± .107
0355+508	**	3C84	.064	.060	.017	± .017	-.012	± .017
0426+273	*	NRAO150	.045	.099	.058	± .041	.010	± .099
0430+289	**		.023	.027	.009	± .016	.019	± .020
0437-454	*		.143	.237	.187	± .174	.203	± .117
0451-282	@@		.085	.225	.004	± .052	.055	± .074
0831-445	@		7.672	4.202	2.883	± 4.621	-.560	± 2.192
1048-313	@		.639	1.317	-.522	± .517	-.400	± 1.146
1101-536	@@		.058	.119	.100	± .035	.140	± .079
1105-680	@		1.781	1.017	.640	± .455	.398	± .313
1252+119	@@		.100	.130	.073	± .024	.059	± .028
1313-333	**		.035	.097	-.017	± .023	-.073	± .052
1622-253	**		.013	.020	-.002	± .005	-.005	± .006
1639+230	*		.060	.085	-.017	± .042	.018	± .051
1741-038	@@		.005	.007	-.020	± .001	.019	± .002
1817-254	@		.279	.376	.286	± .154	.051	± .249
1901+319	@@		.057	.048	-.003	± .035	-.008	± .030
1923+210	**	3C395	.033	.047	-.024	± .009	-.017	± .013
1926+087	*		.144	.172	-.034	± .098	.123	± .084
1932+204	*		.063	.145	.022	± .050	.109	± .107
1955+335	@		.140	.278	.044	± .068	-.156	± .110
2005+403	@		.496	.524	-.157	± .291	.140	± .314
2134+004	**		.034	.060	-.024	± .014	-.032	± .019

Acknowledgements. The general physical description of pulsars was collected from the scientific information websites mentioned in the text. The bibliographic survey made use of the NASA ADS Astronomy Abstract Service.

References

Backer, D. C., Kulkarni, S. R., Heiles, C., Davis, M. M., Goss, W. M., 1982, Nature 300, 615.

Bartel, N., Chandler, J. F., Ratner, M. I., Shapiro, I. I., Pan, R., Cappallo, R. J., 1996, AJ 112, 1690.

Campbell, R. M., 2001, IAU Symp. 205, 404.

Chapront, J., Chapront-Touzé, M., Francou, G., 2002, AA 387, 700.

Chapront, J., Francou, G., 2003, this volume.

Dewey, R. J., Gwinn, C. R., Jones, D. J., Davis, M. M., 1996, AJ 111, 315.

Doroshenko, O., Ilyasov, Yu. P., Oreshko, V. V., 2000, ASP Conf Series 202, 57.

Feissel-Vernier, M., 2003, AA (in press).

Folkner, W. M., Charlot, P., Finger, M. H., Williams, J. G., Newhall, X X, Standish, E. M., 1994, AA 297, 279.

Hanado, Y., Shuibuya, Y., Hosokawa, M., Sekido, M., Gotoh, T., Imae, M., 2002, Publ. Astron. Soc. Japan 54, 305.

Kaspi, V. M., Taylor, J. H., Ryba, M., 1994, ApJ, 713.

Lange, Ch., Wex, N., Kramer,yM., Doroshenko O., Backer, D. C., 2000, ASP Conf Series 202, 61.

Lewandowski, W., Konacki, M., Redmerska, M., Feiler, G., 2000, ASP Conf Series 202, 63.

Lestrade, J.-F., Cognard, I., Maitia, V., 1999, Pulsar Timing, General Relativity and the Internal Structure of Neutron Stars, KNAW (ISBN 90-6984-247-5), p. 65.

Petit, G., 1994, PhD Thesis, Observatoire de Paris.

Potapov, V.A., Ilyasov, Yu. P., Oreshko, V. V., Rodin, A. E., 2003, Astron. Lett. 29, 241.

Sekido, M. and 12 co-authors, 1999, New Astron. Rev. 43, 599.

Wang, Wu, Zhang, Manchester, Yusup, Cheng, 2000, ASP Conf Series 202, 65.

Wolcsczan, A., Doroshenko, O., Konacki, M., Jessner, A., Wielebinski, R., Camilo, F., Nice, D. J., Taylor, J. H., 2000, ApJ 528, 907.

Lunar Laser Ranging: measurements, analysis, and contribution to the reference systems

J. Chapront and G. Francou

Observatoire de Paris - SYstème de Référence Temps-Espace (SYRTE) - UMR 8630/CNRS, 61 Av. de l'Observatoire, 75014, Paris, France

Abstract. On 21 July 1969, the first lunar reflector was placed on the Moon surface by Apollo 11 mission. Since this date 4 more reflectors have been deployed and, today, the Lunar Laser Ranging (LLR) is still operating in USA and France. The complete set of LLR observations covers a time interval longer than 30 years and the accuracy of measurements is regularly improved. This technique has brought remarkable results in lunar science, solar system dynamics, geophysics and fundamental physics. In 1998, the Paris Observatory Lunar Analysis Center (POLAC) has performed analysis of LLR observations. In this contribution we emphasize some results obtained in 2002 such as the orientation of the dynamical ecliptic, the correction to the IAU 1976 value of the precession constant in longitude and the improvement of the tidal acceleration of the Moon.

1 Lunar Laser Ranging measurements

Lunar laser telemetry consists in determining the round-trip travel time of the light between a transmitter on the Earth and a reflector on the Moon, which is an equivalent measurement of the distance between these two points. Neil Armstrong put down the first reflector array in the Sea of Tranquillity in July 1969 and a few weeks later McDonald Observatory succeeded in detecting photons returned from a laser pulse sent to the Moon.

Afterwards, more reflector arrays have been placed by two American Apollo missions in 1971 (Apollo 14 and Apollo 15), and two Soviet automatic missions, Luna 17 (1970) and Luna 21 (1973) which carried French-built reflectors, Lunakhod 1 and 2. Except Lunakhod 1 from which the signal has been lost, the 4 other reflectors are still operating normally (Fig. 1).

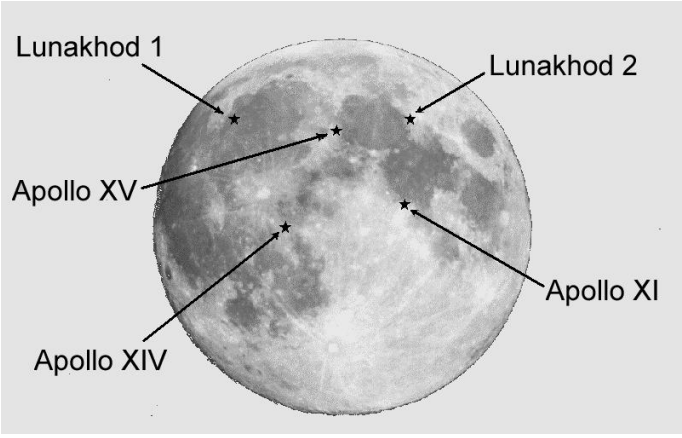

Fig. 1. Distribution of the reflectors on the lunar surface

The Apollo arrays consist of 3.8-cm diameter corner cubes mounted on an aluminium panel (100 for Apollo 11 and 14 and 300 for Apollo 15). The Lunakhod arrays have 14 triangularly faced corner cubes of 11-cm edge. The design of reflector arrays is straightforward: each corner cube reflects incident light back to its point of origin (Fig. 2).

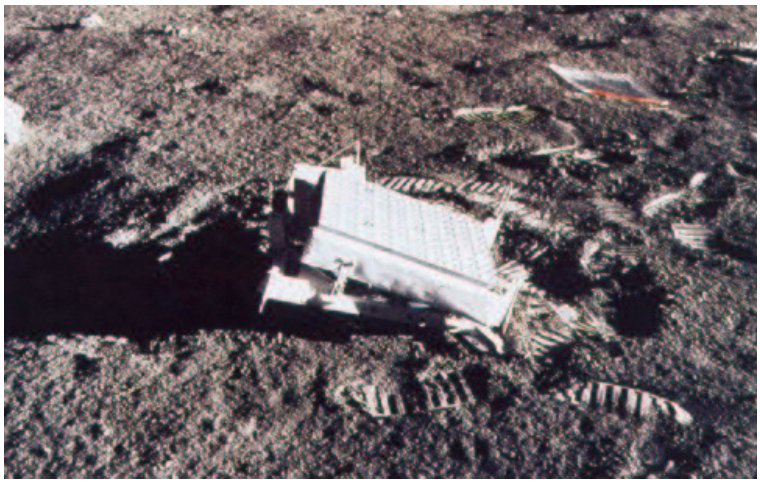

Fig. 2. Photography of the reflector array placed by Apollo 14

Fig. 3. McDonald Laser ranging station (Fort Davis, Texas)

Fig. 4. CERGA Laser ranging station (Plateau de Calern, Caussols, France)

Since 1970 there were few LLR observing stations. The first one was McDonald Observatory (2.7-m telescope) near Fort Davis, Texas (USA). It was fully dedicated to lunar ranging and ceased operation in 1985 after maintaining routine activities for more than 15 years. The transition was made in the mid-1980s to the McDonald Laser Ranging Station (0.76-m telescope) on two sites (Saddle and Mt. Fowlkes): MLRS1 (1983-1988) and MLRS2 (since 1988) which share lunar and artificial satellite ranging facilities (Fig. 3).

In the 1980s, two other stations have carried out Lunar Laser Ranging. The Haleakala Observatory on Maui, Hawaii (USA) produced high quality data over a few years around 1990. Since 1982, the CERGA station (Centre d'Etudes et de Recherche en Géodynamique et Astronomie) has been operating at the 'Observatoire de Côte d'Azur' (OCA) on the 'Plateau de Calern' near Grasse (France), with a 1.54-m Cassegrain telescope which replaced its Rubis laser by a YAG in 1987 (Fig. 4). Occasionally some other artificial-satellite stations have performed successfully LLR observations such as in Australia and in Germany, but all the data used for the analyses come from the 3 observatories: McDonald, Haleakala and CERGA. Today, just two observatories are still operating: McDonald (MLRS2) and CERGA.

The principle of Lunar Laser Ranging is to fire laser pulses towards the target reflectors on the Moon, to receive back localised and recognizable signals and to measure the duration of the round-trip travel of the light. If the concept is elementary, it is in fact a real technical challenge.

At first, the performances of the observations depend on the quality of the time measurements. On average the duration of the round-trip flight is 2.5 seconds varying according to the lunar distance, the mean distance Earth-Moon being 385000 km. If one aims at a precision of 1 cm for the separation between transmitter and reflector, one needs an accuracy of the order of 0.1 nanosecond (10^{-10} second) in the measurement of the round-trip travel duration. The measure of the time is based on a very stable high frequency signal generated by a caesium atomic clock whose the frequency accuracy is better than 10^{-12} yielding an uncertainty below 10 picoseconds (10^{-11} second) over the journey of the light. But several factors affect the precision of the measurements. The atmosphere induces a time delay which is difficult to estimate rigorously, probably between 50 and 100 picoseconds; it depends on temperature, pressure and humidity. The libration of the Moon makes an oscillation of the orientation of the array which produces, in worse cases, an unbiased scatter in distance of few centimeters (about 200 picoseconds in the time of flight). There are other sources of uncertainties such as the photodiodes connected to the start timer or the return detector. The CERGA team has tested several approaches and has converged towards widths of about 200 picoseconds. And to improve the chance to trapping the right return photon several kinds of filtering are performed to eliminate the noisy photons as much as possible. In these conditions, the precision of a measurement of the round-trip travel time of 'one photon' is of the order of 3 cm. With the most unfavourable librations this value can grow up to about 5 cm.

Nevertheless, the main problem stands elsewhere. The outgoing beam has a divergence of 3" to 4" after crossing the Earth atmosphere so that the size of the light spot on the Moon is about 7 km in diameter, which means that only one photon out of 10^9 impacts a reflector array. Besides the reflected beam has a significant angular divergence (12") due to the diffraction by the pupil of the reflector yielding a spot nearly 25 km

back on the Earth. With a 1-meter telescope, only a fraction 10^{-9} of the photons is intercepted.

Finally, allowing for other factors, just one photon is detected out of 10^{20} emitted in the initial pulse. With the YAG laser of the CERGA (since 1987), the energy of the beam is about 300 mJ per pulse at a wavelength of 532 nanometers; it is equivalent to 10^{18} photons. That gives an average of one return every 100 pulses, or every 10 seconds, the laser system producing pulses with a typical rate of 10 pulses per second.

2 Lunar Laser Ranging data

The actual observational data consists of 'Normal Points' built on statistics from the individual time returns. It is essentially a one parameter fitted on the round-trip travel time centered in the middle of the interval of the observations. Since the beginning of the Lunar Laser Ranging, the instrumental quality of the measurements has been noticeably improved. It was around 25 cm in the one-way distance 'station-reflector' in the 1970s and gradually getting better around 10-15 cm in the early 1980s. When the Rubis laser was replaced by a YAG device, after 1985, with much smaller pulse widths and a better timing system, the standard uncertainty in the measurements dropped to 3-cm level.

At the CERGA lunar laser station, a project aiming at sub-centimetric precision was initiated in 1992. Today, the 'Normal Points' provided by the CERGA have an 'instrumental internal precision' of 30-60 picoseconds in the round-trip travel time, which is equivalent to 5-10 mm in one-way distance.

Figure 5 shows the contribution of the 3 LLR stations: McDonald, Haleakala and CERGA since 1970. During the 15 early years, the McDonald Observatory was the only station to range the Moon with the 2.7-m telescope. Around 1990 a second American laser station, Haleakala on Maui, Hawaii, provided several hundreds of 'Normal Points'. Since the 1990s the CERGA station has produced 70% of lunar ranging data. Figure 6 gives the distribution of the Lunar Laser Ranging data between the several reflectors. The reflector Apollo 15 contributes to the major part of the observations (80%) compared with the other reflectors Apollo 11, Apollo 14 and Lunakhod 2.

Figure 7 shows the time distribution of 'Normal Points' for the MLRS2 (in light) and CERGA (in dark) between 1988 and 2001; the maximum of annual data for both stations is about 1000 observations (in 2000), the average being around 700 per year. Figure 8 gives the distribution of the number of returns per 'Normal Point' during the period 1988-2001. The average is respectively 50 returns per 'Normal Point' for CERGA and 15 for MLRS2 with a maximum around 20 for CERGA and 8 for MLRS2.

Figure 9 shows the distribution of observations within a lunar month. Observations are carried out about 25 days per lunation with no observation around New Moon. They are grouped around the First Quarter (evening observations) and the Third Quarter (morning observations). There is no observation at Full Moon because of heavy noise except during Moon eclipses as in 2000 at CERGA station. Figure 10 shows for both stations the distribution of the number of 'Normal Points' per night during the period 1988-2001. In average there are 8 'Normal Points' per night for CERGA and 3-4 for MLRS2. This information is useful in lunar

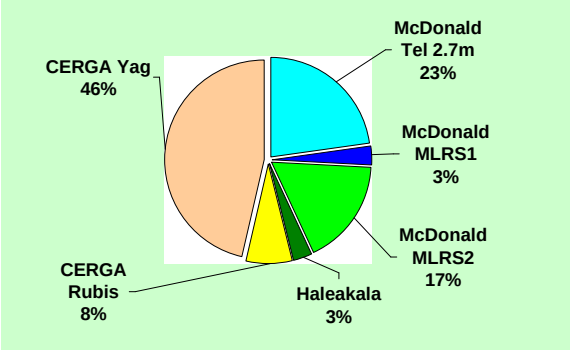

Fig. 5. Distribution of 'Normal Points' per LLR station

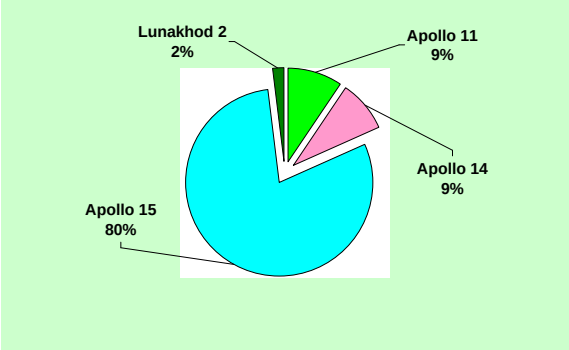

Fig. 6. Distribution of 'Normal Points' per Lunar Reflector

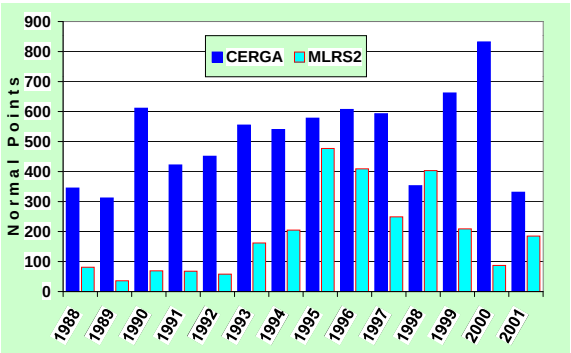

Fig. 7. Distribution of LLR 'Normal Points' over(1988-2001)

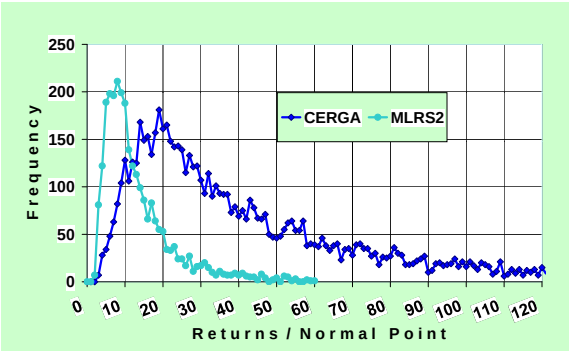

Fig. 8. Distribution of Returns per 'Normal Point'

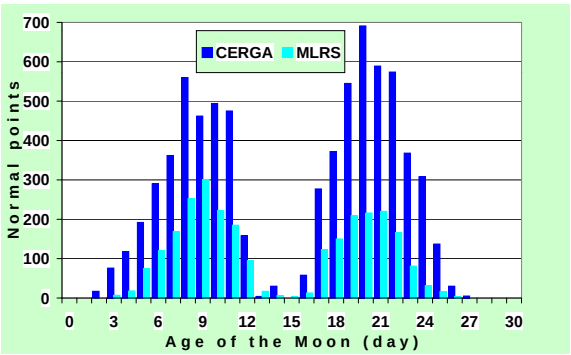

Fig. 9. Distribution of LLR 'Normal Points' within the lunar month

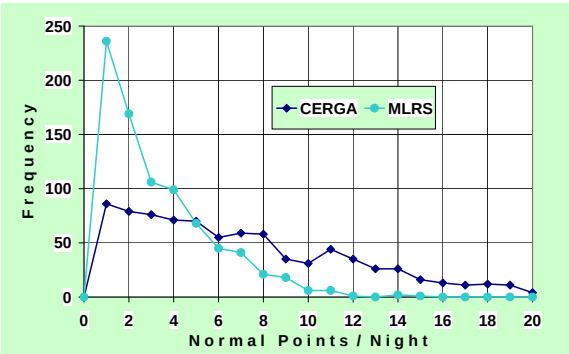

Fig. 10. Distribution of LLR 'Normal Points' per Night

analysis which provide estimations of the Earth orientation parameters (EOP) UT0-UTC and VOL (variation of latitude). Generally we need 3 or 4 'Normal Points' per night and per reflector to determine these parameters.

The thousands of Lunar Laser Ranging data collected since 1970 have given significant contributions to a large scientific domain. We enumerate below a non-exhaustive list of them.

- Ephemerides
  The improvement of the orbital motion of the Moon has followed the accuracy in the LLR measurements. Several numerical integrations (Development Ephemerides at JPL) and analytical solutions (ELP) have been constructed. Libration models (forced and free librations) have been elaborated in parallel.
- Gravitational physics
  It concerns the verification of the equivalence principle, a determination of the PPN parameters β and γ, and the geodetic precession. Correlatively, precise boundaries of the rate of change of G (the gravitational constant) and of the solar J_2 have been also derived. Since 1996, compared to previous determinations, the uncertainties in gravitational physics parameters have been reduced by a factor 2 or more. It is mainly due to the data (an improved range accuracy and a longer time span), some additional solutions (plate motion on the Earth and solid body tides on the Moon), a better determination of Earth Orientation Parameters, and finally, a modeling of the energy dissipation of the Moon.
- Geodynamics
  The LLR technique is also a main contributor to the improvement of various parameters of the Earth-Moon system. We shall mention in particular the determination of the lunar mass and the coefficients of the Earth potential when combined with SLR technique. It contributes, complementary to VLBI, to a better knowledge of the precession constant and of few long-periodic terms in nutation. A domain of excellence is a precise evaluation of the Earth tidal dissipation (Love numbers and time delay) due to the lunar action, which induces a secular acceleration of the lunar longitude.
- Lunar science and selenophysics
  The Moon in rotation is submitted to two different kinds of effects: forced and free librations. Through the analysis of the lunar parameters, one derives an estimate of the principal moment of inertia, low degree gravitational harmonics, Love number κ_2 and dissipation parameter Q. LLR data are combined with lunar orbiting satellites and result in a determination of the parameter C/MR^2 which is fundamental for the knowledge of the Moon's evolution. The free libration is implicit in the equations of motion. Once the total libration is known by the observations and the forced libration modeled, a frequency analysis of the difference: Total Libration - Forced Libration, exhibits 3 frequencies (and 3 modes of libration: a wobble mode, a precession mode and a longitude mode).
- Reference systems
  The lunar motion defines intrinsically a dynamical system. It allows in particular a positioning of the dynamical reference frame in the ICRS. This topic is discussed in the last section.

3 Lunar Laser Ranging data analysis: evaluation of the residuals

LLR data analysis has to be performed rigorously in the frame of General Relativity. We use below the common language of classical mechanics for sake of simplicity, without changing the nature of the physical problem.

The LLR stations provide the 'Normal Points', which are used as 'observed values'. A 'Normal Point' consists in Δt_o, the duration of the round trip travel of the light in atomic time (TAI, Temps Atomique International) and t_1, the date of the starting pulse in Universal Time Coordinated (UTC). The other data supplied are the wavelength of the pulse, the number of returns, the estimated uncertainty of measurements, the signal/noise rate and the temperature, pressure and humidity of the atmosphere.

The principle of the analysis is to compare the 'observed value' Δt_o with a 'computed value' Δt_c and to deduce the residual: $\rho = \Delta t_0 - \Delta t_c$.

The 'computed value' Δt_c is determined in two steps as follows: from the LLR station transmitter O at time t_1 to the lunar reflector R at time t_2, and then from R at time t_2 to O at time t_3.

The propagation time has to be corrected taking into account several effects such as the relativistic curvature of the light beam or the influence of the troposphere. Relativistic changes of time scales have to be performed in order to express the various components in the same time scale. In the frame of the General Relativity theory, the computed Δt_c depends on the barycentric positions of T, L and S, respectively the center of mass of the Earth, of the Moon and of the Sun; B is the barycenter of the solar system.

Hence, as shown on Figure 11, the computation involves the following coordinates in the same celestial barycentric reference system:

- the coordinates of TL (Earth-Moon) provided by a lunar ephemeris, and the barycentric coordinates of the Earth-Moon barycenter BG provided by a planetary ephemeris,
- the coordinates LR (lunar reflector) which requires an ephemeris of the lunar librations and the selenocentric coordinates of the reflectors,
- the coordinates of TO (observing station) which requires a precise knowledge of the Earth rotation (precession, nutation, polar motion, and Universal Time UT through the sidereal time), of the coordinates of the station in a terrestrial reference system, and of relativistic corrections.

The value of Δt_c is given by:

$$\Delta t_c = [t_3 - \Delta T_1(t_3)] - [t_1 - \Delta T_1(t_1)]$$

$$t_3 = t_2 + \frac{1}{c}\,|BR(t_2) - BO(t_3)| + \Delta T_3 + \Delta T_4$$

$$t_2 = t_1 + \frac{1}{c}\,|BR(t_2) - BO(t_1)| + \Delta T_3 + \Delta T_4$$

where c is the velocity of the light, ΔT_1 is a relativistic correction on the time scales, ΔT_3 is the time contribution due to the gravitational curvature of light beam and ΔT_4 is the atmospheric delay. The correction ΔT_2, not mentioned above is the difference between Barycentric Dynamical Time (TDB) and Terrestrial Time (TT).

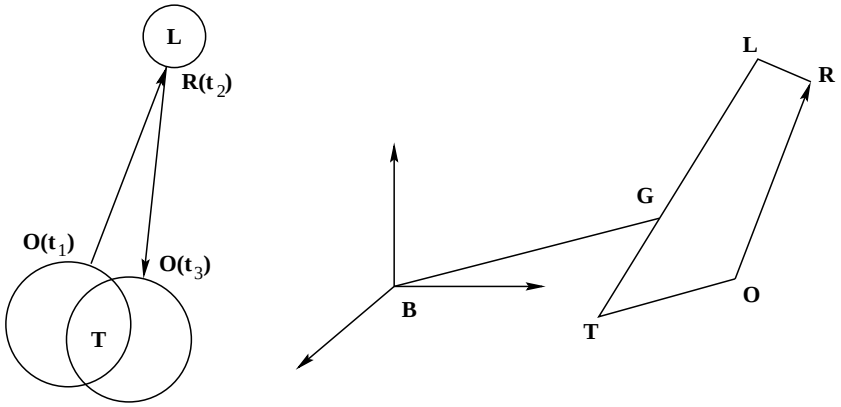

Fig. 11. Light beam OR (Observer-Reflector), Earth T, Earth-Moon barycenter G, Barycenter of the solar system B

Several coordinates transformations are needed in the computations of the barycentric coordinates of the station O and of the reflector R to relate the barycentric reference system (BRS) to the various systems in which the positions are provided: lunar and solar ephemerides, libration and Earth rotation. Actually, the complete model to represent at best the observations is complex and one has to consider a great variety of models: plate motions, atmospheric delay, solid tides of Earth and Moon, ... The ephemeris computations are performed in Barycentric Coordinate Time (TCB). Practically TCB is replaced by a linear function close to the former Barycentric Dynamical Time (TDB). Therefore there are the successive transformations:

$$UTC \rightarrow TAI \rightarrow TT = TAI + 32.184s \rightarrow TDB = TT + \Delta T_2$$

At the end of the computation Δt_c is tranformed from TDB to TAI by means of the relativistic correction ΔT_1.

The global formulation of Δt_c is:

$$\Delta t_c = \frac{1}{c}\,|BR(t_2) - BO(t_1)| + \frac{1}{c}\,|BR(t_2) - BO(t_3)|$$

$$+2\Delta T_3 + 2\Delta T_4 - \Delta T_1(t_3) - \Delta T_1(t_1)$$

with:

$$BR(t) = BG(t) + \frac{m_T}{m_T + m_L} TL(t) + LR(t)$$

$$BO(t) = BG(t) + \frac{m_L}{m_T + m_L} TL(t) + TO(t)$$

where m_T and m_L are respectively the Earth and Moon masses.

The ephemerides of the Moon TL and of the Earth-Moon barycentre BG are referred to the dynamical ecliptic frame of J2000.0 and depend on a large number of physical parameters. Many of them can be fitted to LLR observations: elements of the lunar and terrestrial orbits, coefficients of the gravity field, mass of the Earth-Moon system, tidal dissipation that produces the secular acceleration of the lunar longitude, and relativistic parameters. Indirectly the value of the astronomical unit and the planetary ephemerides play an important role on the lunar motion through various parameters, in particular planetary masses.

The ephemeris of the reflectors LR is dependent of the reflector coordinates in a selenocentric frame defined by the principal axes of inertia of the Moon. They also depend on the lunar rotation which is provided by a theory of the forced libration and the free libration constrained by the elastic deformation of the Moon. The Love numbers and the value of the moments of inertia are fitted parameters. It is worth noticing that a coupling effect exists between the lunar libration and circulation, which is very sensitive to the harmonic coefficients of the lunar potential, in particular in the secular motions of the node and of the perigee. The selenocentric frame is linked to the dynamical ecliptic frame of J2000.0 by the transformation:

$$R_z(-W_1 + 180^\circ) \times M(p_1, p_2, \tau)$$

where R_z is the rotation around the z-axis, W_1 is the mean lunar longitude and M is the matrix fonction of the libration variables p_1, p_2, τ at the time t_2.

The ephemeris of the station TO are primarily defined in the International Terrestrial Reference Frame (ITRF) and are subject to various corrections due to the Earth deformations: terrestrial and oceanic tides and pressure anomaly. For expressing the components of TO in the dynamical ecliptic frame of J2000.0 we have to apply the following transformations:

ITRF → equatorial frame of date
→ equatorial frame of J2000.0
→ dynamical ecliptic frame of J2000.0

The first transformation involves the Earth rotation parameters (EOP): the polar motion (x_p, y_p) and UT1-UTC used through the sidereal time θ as a function of UT1. The second transformation is obtained by the matrix of precession-nutation $P \times N$. The last transformation is performed for referring the station in the dynamical equinox and ecliptic frame defined by the lunar and planetary ephemerides with the position angles: ϵ (obliquity in J2000.0) and ϕ (arc separating the inertial equinox and the origin of the right ascensions on the equator of J2000.0) (see Fig. 13). Hence, the total transformation is:

$$R_x(\epsilon) \times R_z(\phi) \times P^{-1} \times N^{-1} \times R_z(-\theta) \times R_x(y_p) \times R_y(x_p)$$

where R_x, R_y and R_z are respectively the rotations around the x-axis, y-axis and z-axis.

4 Lunar Laser Ranging data analysis: dynamical model and fitted parameters

Two different approaches are possible to represent the planetary and lunar motions: the numerical integrations and the analytical theories.

The Jet Propulsion Laboratory (JPL) has produced very precise ephemerides of the Moon and planets by numerical integration: the Development Ephemerides such as DE200, DE403, or DE405. The most recent integration DE405/LE405 covers 6000 years. It has been fitted to observations and oriented onto the ICRF; it represents presently the most elaborated ephemeris, taking into account the most precise observations

(Radar, Mars spacecraft data, VLBI and LLR) and a very refined dynamical model in the frame of General Relativity, including asteroids. Its main characteristic is a simultaneous integration of the planets, the Moon and the libration.

At Paris Observatory, an analytical approach has been followed. The lunar analytical solution ELP, and its different versions elaborated since 1982, are not as precise as a numerical integration but contains explicitely a large number of parameters. On the short term, it is not adequate to reach the centimeter level required by LLR. Hence, it is completed with numerical complements obtained by difference with a JPL numerical integration as a reference. The numerical complements do not depend on the orbital constants; they improve solely the numerical precision of the analytical solution. ELP plus the numerical complements - fixed once for all - has the precision of a numerical integration and retains the advantages of an analytical solution. Then we can use the analytical form of the solution to fit numerous parameters since the partial derivatives are straightforward. But beyond this practical advantage, the main interest is to make possible an analysis of the perturbations having the same signature by putting aside the various components.

Three important examples can be given:

a) The secular acceleration of the lunar longitude is the sum of several components: Sun and planets, Earth's figure and tides. When observing the total phenomena in LLR residuals it is fundamental to separate the planetary effects from tides, in particular to be able to fit precisely the Love number and the timelag.

b) The libration is composed of a forced component arising from time-varying torques on the lunar figure due to attraction by Earth, Sun and planets and a free component which is a departure of the lunar angular position from an equilibrium state. The separation of the two modes is essential to isolate the free librations to understand the underlying excitation mechanism.

c) Important contributions due to Relativity exist in the sidereal mean motions of the lunar perigee and node, of about 2 arcseconds per century, which have to be separated from other contributions (planets, Earth and lunar figures, tides). Analytical expressions of these motions have been obtained as a function of the PPN parameters β and γ ($\beta = \gamma = 1$ in General Relativity), that can be then tested.

The last version of the analytical solution issued from ELP and fitted to LLR observations is called S2001.

Several improvements were introduced in S2001 with respect to the previous solutions: mainly in the libration model with numerical and analytical complements, but also in the program of reduction with an up-to-date nutation model and a realistic statistical treatment of the data, in particular an adequate distribution of weights among the various observing stations and periods of observations. The fits of the lunar orbital and rotational parameters in S2001 are listed hereunder; the orbital parameters are referred to J2000.0 under the formulation: $Q = Q^{(0)} + Q^{(1)}t + Q^{(2)}t^2 + Q^{(3)}t^3 + Q^{(4)}t^4$ where t is the time in Julian centuries since J2000.0.

- the geocentric lunar orbital parameters $W_1^{(0)}$, $W_2^{(0)}$, $W_3^{(0)}$, (constants of the mean longitude, mean longitudes of perigee and node), $\nu =$

$W_1^{(1)}$, Γ and E (sidereal mean motion, constants for inclination and eccentricity);

- the heliocentric orbital parameters of the Earth-Moon barycenter $T^{(0)}$, and $\varpi'^{(0)}$, (constants of the mean longitude and longitude of perihelion), n' and e' (sidereal mean motion and eccentricity);

- the bias parameters $W_1^{(2)}$, $W_2^{(1)}$, $W_3^{(1)}$, (observed corrections to the computed coefficient of the quadratic term of the lunar mean longitude, and the computed mean motions of perigee and node). $W_1^{(2)}$ yields an observed value of $W_1^{(2,T)}$, the tidal part of the coefficient of the quadratic term of the mean longitude of the Moon (half tidal secular acceleration);

- the 6 libration parameters which are the amplitudes of the 3 main free libration terms and their respective arguments.

Fits of other parameters have been also performed in S2001 such as the position angles of the dynamical ecliptic frame with respect to various systems of axes (ϵ, ϕ, ψ), the correction to the IAU 1976 precession constant Δp and the coordinates of the reflectors and stations. Note that a simultaneous fit of all the parameters produces much correlated values. Hence, the fits have been performed in several steps and tests have been made in order to check the stability of the results. Indeed, strong correlations that exist among some parameters may weaken the accuracy of our determinations; in particular, it is the case of the variables related to the reference frame and the positions of the stations. The correction to IAU 1976 precession constant Δp and the obliquity rate are correlated with the velocities of the stations. The principal nutation term and Δp are also difficult to separate. It is also the case for the selenocentric coordinates of the reflectors and the parameters of the free libration.

We have adopted the following strategy. First, we determine the whole set of parameters mentioned above except the positions and velocities of the stations. Then fixing the value ϕ (position angle, see Fig. 13), we add the positions of the stations to the whole set and make a new improvement. Next, we determine the velocities of the stations separately. Finally, fixing all the parameters, we perform a last analysis including Δp and the principal term of the nutation in longitude. At each step of the process we check the coherence of the determinations; for example we verify that the introduction of the fitted values of the station coordinates does not change significantly the value of ϕ when the first step is reiterated.

Table 1 shows the evolution of the residuals obtained with S2001 for the distance between the LLR stations and the lunar reflectors expressed in centimeters. It gives the time distribution of the root mean square of post-fit residuals obtained with the data provided by the different instruments used since 1972. We note an important gain of precision, between the earliest observations and the recent ones.

The evolution in the quality of the observations is also illustrated in Figure 12 that gives the time distribution of r.m.s. of the residuals obtained with S2001, retaining solely the data provided since1988 by the 2 modern instruments: MLRS2 for McDonald and YAG for the CERGA.

Table 1. LLR residuals: time distribution of the rms (unit:cm). N is the number of LLR 'Normal Points'.

OBSERVATORY *and instruments*	Time Interval	S2001 rms	N
McDONALD	1972-1986	43.5	1487
Telescope 2.70 m	1976-1979	27.7	1035
and MLRS1	1980-1986	29.1	990
CERGA *Rubis*	1984-1986	18.7	1165
HALEAKALA	1987-1990	6.3	451
McDONALD	1987-1991	5.8	232
MLRS1	1991-1995	4.6	586
and MLRS2	1995-2001	3.3	1669
CERGA	1987-1991	5.3	1574
Yag	1991-1995	3.9	2044
	1995-2001	3.0	3273

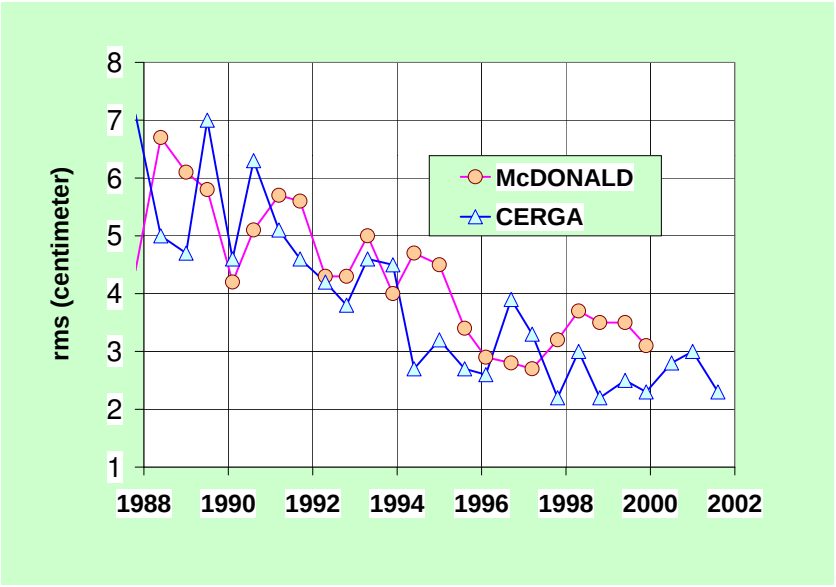

Fig. 12. Residuals of the observations of the 2 operating stations: McDONALD and CERGA

5 Lunar Laser Ranging data analysis: reference system

5.1 Positioning the inertial mean ecliptic of J2000.0

The lunar solution is referred to a dynamical system and introduces the inertial mean ecliptic of J2000.0. With LLR analysis, we can adjust the position of this plane with respect to various equatorial systems. Figure 13 presents the inertial mean ecliptic of J2000.0 and the various equatorial systems (R) involved in our study:

- ICRS: International Celestial Reference System,
- MCEP: Reference system linked to CEP (Celestial Ephemeris Pole),
- JPL: Reference system defined by a JPL numerical integration such as DE403 or DE405.

$\gamma^I_{2000}(R)$ is the ascending node of the inertial mean ecliptic of J2000.0 on the equator of (R), that is the 'inertial equinox of J2000.0', and $o(R)$ is the origin of right ascensions on the equator of (R). The position angles ϵ, ϕ and ψ are:

– $\epsilon(R)$, the inclination of the inertial mean ecliptic to (R),
– $\phi(R)$, the arc between $o(R)$ and $\gamma^I_{2000}(R)$ on (R),
– $\psi(R)$, the arc between $\gamma^I_{2000}(ICRS)$ and $\gamma^I_{2000}(MCEP)$ on the mean ecliptic of J2000.0.

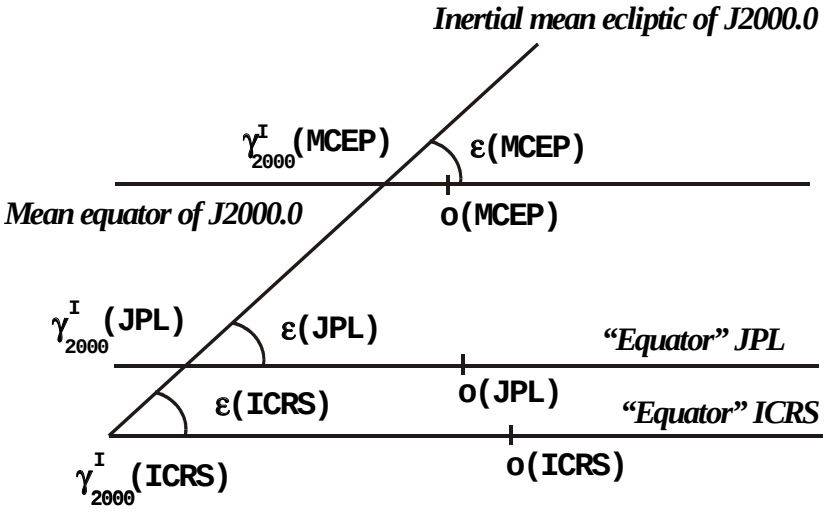

Fig. 13. Position angles of the inertial mean ecliptic of J2000.0

Concerning the ICRS and MCEP reference system, two solutions 'S2001' have been investigated. In both of them the position angles ϵ and ϕ are fitted, but the transformations of the terrestrial coordinates of the stations to celestial ones are different:

- in S2001(ICRS),
  the precession-nutation matrix $P \times N$ is computed via the conventional set of values recommended by the International Earth Rotation System (IERS), in particular the nutation corrections $\delta\epsilon$ and $\delta\psi$ of the series EOP(C04) produced by the Earth Orientation Center,

- in S2001(MCEP),
  the precession-nutation is provided by analytical solutions: polynomial expressions of the precession and theory of nutation; in this case, the correction to the IAU 1976 precession constant Δp is also fitted. In the same way, the lunar solution compared to any JPL ephemeris provides the angles referring the inertial mean ecliptic of J2000.0 with respect to the system defined by the corresponding JPL numerical integration.

Table 2 gives the different values of the position angles ϵ, ϕ and ψ determined for each equatorial reference system. The mean epoch mentioned in this table corresponds to the weighted mean date of LLR observations in the case of ICRS and MCEP. For DE403 and DE405, we have arbitrarily chosen the epoch in function of the dates mentioned in the JPL literature about the observations used in the corresponding numerical integrations.

Table 3 gives the offsets of the Celestial Ephemeris Pole (CEP) with respect to ICRS computed with LLR analysis and a recent value obtained by VLBI measurements; S1998 and S2000 are previous versions of S2001. The notations $\Delta\epsilon_0$ and $\psi\sin\epsilon_0$ are those used in IAU Report on Astronomical Constants.

The separation between the origin of right ascensions in ICRS, $o(ICRS)$, and the projection $o'(JPL)$ of the origin of right ascensions $o(JPL)$ on the ICRS equator (see Fig.13) can be determined using the values of Table 2:

$$o(ICRS)\ o'(DE403) \quad = \quad 1.9\ mas\ \ (Epoch,\ 1985\ Jan\ 1)$$

$$o(ICRS)\ o'(DE405) \quad = \quad 0.7\ mas\ \ (Epoch,\ 1990\ Jan\ 1)$$

Table 2. Position of the inertial mean ecliptic of J2000.0 with respect to various equatorial celestial systems R in S2001. (unit: arcsecond). The uncertainties are formal errors.

R	$\epsilon - 23°26'21"$	ϕ	ψ	Mean Epoch
ICRS	0.41100 ± 0.00005	-0.05542 ± 0.00011		Dec 1994
MCEP	0.40564 ± 0.00009	-0.01460 ± 0.00015	0.0445 ± 0.0003	Dec 1994
DE403	0.40928 ± 0.00000	-0.05294 ± 0.00001	0.0048 ± 0.0004	Jan 1985
DE405	0.40960 ± 0.00001	-0.05028 ± 0.00001	0.0064 ± 0.0003	Jan 1990

Table 3. Offsets of Celestial Ephemeris Pole at J2000.0 with respect to ICRS in S2001, $\Delta\epsilon_0$ and $\psi\sin\epsilon_0$ (unit: arcsecond). The uncertainties are formal errors.

Method	Source	$\Delta\epsilon_0$	$\psi\sin\epsilon_0$
LLR	POLAC S1998	-0.0056 ± 0.0002	-0.0183 ± 0.0004
LLR	POLAC S2000	-0.0054 ± 0.0002	-0.0173 ± 0.0004
LLR	POLAC S2001	-0.0054 ± 0.0002	-0.0177 ± 0.0004
VLBI	IAU2000 (*)	-0.0049 ± 0.0003	-0.0167 ± 0.0005

(*) Fukushima, 2000, Report on Astronomical Constants.

Note that the numerical integration DE405 uses very precise VLBI observations made between 1989 and 1994 and is oriented onto the ICRS.

The angle $\psi(R)$ is the separation between the inertial equinox of J2000.0 in ICRS, $\gamma^I_{2000}(ICRS)$, and the inertial equinox of J2000.0 in the reference system (R), $\gamma^I_{2000}(R)$. It depends of the expression of the lunar mean longitude of the Moon W_1 which has the following secular expansion:

$$W_1 = W_1^{(0)} + W_1^{(1)}t + W_1^{(2)}t^2 + W_1^{(3)}t^3 + W_1^{(4)}t^4$$

where t is the time in Julian centuries since J2000.0.
$W_1^{(0)}$ is the constant term (mean longitude at J2000.0), $W_1^{(1)}$ is the sidereal mean motion (also noted ν) and $W_1^{(2)}$ is the total half-secular acceleration of the Moon. Hence, $\psi(R)$ can be determined by:

$$\psi(R) = W_1(ICRS) - W_1(R) =$$

$$[W_1^{(0)}(ICRS) - W_1^{(0)}(R)] \ +$$

$$[W_1^{(1)}(ICRS) - W_1^{(1)}(R)]t \ +$$

$$[W_1^{(2)}(ICRS) - W_1^{(2)}(R)]t^2$$

where t is the time at a mean epoch, reckoned in centuries from J2000.0 (see Table 2).

5.2 Tidal acceleration

Figure 14 shows the evolution of the correction to the 3 components of W_1: $\Delta W_1^{(0)}$, $\Delta W_1^{(1)}$ and $\Delta W_1^{(2)}$ with the variation of the upper limit of the time span covered by the fit. In other words, the graph represents the different values of $\Delta W_1^{(i)}$ with: $i = 0, 1, 2$ for intermediate solutions in which the characteristics of the fit are the same as in the solution S2001, except the time intervals of the LLR observations that we have successively limited to equidistant dates between 1996 and 2001. We can notice in particular the convergence of the acceleration. This is mainly explained by the evolution of the fitted value of the tidal part of the acceleration when using more and more recent LLR observations.

The tidal component of the secular acceleration of the Moon's longitude is a fundamental parameter, which expresses the dissipation of energy in the Earth-Moon system. It is due to a misalignment of the bulge of the Earth relative to the Earth-Moon direction, which exerts a secular torque. It produces a secular negative acceleration in the lunar longitude of approximately $-25.8"/cy^2$ and correspondingly a decrease in the Earth's rotation rate (or an increase of the length of day). Another consequence is the displacement of the Moon that corresponds to an increase of the Earth-Moon distance of 3.8 $cm/year$.

Table 4 gives a list of determinations of the tidal secular acceleration of the lunar longitude since 1939 and provided by several types of observations: occultations, eclipses and LLR. The most recent values have been obtained with LLR observations. We note for this type of determination a significant improvement of the precision when increasing the number of observations and their accuracy. It is also worth noticing that the most recent determination around $-25.86"/cy^2$ comes closer to the value of Morrison & Ward (1975) obtained with optical observations over a very long time span.

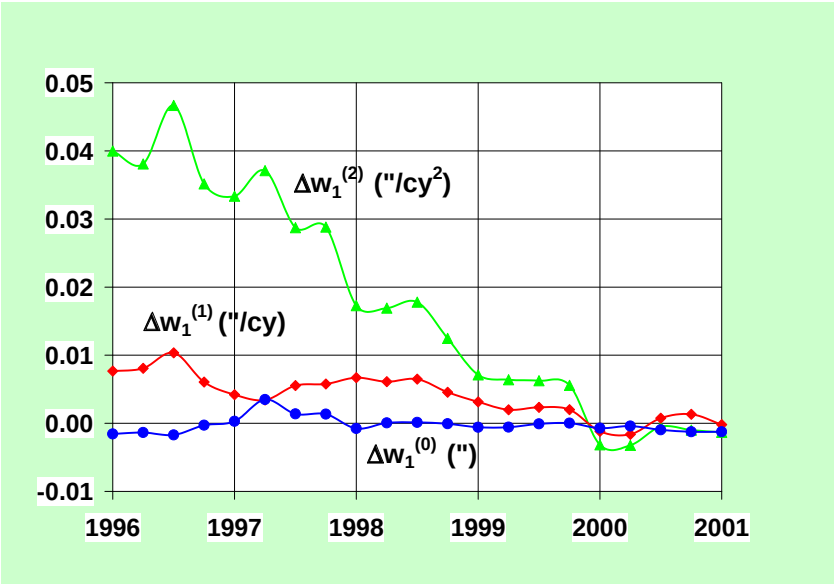

Fig. 14. Evolution of the corrections to the secular components of the mean lunar longitude

Table 4. Tidal acceleration of the lunar mean mean longitude. (unit: arcsecond/cy^2)

Authors	Value	Publication
Spencer Jones [a]	-22	1939
Oesterwinter & Cohen [a]	-38	1975
Morrison & Ward [a]	-26	1975
Muller [b]	-30	1976
Calame & Mulholland [c]	-24.6	1978
Ferrari et al. [d]	-23.8	1980
Dickey et al. [c]	-23.8	1982
Dickey and Williams [c]	-25.10	1982
Newhall et al. [c]	-24.90	1988
Dickey et al. [c]	-25.88	1994
Chapront Touzé et al. [c]	-25.62	1997
(Solution S1998) [c]	-25.78	1999
(Solution S2000) [c]	-25.836	2000
(Solution S2001) [c]	-25.858	2002

Type of observations:
a: Occultations, *b*: Eclipses,
c: LLR, *d*: LLR and Lunar orbiter

Table 5. Tidal acceleration of the lunar mean longitude in various JPL ephemerides (unit: arcsecond/cy^2) (Standish, 1982, 1995, 1998)

JPL ephemeris	Value	Publication
DE200	-23.895	1982
DE245	-25.625	1990
DE403	-25.580	1995
DE405	-25.826	1998

Table 5 gives the intrinsic values of the tidal acceleration in various JPL numerical integrations. The difference between the last JPL value (DE405) and our determination in S2001 gives an idea of the present uncertainty and allows to ensure nowadays a realistic precision of better than $0.03"/cy^2$ in the knowledge of this fundamental lunar parameter. Note that the values presented here as 'JPL values' do not appear explicitly in the list of parameters provided by JPL. We have deduced them from the comparisons of the solution S2001 to the JPL ephemerides.

5.3 Precession constant

In the solution S2001(MCEP), which is linked to the Celestial Ephemeris Pole (CEP), the precession constant has been fitted and the correction Δp to the IAU 1976 constant is equal to $-0.3364"/cy$. We observed that this correction was noticeably divergent from the values of this correction obtained by previous solutions such as S1998 or S2000.

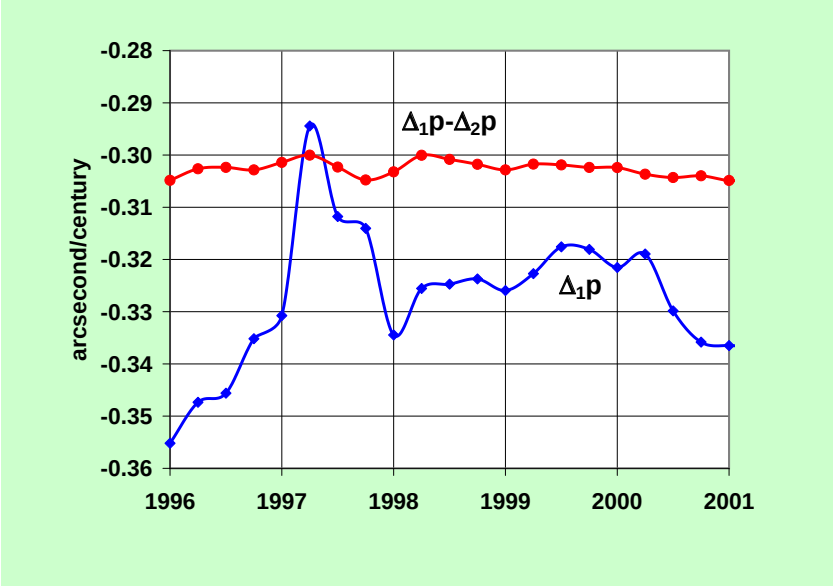

Fig. 15. Evolution of the correction to the IAU 1976 precession constant with the time span covered by the fit: $\Delta_1 p$ for S2001(MCEP) and $\Delta_2 p$ for S2001(ICRS)

Figure 15 illustrates the evolution of Δp with the variation of the upper limit of the time span covered by the fit with the same division in 'slices of time' as we did previously in Figure 14 for the components of the mean lunar longitude. We note $\Delta_1 p$ the evolution of Δp in solution S2001(MCEP). The 'accidental jump' that we observe for 1997 corresponds to an offset of 0.7 nanosecond in the CERGA measurements which has been partly corrected in our analysis. In fact, the relevance of this graph is to put in evidence a residual $\Delta_2 p$ which also arises when we put Δp in the list of the fitted parameters of the solution S2001(ICRS). We note in particular that the difference $\Delta_1 p - \Delta_2 p$ is almost constant on the time interval [1996-2001].

S2001(MCEP) and S2001(ICRS) use the same observations, which are the main source of errors, and the same models, except for the motion of the reference frame due to precession and nutation. If we assume that the series EOP(C04) $\delta\epsilon$ and $\delta\psi$ used in S2001(ICRS) and based on VLBI

observations, contributes ideally to the precession-nutation matrix, we can make the hypothesis that the residual $\Delta_2 p$ is also included in $\Delta_1 p$. Hence, the differences between the two corrections $\Delta p = \Delta_1 p - \Delta_2 p$ gives an better estimate of the corrections to the IAU 1976 precession constant than $\Delta_1 p$. This correction remains around the value $-0.302"/cy$.

Table 6 shows that the last value of the correction to IAU 1976 precession constant Δp obtained by LLR are very close to recent determinations obtained by VLBI analysis: the value presented in the IAU General Assembly in 2000 (Fukushima, 2000) or the value of the theory of nutation MHB2000 (Herring et al., 2002). LLR and VLBI determinations converge nicely with a separation smaller than 0.03 mas/year.

Table 6. Correction to the IAU 1976 precession constant Δp (unit: arcsecond/cy). The uncertainties are formal errors.

Method	Source		Δp
LLR	S2001	(Chapront, 2002)	-0.302 ± 0.003
VLBI	IAU2000	(Fukushima, 2000)	-0.297 ± 0.004
VLBI	MHB2000	(Herring, 2002)	-0.2997 ± 0.0008

6 Conclusion

The improvement of the LLR measurements during the 10 last years associated with a more refined Earth-Moon model have allowed to provide a better determination of the angles involved in the positioning of the dynamical ecliptic reference frame with respect to the ICRS and other equatorial reference systems. This gain in accuracy is also noted for the estimation of the correction to the precession constant and for the determination of the tidal secular acceleration of the lunar longitude. Presently, at the CERGA, an individual LLR measurement shows an error around 30-60 picoseconds. So, there is still a margin between the present 'instrumental' accuracy of the data and the values of the residuals obtained by the LLR analysis. The team of the Paris Observatory lunar analysis center works in cooperation with the LLR staff of the CERGA since 1998. Besides the LLR analysis, we assume also a role of control and validation of LLR data as soon they are provided by the CERGA. Nevertheless, the first goal of our analysis is to improve the analytical solution of the orbital and rotational motions of the Moon. A theory of the lunar motion including new planetary perturbations, ELP/MPP02, will replace the previous solution and in this version the constants will be fitted to LLR data taking into account the results presented here (Chapront and Francou, 2002).

Acknowledgements: We are grateful to LLR staffs of CERGA and McDONALD for providing the LLR observations and normal points. We thank F. Mignard for its fruitful contributions and M. Chapront-Touzé who is a main contributor in the LLR analysis work.

Bibliography and References

Boucher C., Altamimi Z., Feissel M., Sillard P., 1996, IERS Technical Note 20, Central Bureau of IERS, Observatoire de Paris

Calame O., Mulholland J. D., 1978, Science, 199, 3.

Chapront-Touzé M., Chapront J., 1983, Astron. Astrophys., 124, 50-62.

Chapront-Touzé M., Chapront J., 1988, Astron. Astrophys., 190, 342.

Chapront J., Chapront-Touzé M., 1997, Celest. Mech., 66, 31.

Chapront J., Chapront-Touzé M., Francou G., 1999, Celest. Mech., 73, 317-328.

Chapront J., Chapront-Touzé M., Francou G., 1999, Astron. Astrophys., 343, 624-633.

Chapront J., Chapront-Touzé M., Francou G., 2000, in Journées systèmes de référence spatio-temporelles 2000, Observatoire de Paris.

Chapront J., Mignard F., 2000, C R. Acad. Sci. Paris, t.1, Série IV, p. 1233-1243.

Chapront J., Chapront-Touzé M., Francou G., 2002, Astron. Astrophys., 387, 700-709.

Chapront J., Francou G., 2003, Astron. Astrophys., 404, 735-742.

Dickey J. O., Williams J. G., 1982, E.O.S., 63, 301

Dickey J. O., Williams J. G., Yoder C. F., 1982, in High Precision Earth rotation and Earth-Moon dynamics, O. Calame Ed., Reidel, Dordrecht, 209.

Dickey J. O, Bender P. L., Faller J. E, Newhall X X, Ricklefs R. L., Ries J. G., Shelus P. J., Veillet C., Whipple A. L., Wiant J. R., Wiiliams J. G., Yoder C. F., 1994, Science 265, 482-490.

Ferrari A. J., Sinclair W. S., Sjogren W. L., Williams J. G., Yoder C. F., 1980, J. Geophys. Res., 85, 3939.

Folkner W. M., Charlot P., Finger M. H., Williams J. G., Sovers O. J., Newhall X. X, Standish E. M., 1994, Astron. Astrophys., 287, 279.

Fukushima T., 2000, in IAU Colloquium 180, K. J. Johnston et al. Eds., Washington D.C.

Herring T. A., Mathews P. M., Buffett B. A., 2002, Geophys. Res., 105, B4, 10.1029/2001JB000165.

Lucchini C., Gaignebet J., Hatat J. L., 1996, in Processings of the 8th International Laser Workshop, Canberra, Nov. 1994, 2, 628-635.

McCarthy, D. D., 1996, IERS Technical Note 21: IERS Conventions, Central Bureau of IERS, Observatoire de Paris.

Moons M., 1982, The Moon and the Planets, 27, 257-284.

Moons M., 1984, Celest. Mech., 34, 263.

Morrison L. V., Ward C. G., 1975, Monthly Notices Roy. Astron. Soc., 173, 183.

Muller P. M., 1976, JPL Spec. Publ. 43-36.

Newhall X X, Williams J. G, Dickey J. O., 1988, in The Earth's rotations and reference frame for geodesy and geodynamics, A. Babcok and G. Wilkins Eds., Reidel, Dordrecht, 159.

Newhall X X, Williams J. G., 1997, Celest. Mech., 66, 21.

Nordvedt K., 1998, Class. Quantum Grav., 15, 3363-3381.

Oesterwinter C., Cohen C. J., 1975, Celest. Mech., 5, 317.

Samain E., Mangin J. F., Veillet C., Torre J. M., Fridelance P., Chabaudie J. E., Feraudy D., Glentzlin M., Pham Van J., Furia M., Journet A., Vigouroux G., 1998, Astron. Astrophys. Supp. Ser. 130, 235–244.

Simon, J. L., Bretagnon, P., Chapront, J., Chapront-Touzé, M., Francou, G., Laskar, J., 1994, Astron. Astrophys. 282, 663

Spencer Jones H., 1939, Monthly Notices Roy. Astron. Soc., 99, 541.

Standish E. M., 1982, Astron. Astrophys., 114, 297-302.

Standish E. M., 1995, JPL Planetary and Lunar ephemerides, DE403/LE403, IOM, 314.10-127, Pasadena.

Standish E. M., 1998, JPL Planetary and Lunar Ephemerides, DE405/LE405, IOM 312.F-98-048, Pasadena.

Standish E. M., 2000, in IAU Colloquium 180, K. J. Johnston et al. Eds., Washington D.C.

Williams J. G., Newhall X. X., Dickey J. O., 1996, Physical Review D, 53, 12, 6730-6739.

Williams J. G., Newhall X. X., Yoder C. F., Dickey J. O., 1996, Lunar Planetary Sciences, 27, 1439.

Williams J. G., Newhall X. X., Dickey J. O., 1998, Planet. Space Sci., 44, 1077-80.

Global consistency of IERS Earth orientation with the ITRS and ICRS: span 1988–2003

C. Bizouard

Observatoire de Paris, SYRTE, 61 av. de l'Observatoire, 75014 Paris, FRANCE

Abstract. In this technical note we present the problem of global consistency of EOP series, determined from VLBI, GPS, SLR observations. It is possible to quantify the level of consistency of two EOP series if the relative rotation between the reference frames to which they referred, is known. After recalling the way the ,,consistencies" are estimated, we derived them for the last global VLBI solutions received during the year 2004 at the Earth Orientation Center

1 Introduction

The Earth Orientation Parameters (EOP) are routinely provided by three techniques: VLBI, GPS, SLR. One of the tasks of the IERS, committed to the care of the EOP Centre of Paris since 1988 is to check the consistency of these series. Nowadays the time variations of the EOP agree from a series to an other at the level of 60 microarcseconds (μas): for polar motion, 15 microseconds for UT1 and 100 μas for nutation. But these same series can present larger systematic shifts, modelled as linear time function. These systematic offsets are not surprising when considering the fact that these series are referred to different reference frame (terrestrial and celestial). Indeed any rotation between these systems induce biases between the corresponding EOP. The consistency of two EOP series is granted if their bias is fully explained by the rotation angles between the terrestrial (or celestial) frames to which they are referred. From practical point of view biases and trend are computed with respect to combined series of the EOP Centre (C01), which is given in principle in the International Terrestrial Reference Frame (ITRF) and International Celestial Reference Frame (ICRF).

Consistencies were studied since 1988, and reported in the frame of the IERS annual report. The inconsistencies reached in this epoch 1-2 milliarcseconds (mas). They are now reduced to a few tenths of mas. This is too large with respect to the precision of the EOP.

2 Theory

Let us consider two series of EOP (x, y, UT1, dψ, dϵ) and (x', y', UT1', dψ', dϵ') respectively. Each of them is referred to a celestial frame defined by the adopted Radio Source Coordinates (RSC) and to a terrestrial frame defined by the adopted Set of Station Coordinates (SSC) and velocities. The celestial reference frames, respectively denoted CRF and CRF' present systematic differences, which can be described by an elementary rotation matrix A. The coordinates in both system, [CRF] and [CRF'] respectively, are linked by the relation:

$$[\mathrm{CRF}] = \mathrm{A}\ [\mathrm{CRF'}]$$

In the same way the terrestrial reference frames, TRF and TRF' respectively, are linked through an elementary rotation:

$$[\mathrm{TRF}] = \mathrm{R}\ [\mathrm{TRF'}]$$

If both EOP series were consistent with their frames, then the systematic differences in the pole coordinates (Δx = x' - x, Δy = y' - y), in the universal time (ΔUT1 = UT1' - UT1), and in the celestial pole offsets ($\Delta\psi = \delta\psi$' - $\delta\psi$, $\Delta\epsilon = \delta\epsilon$' - $\delta\epsilon$) would be only due to the rotation angles (A1, A2, A3) between the two celestial frames and (R1, R2, R3) between the two terrestrial frames. It can be shown that these systematic differences would satisfy the following relationships with an accuracy of a few microarcseconds:

$$\begin{aligned} \Delta x &= R_2 \\ \Delta y &= R1 \\ f.\Delta UT1 &= -R_3 + A_3 \\ \Delta(\delta\psi) &= A_2/sin(\epsilon_0) \\ \Delta(\delta\epsilon) &= -A_1 \end{aligned} \tag{7}$$

where f is the conversion factor from Universal Time to sidereal time, and ϵ_0 is the obliquity of the ecliptic. It is worthwhile to check to which extent the relationships (1) are satisfied. Each comparison will be made naturally with respect to the same data set (CRF, TRF, EOP), that is the ICRF, the ITRF and the corresponding EOP series of the IERS. The closure of relationships (1) characterises the internal consistency of the set of IERS results, time series and reference frames. In this objective the quantities

$$\begin{aligned} C(x) &= \Delta x - R_2, \\ C(y) &= \Delta y - R_1, \\ C(UT1) &= f.DUT1 - (-R_3 + A_3), \\ C(\delta\psi) &= \Delta(\delta\psi) - A_2/sin(\epsilon_0), \\ C(\delta\epsilon) &= \Delta(\delta\epsilon) - (-A_1) \end{aligned}$$

are computed.

3 Time evolution of the IERS EOP series relative to ITRF

We consider two terrestrial frames, each one having its own velocity field. The series of EOP, the relative drifts between the corresponding series of EOP can be predicted by relationships (2), obtained as the time derivatives of the first three relationships (1):

$$\begin{aligned} d(\Delta x)/dt &= d(R2)/dt \\ d(\Delta y)/dt &= d(R1)/dt \\ f.d(\Delta UT1)/dt &= -d(R3)/dt \end{aligned} \tag{8}$$

where d(R1)/dt, d(R2)/dt, d(R3)/dt are the rates of change of the rotation angles between the two terrestrial reference frames. These relationships are used to compare the drifts of the EOP series relative to EOP(IERS)C01 with their predicted values based on the definition of the corresponding terrestrial velocity field.

4 Results for the EOP VLBI series over the time span 1988–2003

Since the year 1998, the angles between the individual TRF and the ITRF97 have not been computed by the terrestrial frame section of the Central Bureau (located at the Institut Géographique National, France). For that reason consistency analyses for polar motion and UT1 is only pertinent for the series referred to the ITRF (angles R1, R2, R3 equal to zero). That is the case of some VLBI series.

Our analysis is restricted to the last VLBI EOP series, for which we had valuable information on their reference Radio Source Coordinates. They are listed in the Table 1.

Table 1. Analysed EOP VLBI series. We give the time span of the analysis and specify the reference frames to which are referred those series as well as the possible rotation between their associated radio source catalogue and the ICRF. Unit for angles is milliarcsecond.

VLBI EOP Series	Years considered	CRF	TRF	Organization
AUS 04 R 01	1988–2003	ICRF	?	Geoscience Australia
BKG 02 R 01	1988–2001	BKGI 02 R 01 A1 = 0.029±.010 A2 = -0.002±.009 A3 = -0.017±.011	ITRF2000	Bundesamt für Kartographie und Geodäsie
GAOUA 03 R 01	1988–2002	GAOUA 03 R 01 T A1 = 0.008±.011 A2 = -0.047±.010 A3 = -0.017±.012	?	Glavnaya Astronomicheskaya Observatorya Ukraini (MAO)
GSFC 02 R 01	1988–2002	GSFC 02 R 01 A1 = 0.011±.010 A2 = -0.015±.010 A3 = -0.036±.012	?	Goddard Space Flight Center, Washington
IAA 02 R 03	1988–2001	IAA 02 R 03 A1 = 0.003±.012 A2 = -0.012±.011 A3 = -0.007±.014	ITRF2000	Institut of Applied Astronomy Saint-Petersburg
MAO 03 R 02	1988–2002	ICRF	ITRF2000	Main Astronomical Observatory, Ukraine
SHA 04 R 01	1988–2002	ICRF	?	Shanghai Observatory

The present consistency analysis consists in two steps:

- The first step is the computation of the biases and slopes of the individual EOP parameters (nutation in longitude, nutation in obliquity) with respect to the combined parameters of the series EOP(IERS)C01. To this aim the individual series are averaged and interpolated with 0.05-year interval.
- The second step is the comparison, given hereafter, between these biases and those theoretically produced by the rotations between the reference frames, as already explained.

Table 2 gives the evaluations of the internal consistency for data sets involving celestial pole offsets series and RSC, till the date 2003.0. The data before 1988 are not considered because they are considered to be of lower quality. Biases and trends have been computed with respect to the epoch 1997.0.

Table 2. CONSISTENCY OF VLBI EOP SERIES WITH CELESTIAL REFERENCE FRAMES, BASED ON THE ROTATION ANGLES RELATIVE TO ICRF (slope and bias computed at the epoch 1997). The data span is given. Unit are mas (0.001"). For each series the first line gives the second member of consistency relation (1), the second line gives the second member of consistency relation (1), and the third line the consistencies themselves. The satisfactory ,,consistencies" are written in green, the ,,inconsistencies" or badly determined consistencies in red.

SERIES	1 2 3	R_2 Δx C(x)	R_1 Δy C(y)	$-R_3+A_3$ $f.\Delta UT1$ C(UT1)	$A_2/sin(\epsilon_0)$ $\Delta\delta\psi$ C($\delta\psi$)	$-A_1$ $\Delta\delta\epsilon$ C($\delta\epsilon$)
	1	?	?	?	0.000±0.025	0.000±0.010
EOP(AUS) 4 R 01	2	0.007±0.010	0.035±0.009	-0.113±0.015	0.022±0.019	-0.036±0.008
1988-2003 1997.00	3	?	?	?	0.022±0.032	-0.036±0.013
	1	0.000±0.000	0.000±0.000	-0.017±0.011	-0.005±0.023	-0.029±0.010
EOP(BKG) 2 R 01	2	-0.137±0.010	0.181±0.009	0.008±0.012	-0.036±0.016	-0.055±0.007
1988-2001 1997.00	3	-0.137±0.010	0.181±0.009	0.025±0.016	-0.031±0.028	-0.026±0.012
	1	?	?	?	0.118±0.025	-0.008±0.011
EOP(GAOUA)3 R 01	2	-0.081±0.010	0.144±0.009	-0.030±0.011	0.107±0.016	-0.027±0.007
1988-2002 1997.00	3	?	?	?	-0.011±0.030	-0.019±0.013
	1	?	?	?	-0.038±0.025	0.011±0.010
EOP(GSFC) 2 R 01	2	-0.200±0.009	0.064±0.007	0.003±0.009	-0.096±0.014	-0.013±0.006
1988-2002 1997.00	3	?	?	?	-0.058±0.029	-0.024±0.012
	1	0.000±0.000	0.000±0.000	-0.007±0.014	0.030±0.028	0.003±0.012
EOP(IAA) 2 R 03	2	0.037±0.012	-0.002±0.013	0.662±6.415	-0.065±0.021	-0.033±0.010
1994-2001 1997.00	3	0.037±0.012	-0.002±0.013	0.669±6.415	-0.095±0.035	-0.036±0.016
	1	0.000±0.000	0.000±0.000	0.000±0.000	0.000±0.000	0.000±0.010
EOP(MAO) 3 R 02	2	-0.088±0.011	0.144±0.009	-0.027±0.011	0.111±0.016	-0.034±0.007
1988-2002 1997.00	3	-0.088±0.011	0.144±0.009	-0.027±0.015	0.111±0.030	-0.034±0.012
	1	?	?	?	0.000±0.025	0.000±0.010
EOP(SHA) 4 R 01	2	-0.157±0.010	0.188±0.007	0.012±0.009	0.087±0.019	-0.048±0.009
1988-2002 1997.00	3	?	?	?	0.087±0.032	-0.048±0.013

4.1 Nutation offsets consistency

For celestial pole offsets $\delta\psi sin(\epsilon_0)$ and $\delta\epsilon$ the inconsistencies does not stretch over 50 μas. The mean consistency is about 30 μas. This an encouraging result, in the sense that the standard deviation between time series is typically two times more. For some series (BKG, GAOUA, GSFC) the angles between celestial frames explain partly the bias between series.

4.2 UT1 consistency

Three VLBI series allow us to establish consistency for UT1: BKG for which the value is perfectly acceptable, IAA for which the consistency remain poorly known probably because of the shortness of the series which begins in 1994, and MAO showing excellent consistency. Most often VLBI series are determined from sub-network of the ITRF, and it is not a clear issue whether this sub-network has a significant rotation with respect to the ITRF or not. This may be a major source of inconsistency in UT1.

4.3 Polar motion consistency

The inconsistencies in polar motion can be computed for 4 VLBI series. Globally their values are up to 200 μas, except for IAA series. We note that their mean values (for x: -60 μas, for y: 100 μas), are comparable to that ones associated with VLBI series determined from the VLBI-GPS Pilot Campaign 2001, but globally smaller.

5 Conclusion

We can measure the progress achieved in 10 years: in 1995 the mean consistencies were about 300 μas for x, 800 μas for y, 650 μas for the rotation angle, -150 μas for $\delta\psi sin(\delta\epsilon_0)$ and 50 μas for $\delta\epsilon$. The gain is up to 5 for some EOP, inconsistencies tend to the level of the uncertainties of the EOP parameters.

Comments on the VLBI connection between celestial and terrestrial reference frames by means of sidereal time

M. Feissel-Vernier

Observatoire de Paris/SYRTE, CNRS UMR8630, 61 Av. de l'Observatoire, 75014, Paris, FRANCE

Abstract. Causes of inaccurate or instable connection of the celestial and terrestrial VLBI reference frames via sidereal time are reviewed. Their effects after 1990 are in the range 5-10 μs in the short term, 2-7 μs year to year, with expected biases at the 2-5 μs level and spurious drifts smaller than 1 μs/year.

1 Introduction

In the international multi-technique project for measuring the Earth's rotation and deformations, VLBI has the unique role of providing the sidereal reference that is not accessible to the satellite-based techniques. The primary Earth Rotation Parameter (EOP) involved is Universal time UT1-TAI, a measure of the progressive departure of sidereal time with atomic time. In addition to providing the link between the terrestrial (rotating) and the celestial (inertial) reference frames, UT1 measurements provide global information on the dynamics of the various layer of our planet, from the liquid core to the upper atmosphere.

The celestial reference frame (CRF) is materialized by the equatorial coordinates of a set of extragalactic radio sources. Most objects exhibit time variations of their position in some preferred direction (Feissel-Vernier, 2003, 2005a). This is illustrated in Figure 1, which shows the envelopes of the standard deviation of yearly weighted average source positions in local equatorial frames for the most stable sources. The deficiency of sources south of declination -30^o is an effect of their relatively sparse observation history due the biased network distribution.

The terrestrial reference frame (TRF) is materialized by the cartesian coordinates of the position and velocity of the world VLBI network shown on figure 2. The most striking feature of the VLBI antenna network is its non-uniformity. The set of station positions and velocities that can

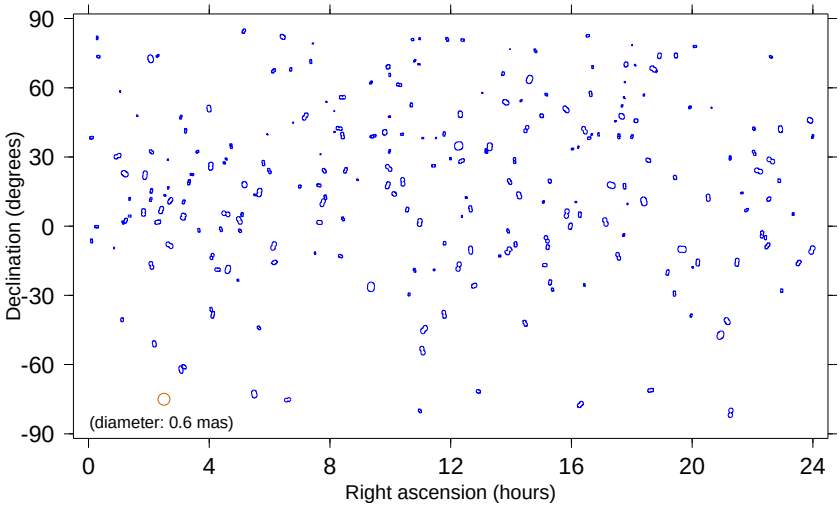

Fig. 1. Map of 245 well-observed radio sources (1989.5-2002.4) with one-year standard deviations smaller than 0.35 mas. Envelopes show the standard deviation of the yearly average coordinates in local equatorial frames ($\alpha \cos\delta$, δ).

be derived from long series of observations will not be perfectly uncorrelated. In addition, the network is normally not used in its entierety. In practice, the CRF-TRF link is implemented by series of 24-hour VLBI sessions involving 4-6 stations sampling a part of the network. On account of this weak geometrical coverage, correlations among EOP estimates can often exceed 0.5. For instance, the weekly IVS R4 network (see section 4) normally has a correlation coefficient between UT1 and polar motion X of about -0.6.

These imperfections of the realization of the celestial and terrestrial reference frames give rise to defects in the estimation of UT1. Various possible causes of inacuracy are reviewed. These concern data analysis options (section 2), the influence of the TRF and CRF incinsistencies (section 3), and the consequences of the observing strategy (section 4).

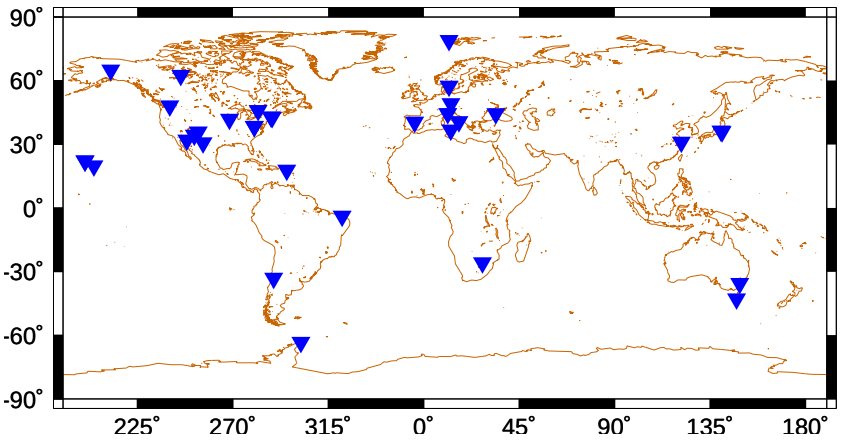

Fig. 2. Geodetic VLBI network.

2 Impact of TRF analysis status

The analysis strategies for deriving a celestial reference frame from multi-year VLBI observations include a number of choices. We consider here choices that concern the definition of the celestial and terrestrial reference frames and their connection in time. Two different approaches are used, as follows.

- In order to free the celestial frame solution from systematic errors that may be propagated from terrestrial network deficiencies, the so-called **CRF** approach was used in the derivation of the ICRF and its extensions (Ma et al., 1998; Fey et al., 2004). The stations positions are set as *arc parameters*, i.e., they are estimated independently for each observing session. Polar motion and universal time are not estimated but nutation corrections (celestial pole offsets) are obtained.
- In the so-called **TRF** approach, most station positions and velocities are set as *global parameters*, i.e. considered as valid over the total data span. Polar motion, universal time and nutation corrections are estimated for each session.

We investigate this possible contamination using test solutions based on the 1980.0-2002.7 data, described in table 1. Data analysis was performed at GSFC with the CALC-SOLVE software package. See Feissel-Vernier et al., 2005b) for more detail. The identification of stable sources is described by Feissel-Vernier (2003). The results considered are the celestial reference frames on the one hand, and the time series of UT1-TAI on the other hand.

Table 1. Test solutions: status of the sources (Global or Arc) and category of sources considered to define the orientation of the frame (No-net-rotation).

Frame	Arc sources	Global sources	No-net-rotation
TRF approach			
cne	unstable	all others	stable
cn7	none	all	ICRF *defining*
CRF approach			
cnh	unstable	all others	stable
cn8	none	all	ICRF *defining*

In order to test the possible perturbation of the orientation of the celestial reference frame due to the consideration of a global terrestrial frame, i.e. one set of station positions and velocities, we compute the relative orientations of pairs of celestial frames obtained with the same source categorization, with the **TRF** and the **CRF** approach.

The relative orientation of two celestial reference frames is modeled by three rotation angles A_1, A_2, A_3 around the axes of the equatorial coordinate system. These angles are estimated using equations (1) and (2), where α, δ are the source coordinates and $\Delta\alpha$, $\Delta\delta$ are the differences of coordinates in the two frames.

$$\Delta\alpha = A_1 \tan\delta \cos\alpha + A_2 \tan\delta \sin\alpha - A_3 \quad (1)$$

$$\Delta\delta = -A_1 \sin\alpha + A_2 \cos\alpha \quad (2)$$

The relative A_3 angles between pairs of celestial reference frames are given in table 2, for the two pairs of of celestial frames described in table 1. The inconsistency of the axes definition between the **TRF** and **CRF** approaches is at the level of 2 μas only (about 0.1 μs).

Table 2. Relative A_3 rotation angles of celestial reference frames obtained respectively with the **TRF** and **CRF** approaches, considering either the stable sources or the conventional defining ones.

Pair	A_3 (μas)
Reference: Stable sources	
cne-cnh	-2.3 ± 0.6
Reference: *Defining* sources	
cn7-cn8	1.7 ± 1.4

3 Sensitivity to consistency of the CRF and TRF

3.1 Internal inconsistencies of the TRF

The instability of a part of the sources in the CRF have been shown to give rise to slightly significant changes in the derived precession and nutation parameters (Feissel-Vernier et al., 2004). We study here the impact of source selection on UT1.

Possible contamination of the stability of the origin of right ascensions by the source instability may be estimated from differences between series of UT1-TAI referred to all sources (*cn7*) or to the stable ones only (*cne*). When modelling these differences over 1990-2002 as a linear variation one finds a bias of 4.7 ± 0.1 μs at J2000.0, a drift of -0.82 ± 0.02 μs/year, and an rms residual of 3 μs for one session.

3.2 Internal inconsistencies of the TRF

Feissel-Vernier et al. (2004) studied how the distribution of the stations that sample the VLBI TRF from year to year may impact UT1, using two different combinations of unconstrained session solutions for station coordinates and EOPs together with the full covariance matrices (SINEX files). The global combination of these parameters in a unique terrestrial reference frame is done using the CATREF (Combination and Analysis of Terrestrial REference Frames) software (Altamimi et al., 2002). The datum definition attaches the results to ITRF2000 using a subset of stations that are judged reliable over the data span considered. Two combination strategies were compared: 1) a global analysis over 1990-2003, using an appropriate set of long-term reliable stations for the datum definition; 2) yearly analyses, with different suitable sets of datum stations for each year.

The UT1 differences derived from the two approaches are plotted in Figure 3 in the form of yearly weighted averages. The year-to-year EOP changes, which increase after 1996, are significant with respect to their internal consistencies, reaching the few-mm level for rotation on the Earth's surface. The pre-1995 TRF effect is comparable in size with the CRF effect, at the level of a few μs. When modelling these differences over 1990-2002 as a linear variation one finds a bias of 3.6 ± 0.7 μs at J2000.0, a drift of $+0.54 \pm 0.16$ μs/year, and an rms residual of 2.4 μs for one year. These effects presumably reflect mostly inconsistencies with the VLBI terrestrial frame and weaknesses in the longer-term interconnection of the network.

The annual averages of the rotation angle A3 of yearly celestial reference frames from a similar computation are also included in the figure, as errors in UT1 may result from either terrestrial or celestial frame axial instabilities. When modelling these differences over 1990-2002 as a linear variation one finds a bias of 0.4 ± 0.3 μs at J2000.0, a drift of $+0.02 \pm 0.07$ μs/year, and an rms residual of 0.7 μs for one year.

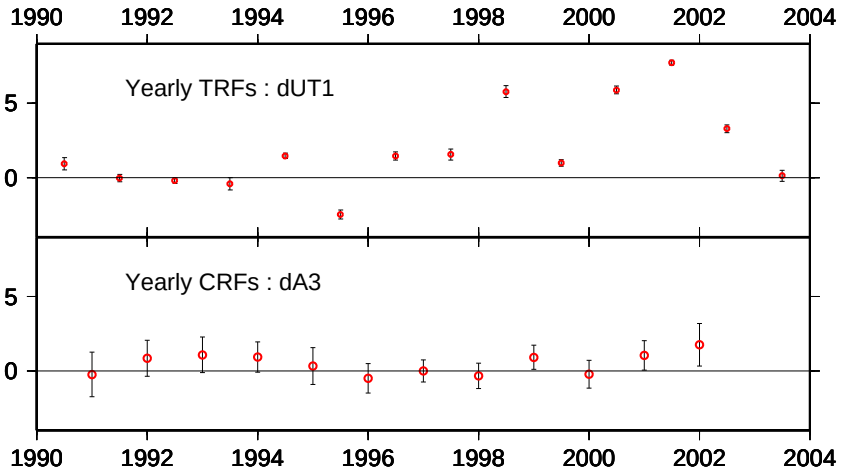

Fig. 3. Yearly average UT1 differences between solutions with the ITRF2000 tie performed separately each year and globally over 1990-2003. Similar variations of the axial rotation of yearly celestial reference frames are shown in the bottom. Unit: μs

4 Impact of the observing strategy

In this section we give two examples of short term effects of internal TRF inconsistencies associated with the VLBI TRF defects.

- The first example, taken from Feissel-Vernier et al. (2004), concerns the weekly operation of the IVS R1 and R4 24-hour EOP sessions, each using different networks. They are run since 2002 on Mondays and Thursdays, respectively, and each includes five to seven stations. Three stations are common: Gilcreek, Wettzell and Concepcion. The differences in the UT1 values derived from either type of session over 2002.0-2003.8 can be modelled as a bias: 1.9 μs, and an rms residual per session: 9.6 μs. The magnitude of the differences is equivalent to 3 to 5 mm on the Earth's surface, probably reflecting station coordinate inconsistencies at a similar level.
- Ray et al. (2005) studied methods for combining GPS and VLBI series of station coordinates together with the corresponding polar motion measurements and evaluated the outcome by comparing the geodetic series with series inferred from the atmospheric and oceanic excitation of Earth orientation variations. They show that
  - the consideration of VLBI polar motion in the combination degrades the accuracy of the GPS-only time series;
  - using GPS polar motion alone indirectly improves the VLBI-based estimation of universal time. The match of Length of Day (LOD) with geophysical data is improved by about 4 μs. The improvement is tiny - about 1% of the residual variance - but systematic. They also suggest that, conversely, the joint consideration of the two series of polar motion globally improves the alignment of the VLBI and GPS reference terrestrial frames.

5 Summary

Table 3 summarizes the orders of magnitude of the perturbation of the VLBI-derived UT1.

Table 3. Level of perturbation of VLBI UT1 due to celestial or terrestrial reference frames defects.

Perturbating Ref. frame	Bias	Drift	Medium term	Short term
TRF	2 μs	0.5 μs/year	7 μs	10 μs
CRF	4 μs	0.8 μs/year	2 μs	5 μs

Acknowledgements. C. Ma (GSFC) provided the test celestial reference frames described in table 1 and the time series of UT1 attached to the *cne* and *cn7* solutions. A.-M. Gontier and C. Barache performed the comparisons of reference frames.

References

Altamimi, Z., P. Sillard and C. Boucher, 2002, JGR 107B, 1, 2002.

Bizouard, C., 2005, This volume.

Feissel-Vernier, M., 2003, A&A 403, 105.

Feissel-Vernier, M., Ray, J., Altamimi, Z., Dehant, V., de Viron, O., 2004, IVS ...

Feissel-Vernier, M., Ma, C., Gontier, A.-M., Barache, C., 2005a, A&A (in press).

Feissel-Vernier, M., 2005, This volume.

Feissel-Vernier, M., Ma, C., Gontier, A.-M., Barache, C., 2005b, IERS Technical Note in preparation, C. Ma (ed.).

Fey, A. L., Ma, C., Arias, E. F., Charlot, P., Feissel-Vernier, Gontier, A.-M., Jacobs, C. S., Li, J., MacMillan, D., Sovers, O. J., 2004, AJ, 127, 3587.

Ma, C., Arias, E. F., Eubanks, T. M., Fey, A. L., Gontier, A.-M., Jacobs, C. S., Sovers, O. J., Archinal, B. A., Charlot, P., 1998, AJ 116, 516

Ray, J., Kouba, J., Altamimi, Z., 2005, Journal of Geodesy (in press)

Dissemination of ICRS products and information on ICRF radio sources

A.-M. Gontier[1], A. L. Fey[2], D. A. Boboltz[2], S. Bouquillon[1] and C. Barache[1]

[1] *Observatoire de Paris - SYstèmes de Référence Temps-Espace (SYRTE) - UMR 8630/CNRS*
[2] *US Naval Observatory - 3450 Massachusetts Avenue, NW - Washington, DC 20392-5420 USA*

Abstract. As agreed in the ICRS-PC terms of reference, the two participating groups (OP, USNO) have set up web sites and the necessary cross access to disseminate results.

1 Organisation of the Paris site

The structure of Paris web site is similar to the Earth Orientation Center one. It was reorganised starting from existing CRF section of IERS Central Bureau. It is divided in four sections (Fig. 1).

- ICRS-PC: contains general information on the ICRS Center.
- ICRS: gives informations on the system
  - definition of ICRS (equator and pole),
  - relation with the preceding conventional celestial reference frame FK5,
  - description of the organisation of the frame maintenance.

  The necessary links with other pages like VLBI techniques or IVS (International VLBI Service for geodesy and astronomy) are provided. References to articles are given at the bottom of the pages.
- ICRF: is devoted to the sources that materialize the frame.
  - ICRF elaborated in 1995 and details on the VLBI analyses used.
  - Extension of ICRF, ICRF-Ext.1 elaborated in 1999 and ICRF-EXT.2 in 2004. Coordinates in ICRS of 109 newly observed sources are provided.
  - For the next realization of ICRF (ICRF2), results of studies on the time stability of source coordinates are made available. Plots of yearly positions (postscript and gif images) and numerical data are proposed for 410 sources.
  - Information on Radio source structure is also necessary to monitor the sources. Structure index data are available through a link to Bordeaux Observatory.
  - An interactive access to all the information available in the various files for a selected source (alias name, ICRF coordinates and category, physical characteristics...) is provided.
- CRF analyses: gives the results of the comparisons between celestial reference frames submited to the ICRS-PC and the ICRF. References and explanations on the method of comparison are described.

In addition, informations on related sites and a contact person is given.

2 Organisation of the USNO site

At USNO the information relative to the ICRS-PC activities is presented in two pages:

Fig. 1. ICRS-PC web page

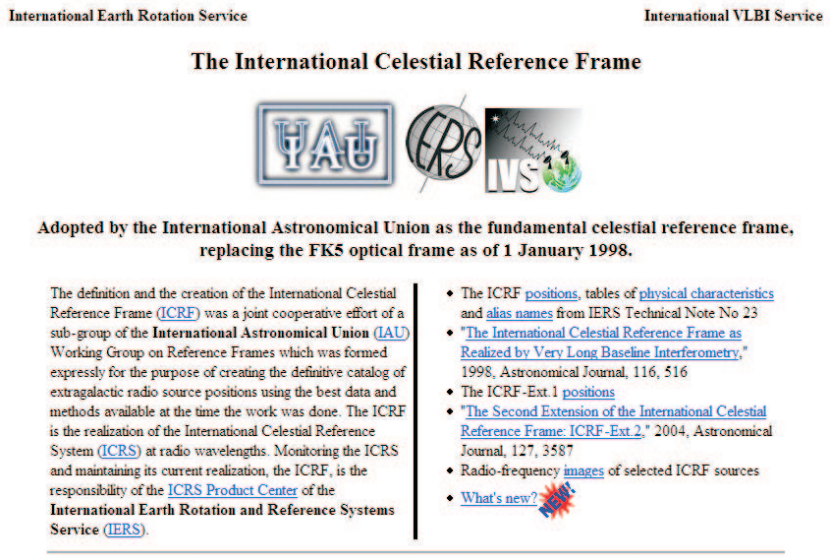

Fig. 2. USNO web page

ICRF (http://rorf.usno.navy.mil/ICRF) and
VLBI (http://rorf.usno.navy.mil/vlbi).

In the project ICRF page, access is given to the various services collaborating for the elaboration and maintenance of the ICRF: the International Astronomical Union (IAU), the IERS and IVS.

The ICRF page (Fig. 2) gives the following informations together with the necessary references:

- a short explanation about the adoption of the ICRF, together with links to the Paris Observatory site about ICRS, ICRF (extension) catalogues and related files.

- Radio frequency images of selected ICRF sources are available from the Radio Frame Frequency Images Database (RFFID).
- Abstract of the ICRF article, description of the settled organisation for the maintenance of the frame.
- Explanations about ICRF-Ext.1 catalogue and the ICRF-Ext.2 abstract article.

The VLBI page give links to the four following activities:

- USNO global VLBI solutions,
- RFFID,
- IVS Special Analysis Center for Source Structure that provides the IVS with intrinsic structure information on ICRF sources at radio wavelength,
- USNO Analysis of VLBA RDV that provides results of investigations of the effects of VLBA RDV data on astrometric position and EOP estimations.

The ICRS-PC/USNO component is the provider of the VLBI images of ICRF sources. The RRFID page (Fig. 3) explains the four different activities made on regular basis:

- VLBA and "VLBA + geodetic antenna" are snapshot images in S/X band (contour and visibility plots available in postscript format). Images and/or visibility in FITS format are distributed only upon request. The database contains actually 3285 images of 463 sources.
- The VLBA K/Q band program (collaboration between NASA, NRAO, Bordeaux Observatory and USNO), to extend ICRF to K, KA and Q bands, consist of 783 snapshot images of 231 sources.

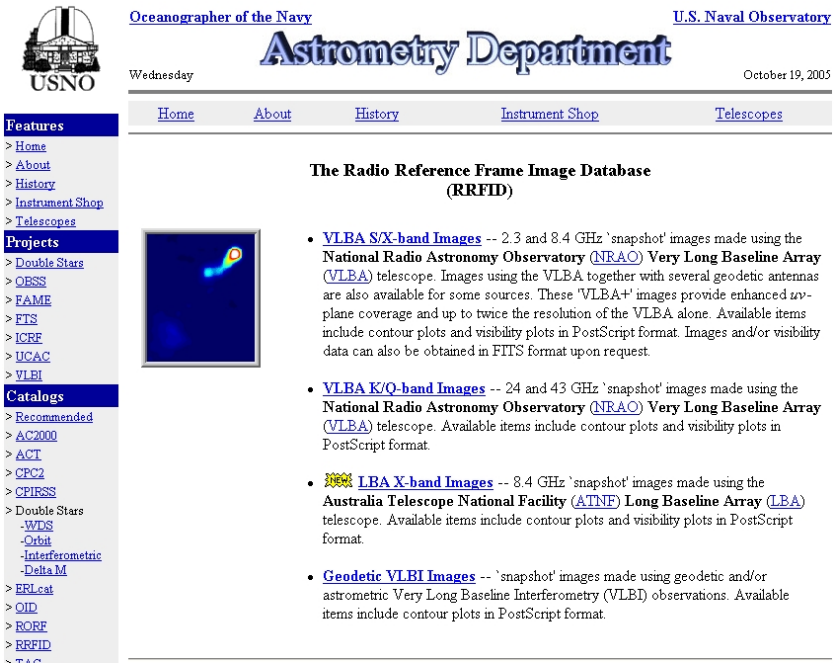

Fig. 3. Radio Frame Frequency Images Databases (RFFID) web page

- LBA X-band images is a joint program of Australian Telescope National Facility (ATNF) and USNO. The aim is to extend and maintain the ICRF in the southern hemisphere, the database contains 74 images of 69 sources.
- Geodetic VLBI images activity provide snapshot images using geodetic and/or astrometric VLBI observations.

The references and article links on source structure are available at the bottom of the page.

3 Plans

The site maintenance and extension plans include the following:

- update with newly available data and products,
- link to optical reference frames informations,
- development of the interactive consultation, in cooperation with the Centre de Données Astronomique de Strasbourg (CDS) and with the Virtual Observatory project in development at Paris Observatory.

References

- http://hpiers.obspm.fr/icrs-pc
- http://rorf.usno.navy.mil/ICRF
- http://rorf.usno.navy.mil/vlbi

Annex:
Share of task for operating the IERS ICRS Center

Abstract. This annex is an extract from the June 2000 agreement between Paris Observatory and the US Naval Observatory, with list of participants over 2001-2004.

Responsibilities

The Paris Observatory (OP) and the U.S. Naval Observatory (USNO) propose to act jointly as the International Celestial Reference System (ICRS) Center of the International Earth Rotation Service. The Product Center will have two co-directors (one from each institution), and a representative to the IERS Directing Board, which will rotate between institutions on a four-year term starting with the Paris Observatory. The proposing institutions will work together to provide the IERS Celestial Reference System. Each agency will perform specific tasks as described below to accomplish this goal.

The sharing of tasks, based on those originally proposed by OP and USNO, is listed hereafter. A capital X indicates the coordinating institution.

	OP	USNO
A. Reference system and frame		
1. Maintenance and extension of the ICRF	X	x
2. Investigation of future realizations of the ICRS	x	X
B. Extragalactic radio-sources		
3. Monitor structure to assess astrometric quality	x	X
4. Maintenance of the time stability of ICRF	X	x
C. Link of other reference frames to ICRS		
5. Maintenance of the link to the Hipparcos catalog	x	X
6. Linking the ICRF to frames at various wavelengths	X	x
7. Maintenance of the link to the solar system dynamical reference frame through millisecond pulsar analysis	X	
8. Maintenance of the link to the solar system dynamical reference frame through Lunar Laser Ranging analysis	X	
9. Maintenance of the link to the ITRF	X	
D. Information systems		
10. Dissemination of ICRS products	X	X

The ICRS Center will accomplish these tasks under direction of the IERS Directing Board and in coordination with the International VLBI Service for Geodesy and Astrometry (IVS) and the IAU Working Group on Reference Frames. It also expects to work closely with researchers of other institutions (with their agreement) who have already provided valuable contributions to reference systems.

Organization of activities

Maintaining the ICRF as the fundamental realization of the ICRS for the scientific community is the primary task of the ICRS Center. The IAU assigns this task to the IERS, therefore it will be performed in coordination with the concerned IAU bodies. As the current ICRF is based on VLBI data, the work will be performed in close collaboration with the IVS (both institutions are IVS Analysis Centers). Performing this primary task at the state of the art level requires a number of supporting activities that will be shared between OP and USNO. The following describes the distribution of efforts.

Task 1. Maintenance and Extension of the ICRF

A permanent VLBI observing program coordinated by the IVS continually brings in new observations of ICRF and prospective ICRF sources. The current coordinates of known sources will be checked for consistency and ICRS coordinates of the new sources will be derived. The ICRS Center will publish extensions to the ICRF as computed by the IVS. This work will be performed on a yearly basis, and results will be used to make recommendations on the relevance of possible revisions to the ICRF.

Revisions to the ICRF will occur only when improvements in modeling and data analysis strategies are sufficient to justify a complete reconstruction of the standard frame. The responsibility for this decision lies with the appropriate IAU and IVS groups of experts, of which ICRS PC personnel from both OP and USNO are members. The actual computation of the revised frame is performed in a single analysis following the specifications and recommendations issued by the above-mentioned groups of experts.

Personnel

OP:	USNO:
A.-M. Gontier (Task coordinator)	R. A. Gaume
E. F. Arias (BIPM)	A. L. Fey
C. Barache	N. Zacharias
S. Bouquillon	D. A. Boboltz
N. Essaifi	

Task 2. Investigation of future realizations of the ICRS

Future astrometric satellite missions such as FAME, SIM and GAIA, may provide fundamental reference frames more accurate than the current VLBI-based ICRF. Proposal personnel have direct ties to both FAME and SIM. This puts Product Center personnel in the unique position to study these prospective reference frames and to prepare possible recommendations of future space-based realizations of the ICRF for adoption by the IAU.

Personnel

OP:	USNO:
A.-M. Gontier	**R.A. Gaume (Task coordinator)**
J. Souchay	A.L. Fey
	N. Zacharias
	D.A. Boboltz

Task 3. Monitor structure to assess astrometric quality

The task of imaging the sources and evaluating their quality will be shared between the two proposing organizations for this task. Proposal personnel have played key roles in assessing astrometric source quality through the use of the source "structure index" (see Boboltz, this volume). In addition, proposal personnel have recently developed an improved method for assessing astrometric source quality, which was used in the selection of sources for the SIM extragalactic frame. Both the images and the structure indices will be made available through the ICRS Center web site. These products will be updated regularly as new data become available. The ICRS Center will work closely with the IVS to provide improved means necessary to assess the astrometric quality of ICRF sources. Future work will be targeted at correcting astrometric positions for the effects of source structures.

Personnel

OP:	USNO:
P. Charlot (Bordeaux Obs.)	**A.L. Fey (Task Coordinator)**
	D.A. Boboltz

Task 4. Maintenance of the time stability of ICRF

In addition to source structure, the stability in time of the ICRF depends on many different aspects of the operation of VLBI programs, such as atmospheric corrections, scheduling of observations and analysis strategies. Its understanding and monitoring is crucial for high accuracy scientific applications in other domains, e.g. precession-nutation studies. Proposal personnel are engaged in an analysis program on this topic (see Feissel-Vernier, this volume). These studies will also be useful to prepare recommendations to the IAU for future ICRS realizations. They will be carried out in coordination with the IAU working group on the International Celestial Reference System and IVS components.

Personnel

OP:	USNO:
M. Feissel-Vernier (Task Coordinator)	A.L. Fey
C. Barache	D.A. Boboltz
S. Bouquillon	
A.-M. Gontier	

Task 5. Maintenance of the link to the Hipparcos catalog

The link between the ICRF and the reference frame resulting from the Hipparcos catalog is considered fundamental to both frames; it extends the ICRF to optical wavelengths by giving access to ICRS coordinates and proper motions for more than 100,000 stars over the entire sky at mas and mas/yr accuracy respectively. In fact, the Hipparcos catalog can be considered the optical counterpart to the ICRF, and the IAU has recommended the Hipparcos catalog as the optical realization of the ICRS. The proposed task will consist of gathering both old and new data concerning Hipparcos stars in order to provide complete information on these objects, and particularly, data enabling the determination of the stellar positions with respect to nearby extragalactic objects. The location of the Hipparcos axes with respect to the ICRF will be an object of particular attention, as well as the effect of Hipparcos proper motion uncertainties. One example is the UCAC program to link the optical

and radio frames via extragalactic sources, which should provide a link at the level of 1 mas. This will be a significant improvement and check on the current ICRF/Hipparcos link via radio stars.

Personnel

OP:	USNO:
J. Souchay	**N. Zacharias (Task Coordinator)**
	A.L. Fey
	D.A. Boboltz

Task 6. Linking the ICRF to frames at various wavelengths

The ICRS Center will also deal with the improvement of the link between the ICRF and the frames related to deep sky surveys at wavelengths not belonging to the radio spectra; that is to say in the optical, infrared, and X-ray bandwidths, based on the various surveys conducted around the world that are able to provide valuable astrometric data through output catalogs.

Personnel

OP:	USNO:
J. Souchay (Task coordinator)	R.A. Gaume
	N. Zacharias
	A.L. Fey
	D.A. Boboltz

Task 7. Maintenance of the link to the solar system dynamical reference frame using millisecond pulsar analysis

Associating the pulsar timing technique with differential VLBI astrometry provides high quality information about the position and motion of the equator, the ecliptic, and the equinox of the ICRF. The proposed task will be to carry out a combined analysis of pulsar timing obtained by the OP/Nançay telescope and differential VLBI.

Personnel

OP:
I. Cognard (Task coordinator)
E. Aleshkina (Pulkovo Observatory)
M. Feissel-Vernier
J. Souchay

Task 8. Maintenance of the link to the solar system dynamical reference frame using Lunar Laser Ranging (LLR) analysis

When combined with VLBI analysis, the LLR technique is one of the most efficient ways to determine the orientation of the planetary reference frame relative to the extragalactic reference frame. The ICRS Center will gather the various data coming from LLR measurements in the framework of the ILRS in order to determine the orientation of the ecliptic in the ICRS.

Personnel

OP:
J. Chapront (Task coordinator)
G. Francou

Task 9. Maintenance of the link to the International Terrestrial Reference Frame (ITRF)

Long-term consistency of the ICRF, ITRF, and Earth Orientation time series is required by the user community. The ICRS PC will participate in this task in close cooperation with the IERS Analysis Coordinator and other IERS Product Centers.

Personnel

OP:
C. Bizouard (Task coordinator)
M. Feissel-Vernier

Task 10. Dissemination of ICRS products

Dissemination of ICRS products will be done through the ICRS Center web sites (identical sites will be hosted at OP and USNO) and through the IERS Data Center proposed by Paris Observatory jointly with CDDIS and BKG. The existing web sites will be reorganized and interlinked in order to provide relevant information related on the ICRS and ICRF. Updating the contents related to each task will be under the responsibility of the corresponding task coordinator. The overall homogeneity of the web site and of the Data Center public files will be the joint responsibility of two local coordinators, one in each institution.

Personnel

OP:
A.-M. Gontier
(Local coordinator)
C. Barache
S. Bouquillon
N. Essaifi

USNO:
A.L. Fey
(Local Coordinator)
D.A. Boboltz